Summer 8-2017

Solution of PDES For First-Order Photobleaching Kinetics Using Krylov Subspace Spectral Methods

Somayyeh Sheikholeslami
University of Southern Mississippi

SOLUTION OF PDES FOR FIRST-ORDER PHOTOBLEACHING KINETICS USING KRYLOV SUBSPACE SPECTRAL METHODS

by

Somayyeh Sheikholeslami

A Dissertation
Submitted to the Graduate School,
the College of Science and Technology,
and the Department of Physics and Astronomy
of The University of Southern Mississippi
in Partial Fulfillment of the Requirements
for the Degree of Doctor of Philosophy

August 2017

SOLUTION OF PDES FOR FIRST-ORDER PHOTOBLEACHING KINETICS USING KRYLOV SUBSPACE SPECTRAL METHODS

by Somayyeh Sheikholeslami

August 2017

Approved by:

Dr. James V. Lambers, Committee Chair
Associate Professor, Mathematics

Dr. Christopher Winstead, Committee Member
Professor, Physics and Astronomy

Dr. C. S. Chen, Committee Member
Professor, Mathematics

Dr. David T. Brown, Committee Member
Professor, Biochemistry, University of Mississippi Medical Center

Dr. Christopher Winstead
Chair, Department of Physics and Astronomy

Dr. Karen S. Coats
Dean of the Graduate School

ABSTRACT

SOLUTION OF PDES FOR FIRST-ORDER PHOTOBLEACHING KINETICS USING KRYLOV SUBSPACE SPECTRAL METHODS

by Somayyeh Sheikholeslami

August 2017

We solve the first order reaction-diffusion equations which describe binding-diffusion kinetics using a photobleaching scanning profile of a confocal laser scanning microscope approximated by a Gaussian laser profile. We show how to solve these equations with prebleach steady-state initial conditions using a time-domain method known as a Krylov Subspace Spectral (KSS) method. KSS methods are explicit methods for solving time-dependent variable-coefficient partial differential equations (PDEs). KSS methods are advantageous compared to other methods because of their stability and their superior scalability. These advantages are obtained by applying Gaussian quadrature rules in the spectral domain developed by Golub and Meurant. We present a simple approximate analytical solution to the reaction-diffusion equations, as well as a computational solution that is first-order accurate in time. We then use this solution to examine short- and long-time behaviors.

ACKNOWLEDGMENTS

This is to thank my precious advisor (Dr. James V. Lambers) who survived me, believed in me and trusted my talent. Words can not describe his unconditional availability, support and patience during my limited research period. I am forever thankful of having him in my academic life.

TABLE OF CONTENTS

LIST OF ILLUSTRATIONS

Figure

LIST OF TABLES

Table

LIST OF ABBREVIATIONS

FRAP - Fluorescence Recovery After Photobleaching
KSS - Krylov Subspace Spectral
FFT - Fast Fourier Transform
CFL - Courant-Friedrichs-Lewy

NOTATION AND GLOSSARY

General Usage and Terminology

The notation used in this text represents fairly standard mathematical and computational usage. In many cases these fields tend to use different preferred notation to indicate the same concept, and these have been reconciled to the extent possible, given the interdisciplinary nature of the material. In particular, the notation for partial derivatives varies extensively, and the notation used is chosen for stylistic convenience based on the application. While it would be convenient to utilize a standard nomenclature for this important symbol, the many alternatives currently in the published literature will continue to be utilized.

The blackboard fonts are used to denote standard sets of numbers: $\mathbb{R}$ for the field of real numbers, $\mathbb{C}$ for the complex field, $\mathbb{Z}$ for the integers, and $\mathbb{Q}$ for the rationals. The capital letters, $A, B, \cdots$ are used to denote matrices, including capital greek letters, e.g., Λ for a diagnonal matrix. Functions which are denoted in boldface type typically represent vector valued functions, and real valued functions usually are set in lower case roman or greek letters. Caligraphic letters, e.g., $\mathcal{V}$, are used to denote spaces such as $\mathcal{V}$ denoting a vector space, $\mathcal{H}$ denoting a Hilbert space, or $\mathcal{F}$ denoting a general function space. Lower case letters such as i, j, k, l, m, n and sometimes p and d are used to denote indices.

Vectors are typset in square brackets, e.g., $[\cdot]$, and matrices are typeset in parenthesese, e.g., $(\cdot)$. In general the norms are typeset using double pairs of lines, e.g., $||\cdot||$, and the abolute value of numbers is denoted using a single pairs of lines, e.g., $|\cdot|$. Single pairs of lines around matrices indicates the determinant of the matrix.

Chapter 1

Background

1.1 Fluorescence Recovery After Photobleaching (FRAP) Method

Consider a membrane of molecules with the same molecular species unbound to the membrane (surrounding the membrane). Suppose there are continuous exchanges between the bound and the unbound molecules. The membrane size is not changing and the system is in a steady state. We bleach only the membrane using a high laser intensity for a short period to reduce fluorescence of the membrane to the background levels. Immediately after bleaching, all molecules in the bleach zone (in the membrane) lose fluorescence. Since there is a continuous exchange of the molecules with the exchange rates of k_{on} and k_{off}, the membrane regains fluorescence over time, which changes the fluorescence level. This is a description of the Fluorescence Recovery After Photobleaching (FRAP) method, which is a tool to investigate the dynamics of molecules within membrane domains. The FRAP method was established by Jacobson et al. in 1976 [15]. The chemical equation of the binding-diffusion process is

$$u + a \underset{k_{off}}{\overset{k_{on}}{\rightleftharpoons}} b \tag{1.1}$$

where u is unbound molecules, a is specific binding sites and b is bound complexes (ua). The rate of the forward binding reaction is called k_{on}, where a molecule binds to a binding site to form a bound complex, and k_{off} refers to the rate of the reverse unbinding reaction where a molecule is released from its binding site.

During the bleaching, there is a fraction of the immobilized molecules in the bleached spot, and a mobile fraction of molecules that contributes to fluorescence recovery. FRAP provides us information about the recovery kinetics and also the fraction of diffuse molecules. The assumption in the photobleaching method is that the molecules could be mobile or immobile [10]. So, after bleaching, the fraction of immobile fluorescence can be calculated by

$$F_{im}(t) = \kappa C_i \gamma \frac{1 - e^{-k_b}}{k_b}, \quad 0 < \gamma < 1 \tag{1.2}$$

where κ is a parameter that depends on properties of the laser and of the detection system, k_b is the bleach constant which is a measure of the intensity of the bleaching laser and the

properties of the fluorophore, C_i is the initial concentration of the fluorescent molecules inside the bleached zone, and γ is the percentage of immobile molecules. The fraction of mobile fluorescence is

$$F_m(t) = \kappa C_i(1-\gamma)\sum_{n=0}^{\infty}\frac{(-k_b)^n}{n!}\left[1+n\left(1+\frac{2t}{\tau_D}\right)\right]^{-1}. \tag{1.3}$$

The diffusion coefficient of mobile molecules is

$$D = \frac{r_\omega^2}{2\tau_D} \tag{1.4}$$

where r_ω is the Gaussian beam radius, and τ_D is the characteristic time of diffusion. The total observed fluorescence inside the bleached zone is the sum of the mobile and immobile fluorescence, which could be monitored over time to produce FRAP recovery curves. FRAP recovery curves from laboratory work will be fit to mathematical models to get estimates of mobile and immobile fractions. D is calculated by fitting a function $I(t)$ to the fluorescence recovery curve. The total normalized fluorescence is

$$I(t) = \gamma\frac{1-e^{-k_b}}{k_b} + (1-\gamma)\sum_{n=0}^{\infty}\frac{(-k_b)^n}{n!}\left[1+n\left(1+\frac{2t}{\tau_D}\right)\right]^{-1}. \tag{1.5}$$

The first order reaction-diffusion equations which describe binding-diffusion kinetics are

$$\begin{aligned}
\frac{\partial u}{\partial t} &= -k_b I_{rn}(x,y)u + D_1\nabla^2 u - k_{on}u + k_{off}b \\
\frac{\partial b}{\partial t} &= -k_b I_{rn}(x,y)b + D_2\nabla^2 b + k_{on}u - k_{off}b \\
\nabla^2 &= \frac{\partial^2}{\partial x^2} + \frac{\partial^2}{\partial y^2}, \quad D_1 > D_2
\end{aligned} \tag{1.6}$$

where D_1 and D_2 are diffusion coefficients of u and b, k_{on} and k_{off} are on and off binding-rate constants, and k_b is a bleach constant which is the intensity of the bleaching laser and the properties of the fluorophore. Also, D_1 and D_2, k_{on} and k_{off} are positive constants. The initial conditions from a prebleach steady state are

$$u(x,y,0) = \frac{k_{off}}{k_{on}+k_{off}}C_i, \tag{1.7}$$

$$b(x,y,0) = \frac{k_{on}}{k_{on}+k_{off}}C_i, \tag{1.8}$$

and the photobleaching scanning profile of a confocal microscope can be approximated by a Gaussian laser profile [3, 4, 11]

$$I_{r_n}(x,y) = \frac{2I_0}{\pi r_n^2}e^{-\frac{2((x-x_c)^2+(y-y_c)^2)}{r_n^2}} \tag{1.9}$$

where r_n is the nominal radius of the laser beam and (x_c, y_c) is the center.

1.2 Gaussian Beam Propagation

The Gaussian intensity distribution of a laser is

$$I(x,y) = \eta EE^* = \eta E_0 E_0^* e^{-\frac{2r^2}{r_{\omega 0}^2}} = I_0 e^{-\frac{2r^2}{r_{\omega 0}^2}} \tag{1.10}$$

where r is the distance from the center of the beam, and $r_{\omega 0}$ is the Gaussian beam radius which has the intensity of $1/e^2(0.135)$ of its peak value [21]. The electric field variation is given by

$$E = E_0 e^{-\frac{r^2}{r_{\omega 0}^2}} \tag{1.11}$$

where $r_{\omega 0}$ is the radius at which the amplitude is $1/e$ of its value. The Gaussian beam radius $r_\omega(z)$ and wavefront radius of curvature $R(z)$ as a function of depth are calculated by

$$\begin{aligned} r_\omega^2(z) &= r_{\omega 0}^2 \left[1 + \left(\frac{\lambda z}{\pi r_{\omega 0}^2}\right)^2\right] \\ R(z) &= z\left[1 + \left(\frac{\pi r_{\omega 0}^2}{\lambda z}\right)^2\right] \end{aligned} \tag{1.12}$$

where λ is the wavelength. The Rayleigh range is

$$z_R = \frac{\pi r_{\omega 0}^2}{\lambda} \tag{1.13}$$

and $R(z)$ has its minimum value at $z = z_R$. The confocal parameter b is defined by

$$b = 2z_R = \frac{2\pi r_{\omega 0}^2}{\lambda}. \tag{1.14}$$

The total power $p(\infty)$ is related to $I(0)$ by

$$\begin{aligned} I(0) &= \frac{2}{\pi r_{\omega 0}^2} p(\infty) \\ p(\infty) &= \frac{\pi r_{\omega 0}^2}{2} I(0) \end{aligned} \tag{1.15}$$

where

$$p(r) = p(\infty)\left[1 - e^{-\frac{2r^2}{r_{\omega 0}^2}}\right]. \tag{1.16}$$

The Gaussian intensity distribution of a laser for beam radius at given depth (z) is

$$I(x,y,z) = \frac{2p(\infty)}{\pi r_\omega^2(z)} e^{\frac{-2r^2}{r_\omega^2(z)}} = \frac{I_0 r_{\omega 0}^2}{r_\omega^2(z)} e^{\frac{-2r^2}{r_\omega^2(z)}} \tag{1.17}$$

where

$$r_\omega^2(z) = r_{\omega 0}^2 \left[1 + \left(\frac{\lambda z}{\pi r_{\omega 0}^2} \right)^2 \right]. \tag{1.18}$$

1.3 Problem and Objectives

First-order photobleaching kinetics which are mathematically modeled in equation (1.6) were solved numerically by Kang et al. [11, 12]. These equations were also solved numerically using an inversion method (backward Euler in time, central differencing in space) in [14]. In this dissertation we apply an explicit time-stepping method known as a Krylov subspace spectral (KSS) method to solve the first-order photobleaching kinetics PDEs. KSS methods, developed by Lambers [16], use Gaussian quadrature rules in the spectral domain, as described in [8], to approximate each Fourier coefficient of the solution. This component-wise approach yields high-order accuracy in time, stability characteristic of implicit methods even though KSS methods are themselves explicit [16, 17], and superior scalability compared to other time-stepping approaches [5]. We will use a KSS method to solve the first-order photobleaching kinetics equations (1.6) with initial conditions (1.7), (1.8). By applying KSS symbolically to compute each Fourier coefficient, we can also obtain an approximate analytical solution valid for a sufficiently small time step, to facilitate qualitative analysis of the solution.

Chapter 2

Methodology

2.1 Krylov Subspace Spectral (KSS) Methods

In order to solve photobleaching kinetics equations (1.6), we will apply a Krylov Subspace Spectral (KSS) Method on $[0,2\pi]^2$ and $t>0$ with periodic boundary conditions. To explain KSS methods, we illustrate with a parabolic PDE in 1-D:

$$\begin{aligned} \frac{\partial u}{\partial t}+L(x,D)u &= 0, \quad u(x,0)=u_0(x), \quad t>0, \quad 0<x<2\pi \\ u(0,t) &= u(2\pi,t) \end{aligned} \tag{2.1}$$

where $D=\frac{\partial}{\partial x}$ is a differentiation operator and $L(x,D)$ is a differential operator which includes both differentiation operators and coefficients that are functions of x. The inner product $\langle .,. \rangle$ is the standard inner product of functions on $[0,2\pi]$. The Fourier coefficients of the exact solution as inner products are calculated as follows:

$$\begin{aligned} \langle f,g \rangle &= \int_0^{2\pi} \overline{f(x)} g(x)\,dx \\ \hat{u}(\omega,t_{n+1}) &= \left\langle \frac{1}{\sqrt{2\pi}} e^{i\omega x}, S(x,D;\Delta t)u(x,t_n) \right\rangle, \quad |\omega|<N/2 \end{aligned} \tag{2.2}$$

where $S(x,D;\Delta t)$ is the exact solution operator, N is the number of grid points and $\hat{u}(\omega,t_{n+1})$ is a Fourier coefficient of the solution after a time step. An approximate Fourier coefficient of the solution in discretized space is

$$[\hat{u}^{n+1}]_\omega = \hat{e}_\omega^H S_N(\Delta t)u(t_n), \quad S_N = e^{-L_N \Delta t} \tag{2.3}$$

where L_N is a matrix that represents the spatial discretization of the operator $L(x,D)$. Vector components on a N-point grid with uniform grid spacing h are defined as follows:

$$[\hat{e}_\omega]_j = \frac{1}{\sqrt{2\pi}} e^{i\omega jh}, \quad [u(t_n)]_j = u(jh,t_n), \quad h=\frac{2\pi}{N}. \tag{2.4}$$

2.2 Gaussian Quadrature Rule

The bilinear form in equation (2.3) that we want to approximate is an example of the generic bilinear form

$$\mathbf{u}^T f(A)\mathbf{v}, \tag{2.5}$$

where $\mathbf{u}$ and $\mathbf{v}$ are N-vectors, f is a smooth function and $A = L_N$ is an $N \times N$ symmetric positive definite matrix with positive and real eigenvalues

$$0 < a = \lambda_N \leq \cdots \leq \lambda_2 \leq \lambda_1 = b \tag{2.6}$$

and also orthogonal eigenvectors $\mathbf{q}_1, \mathbf{q}_2, \ldots, \mathbf{q}_N$ such that

$$A\mathbf{q}_j = \lambda_j \mathbf{q}_j, \quad j = 1, 2, \ldots, N. \tag{2.7}$$

Equation(2.5) can be written as Riemann-Stieltjes integral

$$\begin{aligned} \mathbf{u}^T f(A)\mathbf{v} &= \mathbf{u}^T f\left(\sum_{j=1}^{N} \lambda_j \mathbf{q}_j \mathbf{q}_j^T\right)\mathbf{v} \\ &= \sum_{j=1}^{N} f(\lambda_j)\mathbf{u}^T \mathbf{q}_j \mathbf{q}_j^T \mathbf{v} \\ &= \int_a^b f(\lambda) d\alpha(\lambda) \end{aligned} \tag{2.8}$$

where the measure $\alpha(\lambda)$ is defined as

$$\alpha(\lambda) = \begin{cases} 0, & \lambda < a \\ \sum_{j=i}^{N} \alpha_j \beta_j, & \lambda_i \leq \lambda < \lambda_{i-1} \\ \sum_{j=1}^{N} \alpha_j \beta_j, & b \leq \lambda \end{cases} \tag{2.9}$$

with $\alpha_j = \mathbf{u}^T \mathbf{q}_j$ and $\beta_j = \mathbf{q}_j^T \mathbf{v}$.
This integral can be approximated with a Gaussian quadrature rule, which can be written in terms of nodes t_j and weights w_j, where $j = 1, 2, \ldots, K$, as follows

$$\mathbf{u}^T f(A)\mathbf{v} = \int_a^b f(\lambda)\, d\alpha(\lambda) = I[f] = \sum_{j=1}^{K} w_j f(t_j) + R[f]. \tag{2.10}$$

The weights w_j are defined by

$$w_j = \int_a^b L_j(\lambda) d\alpha(\lambda), \tag{2.11}$$

where the Lagrange polynomial $L_j(\lambda)$ is defined by

$$\begin{aligned} L_j(\lambda) &= \prod_{k=1, k\neq j}^{K} \frac{\lambda - t_k}{\lambda_j - \lambda_k}, \quad j = 1, \ldots, K, \\ L_j(t_k) &= \delta_{jk}. \end{aligned} \tag{2.12}$$

The error can be calculated by

$$R[f] = \frac{f^{2K}(\eta)}{(2K)!} \int_a^b \left[\prod_{j=1}^{K} (\lambda - t_j)\right]^2 d\alpha(\lambda), \quad a < \eta < b. \tag{2.13}$$

2.2.1 The Case $\mathbf{u} = \mathbf{v}$

In order to obtain Gaussian quadrature nodes, we define a sequence of polynomials $q_0(\lambda), q_1(\lambda), \ldots$ that are orthonormal. Orthonormality is defined by the conditions

$$\langle q_i, q_j \rangle = \int_a^b q_i(\lambda) q_j(\lambda)\, d\alpha(\lambda) = \delta_{ij} \tag{2.14}$$

where q_j has degree j. Here we use the inner product

$$\langle f, g \rangle = \int_a^b f(\lambda) g(\lambda)\, d\alpha(\lambda) = \mathbf{u}^T f(A) g(A) \mathbf{u} \tag{2.15}$$

where

$$||f||_\alpha = \langle f, f \rangle^{1/2} = (\mathbf{u}^T f(A)^2 \mathbf{u})^{1/2}. \tag{2.16}$$

The three-term recurrence relation for $j = 1, 2, \ldots$ can be written

$$\begin{aligned} \beta_j q_j(\lambda) &= (\lambda - \alpha_j) q_{j-1}(\lambda) - \beta_{j-1} q_{j-2}(\lambda), \\ q_{-1}(\lambda) \equiv 0, \quad q_0(\lambda) &\equiv \left(\int_a^b d\alpha(\lambda) \right)^{-1/2} \equiv \frac{1}{\beta_0}, \end{aligned} \tag{2.17}$$

where, for $j = 1, 2, \ldots, K$, we have

$$\begin{aligned} \alpha_j &= \langle q_{j-1}, x q_{j-1} \rangle = \mathbf{x}_j^T A \mathbf{x}_j, \\ \beta_j &= \langle p_j, p_j \rangle^{1/2} = ||\mathbf{r}_j||_2, \\ \mathbf{x}_j &= q_{j-1}(A)\mathbf{u}, \\ \mathbf{r}_j &= p_j(A)\mathbf{u} = (A - \alpha_j I) q_{j-1}(A)\mathbf{u} - \beta_{j-1} q_{j-2}(A)\mathbf{u} = \\ &\quad (A - \alpha_j I)\mathbf{x}_j - \beta_{j-1}\mathbf{x}_{j-1}. \end{aligned} \tag{2.18}$$

The recurrence relation can be written in matrix form as follows

$$\lambda \mathbf{q}(\lambda) = J_K \mathbf{q}(\lambda) + \beta_K \mathbf{q}_K(\lambda) \mathbf{e}_K, \tag{2.19}$$

where the vector $\mathbf{q}(\lambda)$ and tridiagonal Jacobi matrix J_K are given by

$$\mathbf{q}(\lambda) = \begin{bmatrix} q_0(\lambda) \\ q_1(\lambda) \\ \vdots \\ q_{K-1}(\lambda) \end{bmatrix}, \quad J_K = \begin{bmatrix} \alpha_1 & \beta_1 & & & \\ \beta_1 & \alpha_2 & \beta_2 & & \\ & \ddots & \ddots & \ddots & \\ & & \beta_{K-2} & \alpha_{K-1} & \beta_{K-1} \\ & & & \beta_{K-1} & \alpha_K \end{bmatrix}. \tag{2.20}$$

The eigenvalues of J_K are the nodes for a K-point Gaussian quadrature rule [8]. The squares of the first elements of the normalized eigenvectors of J_K yield the weights $w_j = (\beta_0 q_0(t_j)/\|\mathbf{q}(t_j)\|_2)^2$. We then have the Gaussian quadrature approximation

$$\mathbf{u}^H f(A)\mathbf{u} = \|\mathbf{u}\|_2^2 \mathbf{e}_1^H f(J_K)\mathbf{e}_1 \tag{2.21}$$

which can easily be evaluated in terms of the quadrature nodes and weights.

2.2.2 The Lanczos Algorithm for Case $\mathbf{u} = \mathbf{v}$

Based on the above vectors and coefficients in (2.18) we can derive the following algorithm:
$\mathbf{r}_0 = \mathbf{u}$
$\mathbf{x}_0 = 0$
for $j = 1, 2, \ldots, K$
$\beta_{j-1} = ||\mathbf{r}_{j-1}||_2$
$\mathbf{x}_j = \mathbf{r}_{j-1}/\beta_{j-1}$
$\alpha_j = \mathbf{x}_j^T A \mathbf{x}_j$
$\mathbf{r}_j = (A - \alpha_j I)\mathbf{x}_j - \beta_{j-1}\mathbf{x}_{j-1}$
end

2.2.3 The Block Case $\mathbf{u} \neq \mathbf{v}$

The block-tridiagonal Jacobi matrix J_K of order $2K$ for the block case $\mathbf{u} \neq \mathbf{v}$ can be written

$$J_K = \begin{bmatrix} M_1 & B_1^T & & & \\ B_1 & M_2 & B_2^T & & \\ & \ddots & \ddots & \ddots & \\ & & B_{K-2} & M_{K-1} & B_{K-1}^T \\ & & & B_{K-1} & M_K \end{bmatrix} \tag{2.22}$$

and for $j = 1, 2, \ldots, K$ we have

$$R_{j-1} = X_j B_{j-1}, \quad M_j = X_j^T A X_j, \quad R_j = A X_j - X_j M_j - X_{j-1} B_{j-1}^T, \quad X_0 \equiv 0 \tag{2.23}$$

where X_j is a $N \times 2$ matrix, $X_j^T X_j = I$, B_j is 2×2 upper triangular and M_j is 2×2 and symmetric [18]. The matrices X_j and B_{j-1} are obtained by performing a QR factorization of R_{j-1}. The initial block is $R_0 = \begin{bmatrix} \mathbf{u} & \mathbf{v} \end{bmatrix}$. Once J_K is obtained, a block Gaussian quadrature approximation of (2.5) is given by

$$\mathbf{u}^H f(A) \mathbf{v} = \mathbf{e}_1^T B_0^H E_{12}^H f(J_K) E_{12} B_0 \mathbf{e}_2, \quad E_{12} = \begin{bmatrix} \mathbf{e}_1 & \mathbf{e}_2 \end{bmatrix}. \tag{2.24}$$

2.2.4 The Lanczos Algorithm Block for Case $\mathbf{u} \neq \mathbf{v}$

Based on the above blocks we can derive the following algorithm:
$R_0 = [\mathbf{u} \ \ \mathbf{v}]$
$X_0 = 0$
for $j = 1, 2, \ldots, K$
$R_{j-1} = X_j B_{j-1}$

$V_j = AX_j$
$M_j = X_j^T AX_j$
$R_j = AX_j - X_j M_j - X_{j-1} B_{j-1}^T$
end

2.2.5 The Arnoldi Block Case $\mathbf{u} \neq \mathbf{v}$

The spatial differential operator for the system that we are solving is not self-adjoint, therefore that would be discretized by an unsymmetric matrix. In the case of unsymmetric A, since the orthogonal tridiagonalization does not exist, instead we could obtain a block Hessenberg matrix. The block Hessenberg matrix H_K of order $2K$ for the block case $\mathbf{u} \neq \mathbf{v}$ can be written

$$H_K = \begin{bmatrix} H_{11} & H_{12} & H_{13} & \cdots & H_{1,K} \\ H_{21} & H_{22} & H_{23} & & \vdots \\ \vdots & \ddots & \ddots & \ddots & \vdots \\ 0 & 0 & H_{K-1,K-2} & H_{K-1,K-1} & H_{K-1,K} \\ 0 & 0 & 0 & H_{K,K-1} & H_{K,K} \end{bmatrix} \tag{2.25}$$

and for $j = 1, 2, \ldots, K$ and $i = 1, 2, \ldots, j$ we have

$$R_{j-1} = X_j H_{j,j-1}, \quad H_{ij} = X_i^H AX_j, \quad R_j = R_j - X_i H_{ij} \tag{2.26}$$

where $X_i^H X_i = I$ [5]. The main reason for using Arnoldi for the block case is the loss of orthogonality of the Lanczos vectors in iterations which makes the unsymmetric Lanczos method unstable. Another problem with the unsymmetric Lanczos method is lack of convergence of the eigenvalues of M_j to the eigenvalues of A and also unsymmetric Lanczos can experience serious breakdown [7]. In other words, the iterations terminates while there is no invariant subspace information for A. For each time step and each frequency ω, the block KSS method proceeds by defining $R_0 = [\mathbf{u} \;\; \mathbf{v}] = \begin{bmatrix} \frac{1}{\sqrt{2\pi}} e^{i\omega x} & u(x, t_n) \end{bmatrix}$ as the initial block for the block Arnoldi algorithm [7] described below. We compute the QR factorization $R_{j-1} = X_j H_{j,j-1}$. Then, block Arnoldi [20, 6] is applied to produce the Hessenberg matrix H_K, which in turn yields the nodes and weights for the Gaussian quadrature rule needed to approximate each Fourier coefficient of the solution at time t_{n+1}. The details of these steps are discussed in the next two chapters.

2.2.6 The Arnoldi Algorithm Block for Case $\mathbf{u} \neq \mathbf{v}$

Based on the above blocks we can derive the following algorithm:

$R_0 = [\mathbf{u}\ \ \mathbf{v}]$
for $j = 1, 2, \ldots, K$
    $R_{j-1} = X_j H_{j,j-1}$
    $R_j = AX_j$
    for $i = 1, 2, \ldots, j$
        $H_{ij} = X_i^H R_j$
        $R_j = R_j - X_i H_{ij}$
    end
end

Chapter 3

First Order Photobleaching Kinetics Analytic Solution

3.1 First Order Photobleaching Kinetics Analytic Solution

3.1.1 Construction of Basis Functions

For convenience, we use the spatial domain $E = [0, 2\pi]^2$, and impose periodic boundary conditions. Homogeneous Dirichlet or Neumann boundary conditions can be handled in a similar manner [5]. With this domain and boundary conditions, we use as our basis functions the eigenfunctions of a constant-coefficient problem obtained by averaging the variable coefficient $k_b I_{r_n}$, as described in [18].

Let $\omega = (\omega_1, \omega_2) \in \mathbb{Z}^2$. We denote points in E by $\mathbf{x} = (x, y)$. For convenience, we introduce

$$L_{ij}(x, y, D) = \sum_{\mu,\nu=0} Q^{ij}_{\mu\nu}(x, y) D^{\mu\nu}, \quad D = \frac{\partial}{\partial \mathbf{x}}. \tag{3.1}$$

If we set

$$\begin{aligned}
Q^{11}_{00}(x, y) &= -k_b I_{r_n}(x, y) - k_{on} \\
Q^{11}_{20}(x, y) &= D_1 \\
Q^{11}_{02}(x, y) &= D_1 \\
Q^{12}_{00}(x, y) &= k_{off} \\
Q^{21}_{00}(x, y) &= k_{on} \\
Q^{22}_{00}(x, y) &= -k_b I_{r_n}(x, y) - k_{off} \\
Q^{22}_{20}(x, y) &= D_2 \\
Q^{22}_{02}(x, y) &= D_2.
\end{aligned} \tag{3.2}$$

and then define

$$L = \begin{bmatrix} -k_b I_{r_n}(x, y) - k_{on} + D_1\Delta & k_{off} \\ k_{on} & -k_b I_{r_n}(x, y) - k_{off} + D_2\Delta \end{bmatrix}, \quad \mathbf{v}(t) = \begin{bmatrix} u(x, y, t) \\ b(x, y, t) \end{bmatrix} \tag{3.3}$$

then (1.6) takes the form $\mathbf{v}_t = L\mathbf{v}$. We now seek to solve a constant-coefficient approximation of this system of PDEs.

To that end, the average of $I_{r_n}(x,y)$ over a rectangular domain E is given by

$$\bar{I}_{r_n} = \frac{1}{A(E)} \int\int_E I_{r_n}\, dx\, dy = \frac{1}{A(E)} \int\int_{x^2+y^2<r_n} \frac{I_0}{\pi r_n^2}\, dx\, dy = \frac{I_0}{A(E)}. \tag{3.4}$$

We then compute the 2×2 matrix

$$\bar{L}(\omega) = \begin{bmatrix} \langle e^{i\omega\cdot\mathbf{x}}, \bar{L}_{11}(x,y,D)e^{i\omega\cdot\mathbf{x}}\rangle & \langle e^{i\omega\cdot\mathbf{x}}, \bar{L}_{12}(x,y,D)e^{i\omega\cdot\mathbf{x}}\rangle \\ \langle e^{i\omega\cdot\mathbf{x}}, \bar{L}_{21}(x,y,D)e^{i\omega\cdot\mathbf{x}}\rangle & \langle e^{i\omega\cdot\mathbf{x}}, \bar{L}_{22}(x,y,D)e^{i\omega\cdot\mathbf{x}}\rangle \end{bmatrix} \tag{3.5}$$

where, for $i,j = 1,2$, $\bar{L}_{ij}(x,y,D)$ is obtained from $\bar{L}_{ij}(x,y,D)$ by replacing I_{r_n} by $\bar{I}_{r_n}$. Then, the eigenvalues of $\bar{L}(\omega)$ are

$$\begin{aligned} \lambda_1 &= -\frac{k_b I_0}{A(E)} - \frac{1}{2}\|\omega\|^2(D_1+D_2) - \frac{1}{2}(k_{on}+k_{off}) + \\ &\quad \frac{1}{2}\left[\|\omega\|^4(D_1-D_2)^2 + \|\omega\|^2(2(D_1+D_2)(k_{on}+k_{off}) - \right. \\ &\quad \left. 4(D_1k_{off}+D_2k_{on})) + (k_{on}+k_{off})^2\right]^{1/2} \\ \lambda_2 &= -\frac{k_b I_0}{A(E)} - \frac{1}{2}\|\omega\|^2(D_1+D_2) - \frac{1}{2}(k_{on}+k_{off}) - \\ &\quad \frac{1}{2}\left[\|\omega\|^4(D_1-D_2)^2 + \|\omega\|^2(2(D_1+D_2)(k_{on}+k_{off}) - \right. \\ &\quad \left. 4(D_1k_{off}+D_2k_{on})) + (k_{on}+k_{off})^2\right]^{1/2}. \end{aligned} \tag{3.6}$$

If we write

$$\begin{bmatrix} u_{11} \\ u_{21} \end{bmatrix} = \begin{bmatrix} k_{off} \\ \frac{k_b I_0}{A(E)} + D_1\|\omega\|^2 + k_{on} + \lambda_1 \end{bmatrix} \tag{3.7}$$

then one eigenvector of $\bar{L}(\omega)$ is

$$\begin{bmatrix} u_{11} \\ u_{21} \end{bmatrix} = \begin{bmatrix} k_{off} \\ c_1 \end{bmatrix} \tag{3.8}$$

where

$$\begin{aligned} c_1 &= \frac{1}{2}\|\omega\|^2(D_1-D_2) + \frac{1}{2}(k_{on}-k_{off}) + \\ &\quad \frac{1}{2}\left[\|\omega\|^4(D_1-D_2)^2 + \|\omega\|^2(2(D_1+D_2)(k_{on}+k_{off}) - \right. \\ &\quad \left. 4(D_1k_{off}+D_2k_{on})) + (k_{on}+k_{off})^2\right]^{1/2}. \end{aligned} \tag{3.9}$$

Similarly, the other eigenvector of $\bar{L}(\omega)$ is

$$\begin{bmatrix} u_{12} \\ u_{22} \end{bmatrix} = \begin{bmatrix} k_{off} \\ c_2 \end{bmatrix} \tag{3.10}$$

where

$$\begin{aligned} c_2 &= \frac{1}{2}\|\omega\|^2(D_1-D_2)+\frac{1}{2}(k_{on}-k_{off})- \\ &\quad \frac{1}{2}\left[\|\omega\|^4(D_1-D_2)^2+\|\omega\|^2(2(D_1+D_2)(k_{on}+k_{off})-\right. \\ &\quad \left.4(D_1k_{off}+D_2k_{on}))+(k_{on}+k_{off})^2\right]^{1/2}. \end{aligned} \tag{3.11}$$

Let U be the 2×2 matrix with entries u_{ij}, $j=1,2$. By computing $V=U^{-T}$, we obtain the left eigenvectors of $\overline{L}(\omega)$:

$$\begin{aligned} U^{-1}(\omega)=V^T(\omega) &= \frac{1}{k_{off}(c_2-c_1)}\begin{bmatrix} c_2 & -c_1 \\ -k_{off} & k_{off}\end{bmatrix} \\ &= \frac{-1}{(D_1-D_2)(\omega_1^2+\omega_2^2)+(k_{on}-k_{off})}\begin{bmatrix} \frac{u_{22}}{k_{off}} & \frac{-u_{21}}{k_{off}} \\ -1 & 1\end{bmatrix}. \end{aligned} \tag{3.12}$$

If we write

$$U(\omega)=\begin{bmatrix}\mathbf{u}_1(\omega) & \mathbf{u}_2(\omega)\end{bmatrix} \tag{3.13}$$

and similar for $V(\omega)$, then the right and left eigenfunctions, respectively, of the frozen-coefficient operator $\overline{L}$ are, for $j=1,2$,

$$\begin{aligned} \mathbf{u}_{j,\omega}(\mathbf{x}) &= \mathbf{u}_j(\omega)\otimes e^{i(\omega\cdot\mathbf{x})}=\begin{bmatrix} u_{1j}e^{i(\omega\cdot\mathbf{x})} \\ u_{2j}e^{i(\omega\cdot\mathbf{x})}\end{bmatrix}, \\ \mathbf{v}_{j,\omega}(\mathbf{x}) &= \mathbf{v}_j(\omega)\otimes e^{i(\omega\cdot\mathbf{x})}=\begin{bmatrix} v_{1j}e^{i(\omega\cdot\mathbf{x})} \\ v_{2j}e^{i(\omega\cdot\mathbf{x})}\end{bmatrix}. \end{aligned} \tag{3.14}$$

We then seek a solution of (1.6) of the form

$$\begin{bmatrix} u(x,y,t) \\ b(x,y,t)\end{bmatrix} = \sum_{\omega\in\mathbb{Z}^2}\sum_{j=1}^{2}\mathbf{u}_{j,\omega}(\mathbf{x})\left\langle \mathbf{v}_{j,\omega}, e^{Lt}\begin{bmatrix} u(x,y,0) \\ b(x,y,0)\end{bmatrix}\right\rangle \tag{3.15}$$

We can then approximate each inner product in the above linear combination by treating it as a Riemann-Stieltjes integral, as described in chapter 2.

In this section and the next, we use the continuous inner product of functions on $[0,2\pi]^2$ and its induced L^2-norm; in implementation the formulas are adjusted accordingly to use discrete inner products.

3.2 *QR* Factorization

By computing the *QR* factorization of R_0

$$R_0 = \begin{bmatrix} a & b\end{bmatrix} = \begin{bmatrix} x_{11} & x_{12}\end{bmatrix}\begin{bmatrix} b_{11} & b_{12} \\ 0 & b_{22}\end{bmatrix} \tag{3.16}$$

we can obtain X_1, where

$$X_1 = \begin{bmatrix} x_{11} & x_{12} \end{bmatrix}. \tag{3.17}$$

Therefore we have

$$\begin{aligned} a &= x_{11}b_{11} \\ b &= x_{11}b_{12} + x_{12}b_{22} \end{aligned} \tag{3.18}$$

where

$$\begin{aligned} b_{11} &= \|a\|_2 \\ x_{11} &= a/b_{11} \\ b_{12} &= x_{11} \cdot b \\ w &= b - x_{11}b_{12} \\ b_{22} &= \|w\|_2 \\ x_{12} &= w/b_{22}. \end{aligned} \tag{3.19}$$

3.2.1 Block Arnoldi, $\omega \neq 0$

Now that our basis functions have been chosen, we will approximate each coefficient of the form

$$\left\langle \mathbf{v}_{j,\omega}, e^{Lt} \begin{bmatrix} u(x,y,t^n) \\ b(x,y,t^n) \end{bmatrix} \right\rangle \tag{3.20}$$

using a two-node Gaussian quadrature rule. This entails performing a single iteration of block Arnoldi, with initial blocks

$$\begin{aligned} R_0 &= \begin{bmatrix} v_{11}(\omega)e^{i\omega\cdot\mathbf{x}} & u(x,y,0) \\ v_{21}(\omega)e^{i\omega\cdot\mathbf{x}} & b(x,y,0) \end{bmatrix} \\ \tilde{R}_0 &= \begin{bmatrix} v_{12}(\omega)e^{i\omega\cdot\mathbf{x}} & u(x,y,0) \\ v_{22}(\omega)e^{i\omega\cdot\mathbf{x}} & b(x,y,0) \end{bmatrix}. \end{aligned} \tag{3.21}$$

Then, as the first step in block Arnoldi, we perform a QR factorization of R_0 and $\tilde{R}_0$, which yields

$$R_0 = X_1 B_0, \quad \tilde{R}_0 = \tilde{X}_1 \tilde{B}_0. \tag{3.22}$$

All inner products are defined with scaling factor $W = \langle 1,1 \rangle$ in continuous and discrete spaces:

$$W = \begin{cases} (2\pi)^2, & \textit{Continuous inner product}, \\ N^2, & \textit{Discrete inner product}. \end{cases} \tag{3.23}$$

We then have

$$
\begin{aligned}
b_{11} &= \|a\|_2 = \sqrt{W\|\mathbf{v}_1(\omega)\|^2} \\
x_{11} &= a/b_{11} = \frac{\begin{bmatrix} v_{11}(\omega)e^{i\omega\cdot\mathbf{x}} \\ v_{21}(\omega)e^{i\omega\cdot\mathbf{x}} \end{bmatrix}}{\sqrt{W\|\mathbf{v}_1(\omega)\|^2}} \\
b_{12} &= x_{11}\cdot b = \frac{v_{11}(\omega)\hat{u}+v_{21}(\omega)\hat{b}}{\sqrt{W\|\mathbf{v}_1(\omega)\|^2}} \\
w &= b - x_{11}b_{12} = \begin{bmatrix} \dfrac{f}{W\|\mathbf{v}_1(\omega)\|^2} \\ \dfrac{g}{W\|\mathbf{v}_1(\omega)\|^2} \end{bmatrix} \\
b_{22} &= \|w\|_2 = \sqrt{\frac{f^2+g^2}{(W\|\mathbf{v}_1(\omega)\|^2)^2}} \\
x_{12} &= w/b_{22} = \frac{\begin{bmatrix} f \\ g \end{bmatrix}}{\sqrt{f^2+g^2}} \\
f &= uW\|\mathbf{v}_1(\omega)\|^2 - (v_{11}^2(\omega)\hat{u}+v_{21}(\omega)v_{11}(\omega)\hat{b})e^{i\omega\cdot\mathbf{x}} \\
g &= bW\|\mathbf{v}_1(\omega)\|^2 - (v_{21}^2(\omega)\hat{b}+v_{21}(\omega)v_{11}(\omega)\hat{u})e^{i\omega\cdot\mathbf{x}} \\
\|\mathbf{v}_1(\omega)\|^2 &= v_{11}^2(\omega)+v_{21}^2(\omega) \\
\tilde{b}_{11} &= \|\tilde{a}\|_2 = \sqrt{W\|\mathbf{v}_2(\omega)\|^2} \\
\tilde{x}_{11} &= \tilde{a}/\tilde{b}_{11} = \frac{\begin{bmatrix} v_{12}(\omega)e^{i\omega\cdot\mathbf{x}} \\ v_{22}(\omega)e^{i\omega\cdot\mathbf{x}} \end{bmatrix}}{\sqrt{W\|\mathbf{v}_2(\omega)\|^2}} \\
\tilde{b}_{12} &= \tilde{x}_{11}\cdot\tilde{b} = \frac{v_{12}(\omega)\hat{u}+v_{22}(\omega)\hat{b}}{\sqrt{W\|\mathbf{v}_2(\omega)\|^2}} \\
\tilde{w} &= \tilde{b} - \tilde{x}_{11}\tilde{b}_{12} = \begin{bmatrix} \dfrac{h}{W\|\mathbf{v}_2(\omega)\|^2} \\ \dfrac{k}{W\|\mathbf{v}_2(\omega)\|^2} \end{bmatrix} \\
\tilde{b}_{22} &= \|\tilde{w}\|_2 = \sqrt{\frac{h^2+k^2}{(W\|\mathbf{v}_2(\omega)\|^2)^2}} \\
\tilde{x}_{12} &= \tilde{w}/\tilde{b}_{22} = \frac{\begin{bmatrix} h \\ k \end{bmatrix}}{\sqrt{h^2+k^2}}
\end{aligned}
$$

$$
\begin{aligned}
h &= uW\|\mathbf{v}_2(\omega)\|^2 - (v_{12}^2(\omega)\hat{u} + v_{22}(\omega)v_{12}(\omega)\hat{b})e^{i\omega\cdot\mathbf{x}} \\
k &= bW\|\mathbf{v}_2(\omega)\|^2 - (v_{22}^2(\omega)\hat{b} + v_{22}(\omega)v_{12}(\omega)\hat{u})e^{i\omega\cdot\mathbf{x}} \\
\|\mathbf{v}_2(\omega)\|^2 &= v_{12}^2(\omega) + v_{22}^2(\omega)
\end{aligned} \tag{3.24}
$$

which yields

$$
\begin{aligned}
X_1 &= \begin{bmatrix} x_{11} & x_{12} \end{bmatrix} = \begin{bmatrix} \dfrac{\begin{bmatrix} v_{11}(\omega)e^{i\omega\cdot\mathbf{x}} \\ v_{21}(\omega)e^{i\omega\cdot\mathbf{x}} \end{bmatrix}}{\sqrt{W}\|\mathbf{v}_1(\omega)\|} & \dfrac{\begin{bmatrix} f \\ g \end{bmatrix}}{\sqrt{f^2+g^2}} \end{bmatrix} \\
\tilde{X}_1 &= \begin{bmatrix} \tilde{x}_{11} & \tilde{x}_{12} \end{bmatrix} = \begin{bmatrix} \dfrac{\begin{bmatrix} v_{12}(\omega)e^{i\omega\cdot\mathbf{x}} \\ v_{22}(\omega)e^{i\omega\cdot\mathbf{x}} \end{bmatrix}}{\sqrt{W}\|\mathbf{v}_2(\omega)\|} & \dfrac{\begin{bmatrix} h \\ k \end{bmatrix}}{\sqrt{h^2+k^2}} \end{bmatrix}
\end{aligned} \tag{3.25}
$$

where u and b are shorthand for $u(x,y,t^n)$ and $b(x,y,t^n)$, respectively. Then, M_1 and $\tilde{M}_1$, which correspond to H_{11} from the block Arnoldi algorithm, can be calculated by

$$
\begin{aligned}
M_1 &= X_1^H L X_1 = \\
&\begin{bmatrix} \dfrac{\begin{bmatrix} v_{11}(\omega)e^{i\omega\cdot\mathbf{x}} \\ v_{21}(\omega)e^{i\omega\cdot\mathbf{x}} \end{bmatrix}}{\sqrt{W}\|\mathbf{v}_1(\omega)\|} & \dfrac{\begin{bmatrix} f \\ g \end{bmatrix}}{\sqrt{f^2+g^2}} \end{bmatrix}^H \times \\
&\begin{bmatrix} -k_b I_{r_n}(x,y) - k_{on} + D_1\Delta & k_{off} \\ k_{on} & -k_b I_{r_n}(x,y) - k_{off} + D_2\Delta \end{bmatrix} \times \\
&\begin{bmatrix} \dfrac{\begin{bmatrix} v_{11}(\omega)e^{i\omega\cdot\mathbf{x}} \\ v_{21}(\omega)e^{i\omega\cdot\mathbf{x}} \end{bmatrix}}{\sqrt{W}\|\mathbf{v}_1(\omega)\|} & \dfrac{\begin{bmatrix} f \\ g \end{bmatrix}}{\sqrt{f^2+g^2}} \end{bmatrix} = \\
&\begin{bmatrix} M_{11} & M_{12} \\ M_{21} & M_{22} \end{bmatrix}
\end{aligned} \tag{3.26}
$$

$$
\begin{aligned}
\tilde{M}_1 &= \tilde{X}_1^H L \tilde{X}_1 = \\
&\begin{bmatrix} \dfrac{\begin{bmatrix} v_{12}(\omega)e^{i\omega\cdot\mathbf{x}} \\ v_{22}(\omega)e^{i\omega\cdot\mathbf{x}} \end{bmatrix}}{\sqrt{W}\|\mathbf{v}_2(\omega)\|} & \dfrac{\begin{bmatrix} h \\ k \end{bmatrix}}{\sqrt{h^2+k^2}} \end{bmatrix}^H \times \\
&\begin{bmatrix} -k_b I_{r_n}(x,y) - k_{on} + D_1\Delta & k_{off} \\ k_{on} & -k_b I_{r_n}(x,y) - k_{off} + D_2\Delta \end{bmatrix} \times \\
&\begin{bmatrix} \dfrac{\begin{bmatrix} v_{12}(\omega)e^{i\omega\cdot\mathbf{x}} \\ v_{22}(\omega)e^{i\omega\cdot\mathbf{x}} \end{bmatrix}}{\sqrt{W}\|\mathbf{v}_2(\omega)\|} & \dfrac{\begin{bmatrix} h \\ k \end{bmatrix}}{\sqrt{h^2+k^2}} \end{bmatrix} = \\
&\begin{bmatrix} \tilde{M}_{11} & \tilde{M}_{12} \\ \tilde{M}_{21} & \tilde{M}_{22} \end{bmatrix}
\end{aligned} \tag{3.27}
$$

where

$$
\begin{aligned}
M_{11} &= -k_b\overline{I_{r_n}} + \frac{n_1}{\|\mathbf{v}_1(\omega)\|^2} \\
M_{12} &= \frac{n_2}{d_1} \\
M_{21} &= \frac{n_3}{d_1} \\
M_{22} &= \frac{n_4}{d_2} \\
\tilde{M}_{11} &= -k_b\overline{I_{r_n}} + \frac{n_5}{\|\mathbf{v}_2(\omega)\|^2} \\
\tilde{M}_{12} &= \frac{n_6}{d_3} \\
\tilde{M}_{21} &= \frac{n_7}{d_3} \\
\tilde{M}_{22} &= \frac{n_8}{d_4} \\
T_1 &= v_{11}^2(\omega)\hat{u} + v_{21}(\omega)v_{11}(\omega)\hat{b} \\
T_2 &= v_{21}^2(\omega)\hat{b} + v_{21}(\omega)v_{11}(\omega)\hat{u} \\
T_3 &= v_{11}^2(\omega)\overline{\hat{u}} + \overline{v_{21}(\omega)v_{11}(\omega)}\overline{\hat{b}} \\
T_4 &= v_{21}^2(\omega)\overline{\hat{b}} + \overline{v_{21}(\omega)v_{11}(\omega)}\overline{\hat{u}} \\
T_5 &= v_{12}^2(\omega)\hat{u} + v_{22}(\omega)v_{12}(\omega)\hat{b} \\
T_6 &= v_{22}^2(\omega)\hat{b} + v_{22}(\omega)v_{12}(\omega)\hat{u} \\
T_7 &= v_{12}^2(\omega)\overline{\hat{u}} + \overline{v_{22}(\omega)v_{12}(\omega)}\overline{\hat{b}} \\
T_8 &= v_{22}^2(\omega)\overline{\hat{b}} + \overline{v_{22}(\omega)v_{12}(\omega)}\overline{\hat{u}} \\
n_1 &= k_{off}\overline{v_{11}(\omega)}v_{21}(\omega) + k_{on}\overline{v_{21}(\omega)}v_{11}(\omega) - (D_1v_{11}^2(\omega) + D_2v_{21}^2(\omega))\|\omega\|^2 - k_{off}v_{21}^2(\omega) - \\
&\quad k_{on}v_{11}^2(\omega) \\
n_2 &= -k_b\|\mathbf{v}_1(\omega)\|^2(\widehat{I_{r_n}u}\overline{v_{11}(\omega)} + \widehat{I_{r_n}b}\overline{v_{21}(\omega)}) + k_b\overline{I_{r_n}}[T_1\overline{v_{11}(\omega)} + T_2\overline{v_{21}(\omega)}] - \\
&\quad \|\omega\|^2\|\mathbf{v}_1(\omega)\|^2(D_1\overline{v_{11}(\omega)}\hat{u} + D_2\overline{v_{21}(\omega)}\hat{b}) + \|\omega\|^2[(D_1\overline{v_{11}(\omega)}T_1 + D_2\overline{v_{21}(\omega)}T_2] + \\
&\quad \|\mathbf{v}_1(\omega)\|^2(\overline{v_{11}(\omega)}(k_{off}\hat{b} - k_{on}\hat{u}) + \overline{v_{21}(\omega)}(k_{on}\hat{u} - k_{off}\hat{b})) + \\
&\quad (\overline{v_{11}(\omega)} - \overline{v_{21}(\omega)})[k_{on}T_1 - k_{off}T_2] \\
n_3 &= -k_b\|\mathbf{v}_1(\omega)\|^2(\overline{\widehat{I_{r_n}u}}v_{11}(\omega) + \overline{\widehat{I_{r_n}b}}v_{21}(\omega)) + k_b\overline{I_{r_n}}[T_3v_{11}(\omega) + T_4v_{21}(\omega)] - \\
&\quad \|\omega\|^2\|\mathbf{v}_1(\omega)\|^2((D_1v_{11}(\omega)\overline{\hat{u}} + D_2v_{21}(\omega)\overline{\hat{b}}) + \|\omega\|^2[(D_1v_{11}(\omega)T_3 + D_2v_{21}(\omega)T_4] + \\
&\quad \|\mathbf{v}_1(\omega)\|^2(v_{11}(\omega)(k_{on}\overline{\hat{b}} - k_{on}\overline{\hat{u}}) + v_{21}(\omega)(k_{off}\overline{\hat{u}} - k_{off}\overline{\hat{b}})) + \\
&\quad (v_{11}(\omega)k_{on} - v_{21}(\omega)k_{off})[T_3 - T_4]
\end{aligned}
$$

$$
\begin{aligned}
d_1 &= \sqrt{\|\mathbf{v}_1(\omega)\|^2}\times \\
&\quad \sqrt{(W\|\mathbf{v}_1(\omega)\|^2(\|u^2\|+\|b^2\|)-Real(2\|\mathbf{v}_1(\omega)\|^2[\bar{\hat{u}}T_1+\bar{\hat{b}}T_2])+[(T_2)^2+(T_1)^2]} \\
d_2 &= W\|\mathbf{v}_1(\omega)\|^2(\|u^2\|+\|b^2\|)-Real(2\|\mathbf{v}_1(\omega)\|^2[\bar{\hat{u}}T_1+\bar{\hat{b}}T_2])+[(T_2)^2+(T_1)^2] \\
n_4 &= [-k_{off}(T_2)^2-k_{on}(T_1)^2]+k_{on}T_1T_4+k_{off}T_3T_2-W^2k_b\|\mathbf{v}_1(\omega)\|^4(\widehat{\overline{I_{r_n,u}}}+\widehat{\overline{I_{r_n,b}}})+ \\
&\quad k_b\|\mathbf{v}_1(\omega)\|^2[\widehat{\overline{I_{r_n}}u}T_3+\widehat{\overline{I_{r_n}}b}T_4]-W\|\mathbf{v}_1(\omega)\|^4(D_1\|\nabla u\|^2+D_2\|\nabla b\|^2)- \\
&\quad \|\mathbf{v}_1(\omega)\|^2T_1[-k_{on}\bar{\hat{b}}+D_1\|\omega\|^2\bar{\hat{u}}+k_{on}\bar{\hat{u}}]+\|\mathbf{v}_1(\omega)\|^2T_2[-k_{off}\bar{\hat{u}}+D_2\|\omega\|^2\bar{\hat{b}}+k_{off}\bar{\hat{b}}]- \\
&\quad k_b\overline{I_{r_n}}[(T_2)^2+(T_1)^2]+(k_{off}\hat{b}-k_{on}\hat{u})\|\mathbf{v}_1(\omega)\|^2T_4- \\
&\quad \|\omega\|^2[D_1(T_3)^2+D_2(T_4)^2]+(k_{on}\hat{u}-k_{off}\hat{b})\|\mathbf{v}_1(\omega)\|^2T_3+ \\
&\quad W\|\mathbf{v}_1(\omega)\|^4[-k_{on}\|u\|^2+Wk_{off}\overline{ub}+Wk_{on}\overline{bu}-k_{off}\|b\|^2]- \\
&\quad \|\omega\|^2\|\mathbf{v}_1(\omega)\|^2[D_1\hat{u}T_3+D_2\hat{b}T_4]+k_b\|\mathbf{v}_1(\omega)\|^2[\widehat{\overline{I_{r_n}}b}T_2+\widehat{\overline{I_{r_n}}u}T_1] \\
n_5 &= k_{off}\overline{v_{12}(\omega)}v_{22}(\omega)+k_{on}\overline{v_{22}(\omega)}v_{12}(\omega)-(D_1v_{12}^2(\omega)+D_2v_{22}^2(\omega))\|\omega\|^2-k_{off}v_{22}^2(\omega)- \\
&\quad k_{on}v_{12}^2(\omega) \\
n_6 &= -k_b\|\mathbf{v}_2(\omega)\|^2(\widehat{I_{r_n}u}\overline{v_{12}(\omega)}+\widehat{I_{r_n}b}\overline{v_{22}(\omega)})+k_b\overline{I_{r_n}}[T_5\overline{v_{12}(\omega)}+T_6\overline{v_{22}(\omega)}]- \\
&\quad \|\omega\|^2\|\mathbf{v}_2(\omega)\|^2(D_1\overline{v_{12}(\omega)}\hat{u}+D_2\overline{v_{22}(\omega)}\hat{b})+\|\omega\|^2[(D_1\overline{v_{12}(\omega)}T_5+D_2\overline{v_{22}(\omega)}T_6]+ \\
&\quad \|\mathbf{v}_2(\omega)\|^2(\overline{v_{12}(\omega)}(k_{off}\hat{b}-k_{on}\hat{u})+\overline{v_{22}(\omega)}(k_{on}\hat{u}-k_{off}\hat{b}))+ \\
&\quad (\overline{v_{12}(\omega)}-\overline{v_{22}(\omega)})[k_{on}T_5-k_{off}T_6] \\
n_7 &= -k_b\|\mathbf{v}_2(\omega)\|^2\widehat{\overline{I_{r_n}}u}v_{12}(\omega)+\widehat{\overline{I_{r_n}}b}v_{22}(\omega)+k_b\overline{I_{r_n}}[T_7v_{12}(\omega)+T_8v_{22}(\omega)]- \\
&\quad \|\omega\|^2\|\mathbf{v}_2(\omega)\|^2((D_1v_{12}(\omega)\bar{\hat{u}}+D_2v_{22}(\omega)\bar{\hat{b}})+\|\omega\|^2[(D_1v_{12}(\omega)T_7+D_2v_{22}(\omega)T_8]+ \\
&\quad \|\mathbf{v}_2(\omega)\|^2(v_{12}(\omega)(k_{on}\bar{\hat{b}}-k_{on}\bar{\hat{u}})+v_{22}(\omega)(k_{off}\bar{\hat{u}}-k_{off}\bar{\hat{b}}))+ \\
&\quad (v_{12}(\omega)k_{on}-v_{22}(\omega)k_{off})[T_7-T_8] \\
d_3 &= \sqrt{\|\mathbf{v}_2(\omega)\|^2}\times \\
&\quad \sqrt{(W\|\mathbf{v}_2(\omega)\|^2(\|u^2\|+\|b^2\|)-Real(2\|\mathbf{v}_2(\omega)\|^2[\bar{\hat{u}}T_5+\bar{\hat{b}}T_6])+[(T_6)^2+(T_5)^2]} \\
d_4 &= W\|\mathbf{v}_2(\omega)\|^2(\|u^2\|+\|b^2\|)-Real(2\|\mathbf{v}_2(\omega)\|^2[\bar{\hat{u}}T_5+\bar{\hat{b}}T_6])+[(T_6)^2+(T_5)^2] \\
n_8 &= [-k_{off}(T_6)^2-k_{on}(T_5)^2]+k_{on}T_5T_8+k_{off}T_7T_6-W^2k_b\|\mathbf{v}_2(\omega)\|^4(\widehat{\overline{I_{r_n,u}}}+\widehat{\overline{I_{r_n,b}}})+ \\
&\quad k_b\|\mathbf{v}_2(\omega)\|^2[\widehat{\overline{I_{r_n}}u}T_7+\widehat{\overline{I_{r_n}}b}T_8]-W\|\mathbf{v}_2(\omega)\|^4(D_1\|\nabla u\|^2+D_2\|\nabla b\|^2)- \\
&\quad \|\mathbf{v}_2(\omega)\|^2T_5[-k_{on}\bar{\hat{b}}+D_1\|\omega\|^2\bar{\hat{u}}+k_{on}\bar{\hat{u}}]+\|\mathbf{v}_2(\omega)\|^2T_6[-k_{off}\bar{\hat{u}}+D_2\|\omega\|^2\bar{\hat{b}}+k_{off}\bar{\hat{b}}]- \\
&\quad k_b\overline{I_{r_n}}[(T_6)^2+(T_5)^2]+(k_{off}\hat{b}-k_{on}\hat{u})\|\mathbf{v}_2(\omega)\|^2T_8- \\
&\quad \|\omega\|^2[D_1(T_7)^2+D_2(T_8)^2]+(k_{on}\hat{u}-k_{off}\hat{b})\|\mathbf{v}_2(\omega)\|^2T_7+ \\
&\quad W\|\mathbf{v}_2(\omega)\|^4[-k_{on}\|u\|^2+Wk_{off}\overline{ub}+Wk_{on}\overline{bu}-k_{off}\|b\|^2]- \\
&\quad \|\omega\|^2(\|\mathbf{v}_2(\omega)\|^2[D_1\hat{u}T_7+D_2\hat{b}T_8]+k_b\|\mathbf{v}_2(\omega)\|^2[\widehat{\overline{I_{r_n}}b}T_6+\widehat{\overline{I_{r_n}}u}T_5]. \qquad (3.28)
\end{aligned}
$$

Here, we have used the inner products

$$\begin{aligned}
\left\langle \overline{b}, I_{r_n} \right\rangle &= W\overline{I_{r_n} b} \\
\left\langle \overline{u}, I_{r_n} \right\rangle &= W\overline{I_{r_n} u} \\
\left\langle \overline{b}, I_{r_n} b \right\rangle &= W\overline{I_{r_n,b}} \\
\left\langle \overline{u}, I_{r_n} u \right\rangle &= W\overline{I_{r_n,u}} \\
\left\langle \overline{u}, I_{r_n} b \right\rangle &= W\overline{I_{r_n,ub}} \\
\left\langle \overline{b}, I_{r_n} u \right\rangle &= W\overline{I_{r_n,bu}} \\
\left\langle \overline{b}, e^{i\omega\cdot\mathbf{x}} \right\rangle &= \overline{\hat{b}} \\
\left\langle \overline{u}, e^{i\omega\cdot\mathbf{x}} \right\rangle &= \overline{\hat{u}} \\
\left\langle e^{i\omega\cdot\mathbf{x}}, I_{r_n} b \right\rangle &= \widehat{I_{r_n} b} \\
\left\langle e^{i\omega\cdot\mathbf{x}}, I_{r_n} u \right\rangle &= \widehat{I_{r_n} u} \\
\left\langle \overline{u}, I_{r_n} e^{i\omega\cdot\mathbf{x}} \right\rangle &= \overline{\widehat{I_{r_n} u}} \\
\left\langle \overline{b}, I_{r_n} e^{i\omega\cdot\mathbf{x}} \right\rangle &= \overline{\widehat{I_{r_n} b}} \\
\left\langle e^{i\omega\cdot\mathbf{x}}, I_{r_n} \right\rangle &= \widehat{I_{r_n}} \\
\left\langle I_{r_n}, e^{i\omega\cdot\mathbf{x}} \right\rangle &= \overline{\widehat{I_{r_n}}} \\
\left\langle e^{i\omega\cdot\mathbf{x}}, e^{i\omega\cdot\mathbf{x}} \right\rangle &= W \\
\left\langle \overline{b}, \Delta b \right\rangle &= -\|\nabla b\|^2 \\
\left\langle \overline{u}, \Delta u \right\rangle &= -\|\nabla u\|^2 \\
\left\langle \overline{\Delta u}, e^{i\omega\cdot\mathbf{x}} \right\rangle &= -\overline{\hat{u}}\|\omega\|^2 \\
\left\langle \overline{\Delta b}, e^{i\omega\cdot\mathbf{x}} \right\rangle &= -\overline{\hat{b}}\|\omega\|^2 \\
\left\langle \overline{u}, \overline{u} \right\rangle &= \|\overline{u}\|^2 \\
\left\langle \overline{b}, \overline{b} \right\rangle &= \|\overline{b}\|^2 \\
\left\langle \overline{u}, 1 \right\rangle &= \langle 1, \overline{u} \rangle = W\overline{u} \\
\left\langle \overline{b}, 1 \right\rangle &= \left\langle 1, \overline{b} \right\rangle = W\overline{b} \\
\left\langle u, \overline{b} \right\rangle &= \langle \overline{u}, b \rangle = W\overline{bu} \\
\left\langle \overline{u}, u \right\rangle &= \langle u, \overline{u} \rangle = \|u\|^2 \\
\left\langle \overline{b}, b \right\rangle &= \left\langle b, \overline{b} \right\rangle = \|b\|^2.
\end{aligned} \tag{3.29}$$

After computing the eigenvalues $\lambda_{1,\omega}, \lambda_{2,\omega}$ of M_1, the coefficient of $\mathbf{u}_{1,\omega}$ in the solution at time t can be approximated by

$$[B_0^H e^{M_1 t} B_0]_{12} = \left\langle \mathbf{v}_1(\omega) \otimes e^{i\omega\cdot\mathbf{x}}, \rho_{1,\omega}(L) \begin{bmatrix} u(x,y,0) \\ b(x,y,0) \end{bmatrix} \right\rangle \tag{3.30}$$

where $\rho_{1,\omega}$ is a polynomial of degree 1 which interpolates $e^{\lambda t}$ at $\lambda_{1,\omega}$ and $\lambda_{2,\omega}$ and is given by

$$\rho_{1,\omega}(L) = \frac{e^{\lambda_{1,\omega}t}}{\lambda_{1,\omega}-\lambda_{2,\omega}}[L-\lambda_{2,\omega}I] + \frac{e^{\lambda_{2,\omega}t}}{\lambda_{2,\omega}-\lambda_{1,\omega}}[L-\lambda_{1,\omega}I]. \tag{3.31}$$

The coefficient of $\mathbf{u}_{2,\omega}$ can be approximated in a similar manner, using the eigenvalues $\tilde{\lambda}_{1,\omega}, \tilde{\lambda}_{2,\omega}$ of $\tilde{M}_1$.

The value of t can be chosen sufficiently small to ensure desired accuracy, and then this process can be repeated in subsequent time steps. By using the integrand $g(\lambda) = \lambda e^{\lambda t}$ in place of $f(\lambda) = e^{\lambda t}$, one can easily use the above M_1 and $\tilde{M}_1$ to compute an approximate time derivative, which can then be used to obtain a residual $\mathbf{v}_t - L\mathbf{v}$. This residual can serve as an estimate of local truncation error, for the purpose of adaptive time-stepping.

3.2.2 Block Arnoldi, $\omega_1 = \omega_2 = 0$

We now use block Arnoldi for the case $\omega_1 = \omega_2 = 0$, for which we use the initial block

$$R_0 = \begin{bmatrix} a & b \end{bmatrix} = \begin{bmatrix} \dfrac{-u_{22}}{k_{off}(k_{on}-k_{off})} & u(x,y,0) \\ \dfrac{1}{k_{on}-k_{off}} & b(x,y,0) \end{bmatrix} \tag{3.32}$$

where variables obtained by substituting $u_{22} = -k_{off}$ are

$$\begin{aligned}
b_{11} &= \|a\|_2 = \sqrt{\frac{2W}{(k_{on}-k_{off})^2}} \\
x_{11} &= a/b_{11} = \frac{\begin{bmatrix} k_{off} \\ k_{off} \end{bmatrix}}{\sqrt{W(k_{off}^2+k_{off}^2)}} = \frac{\begin{bmatrix} 1 \\ 1 \end{bmatrix}}{\sqrt{2W}} \\
b_{12} &= x_{11}\cdot b = \frac{\sqrt{W}(u_0+b_0)}{\sqrt{2}} \\
w &= b - x_{11}b_{12} = \begin{bmatrix} u - \dfrac{u_0+b_0}{2} \\ b - \dfrac{u_0+b_0}{2} \end{bmatrix} \\
b_{22} &= \|w\|_2 = \sqrt{\|u\|^2+\|b\|^2-\frac{W(b_+u_0)^2}{2}} \\
x_{12} &= w/b_{22} = \begin{bmatrix} \dfrac{u-\dfrac{u_0+b_0}{2}}{\sqrt{\|u\|^2+\|b\|^2-\dfrac{W(b_+u_0)^2}{2}}} \\ \dfrac{b-\dfrac{u_0+b_0}{2}}{\sqrt{\|u\|^2+\|b\|^2-\dfrac{W(b_+u_0)^2}{2}}} \end{bmatrix}.
\end{aligned} \tag{3.33}$$

Then, after computing the QR factorization $R_0 = X_1 B_0$, we have

$$X_1 = \begin{bmatrix} \frac{1}{\sqrt{2W}} & \frac{u - \frac{u_0+b_0}{2}}{\sqrt{\|u\|^2+\|b\|^2-\frac{W(b_+u_0)^2}{2}}} \\ \frac{1}{\sqrt{2W}} & \frac{b - \frac{u_0+b_0}{2}}{\sqrt{\|u\|^2+\|b\|^2-\frac{W(b_+u_0)^2}{2}}} \end{bmatrix}. \tag{3.34}$$

Then, M_1 is given by

$$M_1 = X_1^H L X_1 =$$

$$\begin{bmatrix} \frac{1}{\sqrt{2W}} & \frac{u - \frac{u_0+b_0}{2}}{\sqrt{\|u\|^2+\|b\|^2-\frac{W(b_+u_0)^2}{2}}} \\ \frac{1}{\sqrt{2W}} & \frac{b - \frac{u_0+b_0}{2}}{\sqrt{\|u\|^2+\|b\|^2-\frac{W(b_+u_0)^2}{2}}} \end{bmatrix}^H \times$$

$$\begin{bmatrix} -k_b I_{r_n}(x,y) - k_{on} + D_1\Delta & k_{off} \\ k_{on} & -k_b I_{r_n}(x,y) - k_{off} + D_2\Delta \end{bmatrix} \times$$

$$\begin{bmatrix} \frac{1}{\sqrt{2W}} & \frac{u - \frac{u_0+b_0}{2}}{\sqrt{\|u\|^2+\|b\|^2-\frac{W(b_+u_0)^2}{2}}} \\ \frac{1}{\sqrt{2W}} & \frac{b - \frac{u_0+b_0}{2}}{\sqrt{\|u\|^2+\|b\|^2-\frac{W(b_+u_0)^2}{2}}} \end{bmatrix} =$$

$$\begin{bmatrix} M_{11} & M_{12} \\ M_{21} & M_{22} \end{bmatrix} \tag{3.35}$$

where

$$\begin{aligned} M_{11} &= -\overline{I_{r_n}} k_b \\ M_{12} &= \frac{-\sqrt{W} k_b (\overline{uI_{r_n}} + \overline{bI_{r_n}} + \overline{I_{r_n}}(u_0+b_0))}{\sqrt{2d_{15}}} \\ M_{21} &= \frac{\sqrt{W}((k_{off}-k_{on})(u_0-b_0) - k_b(\overline{uI_{r_n}} + \overline{bI_{r_n}} + \overline{I_{r_n}}(u_0+b_0)))}{\sqrt{2d_{15}}} \\ M_{22} &= \frac{n_{14}}{d_{15}} \end{aligned}$$

$$
\begin{aligned}
n_{14} &= -k_b W\left(\overline{I_{r_n,u}}+\overline{I_{r_n,b}}-(u_0+b_0)\overline{I_{r_n}u}-(u_0+b_0)\overline{I_{r_n}b}+\overline{I_{r_n}}\left(\frac{u_0^2}{2}+\frac{b_0^2}{2}+u_0b_0\right)\right)- \\
&\quad k_{on}\left(\|u\|^2-Wu_0(u_0+b_0)+\frac{W(b_0+u_0)^2}{4}\right)-k_{off}\left(\|b\|^2-Wb_0(u_0+b_0)+\frac{W(b_0+u_0)^2}{4}\right)+ \\
&\quad W(k_{on}+k_{off})\left((ub)_0-\frac{(b_0^2+u_0^2)}{4}-\frac{b_0u_0}{2}\right)-(D_1\|\nabla u\|^2+D_2\|\nabla b\|^2) \\
d_{15} &= \|u\|^2+\|b\|^2-\frac{W(b_+u_0)^2}{2}.
\end{aligned}
\tag{3.36}
$$

We then proceed as in the previous discussion to obtain the coefficient of $\mathbf{u}_{1,(0,0)}$ in the solution.

Similarly, for the coefficient of $\mathbf{u}_{2,(0,0)}$, our initial block is

$$
\tilde{R}_0 = \begin{bmatrix} \frac{u_{21}}{k_{off}(k_{on}-k_{off})} & u(x,y,0) \\ \frac{-1}{k_{on}-k_{off}} & b(x,y,0) \end{bmatrix}. \tag{3.37}
$$

Computing the *QR* factorization, variables by plugging $u_{21}=k_{on}$ are

$$
\begin{aligned}
\tilde{b}_{11} &= \|\tilde{a}\|_2=\sqrt{\frac{W(k_{on}^2+k_{off}^2)}{k_{off}^2(k_{on}-k_{off})^2}} \\
\tilde{x}_{11} &= \tilde{a}/\tilde{b}_{11}=\frac{\begin{bmatrix} k_{on} \\ -k_{off}\end{bmatrix}}{\sqrt{W(k_{on}^2+k_{off}^2)}} \\
\tilde{b}_{12} &= \tilde{x}_{11}\cdot\tilde{b}=\frac{\sqrt{W}(k_{on}u_0-k_{off}b_0)}{\sqrt{k_{on}^2+k_{off}^2}} \\
\tilde{w} &= \tilde{b}-\tilde{x}_{11}\tilde{b}_{12}=\begin{bmatrix} \frac{u(k_{on}^2+k_{off}^2)-k_{on}^2u_0+k_{on}k_{off}b_0}{k_{on}^2+k_{off}^2} \\ \frac{b(k_{on}^2+k_{off}^2)-k_{off}^2b_0+k_{on}k_{off}u_0}{k_{on}^2+k_{off}^2}\end{bmatrix} \\
\tilde{b}_{22} &= \|\tilde{w}\|_2=\sqrt{\|u\|^2+\|b\|^2-\frac{Wu_0^2k_{on}^2}{k_{on}^2+k_{off}^2}-\frac{Wb_0^2k_{off}^2}{k_{on}^2+k_{off}^2}+\frac{2Wu_0b_0k_{on}k_{off}}{k_{on}^2+k_{off}^2}} \\
\tilde{x}_{12} &= \tilde{w}/\tilde{b}_{22}=\begin{bmatrix} \frac{u(k_{on}^2+k_{off}^2)-k_{on}^2u_0+k_{on}k_{off}b_0}{\sqrt{d_{21}}} \\ \frac{b(k_{on}^2+k_{off}^2)-k_{off}^2b_0+k_{on}k_{off}u_0}{\sqrt{d_{21}}}\end{bmatrix} \\
d_{21} &= \|u\|^2+\|b\|^2-\frac{Wu_0^2k_{on}^2}{k_{on}^2+k_{off}^2}-\frac{Wb_0^2k_{off}^2}{k_{on}^2+k_{off}^2}+\frac{2Wu_0b_0k_{on}k_{off}}{k_{on}^2+k_{off}^2}
\end{aligned}
\tag{3.38}
$$

where $\tilde{R}_0 = \tilde{X}_1 \tilde{B}_0$ yields

$$\begin{aligned}
\tilde{X}_1 &= \begin{bmatrix} \frac{k_{on}}{\sqrt{W(k_{on}^2+k_{off}^2)}} & \frac{u(k_{on}^2+k_{off}^2)-k_{on}^2u_0+k_{on}k_{off}b_0}{\sqrt{d_{21}}} \\ \frac{-k_{off}}{\sqrt{W(k_{on}^2+k_{off}^2)}} & \frac{b(k_{on}^2+k_{off}^2)-k_{off}^2b_0+k_{on}k_{off}u_0}{\sqrt{d_{21}}} \end{bmatrix} \\
d_{21} &= \|u\|^2+\|b\|^2-\frac{Wu_0^2k_{on}^2}{k_{on}^2+k_{off}^2}-\frac{Wb_0^2k_{off}^2}{k_{on}^2+k_{off}^2}+\frac{2Wu_0b_0k_{on}k_{off}}{k_{on}^2+k_{off}^2}.
\end{aligned} \tag{3.39}$$

Then, we compute

$$\begin{aligned}
\tilde{M}_1 &= \tilde{X}_1^H L \tilde{X}_1 = \\
&\begin{bmatrix} \frac{k_{on}}{\sqrt{W(k_{on}^2+k_{off}^2)}} & \frac{u(k_{on}^2+k_{off}^2)-k_{on}^2u_0+k_{on}k_{off}b_0}{\sqrt{d_{21}}} \\ \frac{-k_{off}}{\sqrt{W(k_{on}^2+k_{off}^2)}} & \frac{b(k_{on}^2+k_{off}^2)-k_{off}^2b_0+k_{on}k_{off}u_0}{\sqrt{d_{21}}} \end{bmatrix}^H \times \\
&\begin{bmatrix} -k_bI_{r_n}(x,y)-k_{on}+D_1\Delta & k_{off} \\ k_{on} & -k_bI_{r_n}(x,y)-k_{off}+D_2\Delta \end{bmatrix} \times \\
&\begin{bmatrix} \frac{k_{on}}{\sqrt{W(k_{on}^2+k_{off}^2)}} & \frac{u(k_{on}^2+k_{off}^2)-k_{on}^2u_0+k_{on}k_{off}b_0}{\sqrt{d_{21}}} \\ \frac{-k_{off}}{\sqrt{W(k_{on}^2+k_{off}^2)}} & \frac{b(k_{on}^2+k_{off}^2)-k_{off}^2b_0+k_{on}k_{off}u_0}{\sqrt{d_{21}}} \end{bmatrix} = \\
&\begin{bmatrix} \tilde{M}_{11} & \tilde{M}_{12} \\ \tilde{M}_{21} & \tilde{M}_{22} \end{bmatrix}
\end{aligned} \tag{3.40}$$

which yields

$$\begin{aligned}
\tilde{M}_{11} &= -\overline{I_{r_n}}k_b-k_{on}-k_{off} \\
\tilde{M}_{12} &= \frac{k_bW(-k_{on}\overline{I_{r_n}u}+k_{off}\overline{I_{r_n}b}+\overline{I_{r_n}}(u_0k_{on}-b_0k_{off}))}{\sqrt{W(k_{on}^2+k_{off}^2)d_{16}}} \\
\tilde{M}_{21} &= \frac{n_{18}}{\sqrt{W(k_{on}^2+k_{off}^2)d_{16}}} \\
\tilde{M}_{22} &= \frac{n_{19}}{d_{16}}
\end{aligned}$$

$$
\begin{aligned}
n_{18} &= k_b W(-k_{on}\overline{I_{r_n}u}+k_{off}\overline{I_{r_n}b}+\overline{I_{r_n}}(u_0k_{on}-b_0k_{off}))+ \\
&\quad W\left(u_0\left(-k_{off}^2+\frac{k_{on}k_{off}^3}{k_{on}^2+k_{off}^2}\right)+b_0\left(k_{on}^2-\frac{k_{on}k_{off}^3}{k_{on}^2+k_{off}^2}\right)\right) \\
d_{16} &= \|u\|^2+\|b\|^2-\frac{Wu_0^2k_{on}^2}{k_{on}^2+k_{off}^2}-\frac{Wb_0^2k_{off}^2}{k_{on}^2+k_{off}^2}+\frac{2Wu_0b_0k_{on}k_{off}}{k_{on}^2+k_{off}^2} \\
n_{19} &= -k_bW\left[\overline{I_{r_n,u}}+\overline{I_{r_n,b}}+\overline{I_{r_n}u}\left(\frac{2u_0k_{on}^2}{k_{on}^2+k_{off}^2}-\frac{2b_0k_{off}k_{on}}{k_{on}^2+k_{off}^2}\right)+\overline{I_{r_n}b}\left(\frac{-2u_0k_{on}k_{off}}{k_{on}^2+k_{off}^2}+\frac{2b_0k_{off}^2}{k_{on}^2+k_{off}^2}\right)+\right. \\
&\quad \left.\overline{I_{r_n}}\left(-\frac{u_0^2k_{on}^2}{k_{on}^2+k_{off}^2}-\frac{b_0^2k_{off}^2}{k_{on}^2+k_{off}^2}+u_0b_0\frac{2k_{on}k_{off}}{k_{on}^2+k_{off}^2}\right)\right]+ \\
&\quad W((ub)_0(k_{on}+k_{off})+u_0^2k_{on}+b_0^2k_{off}-b_0u_0(k_{on}+k_{off}))- \\
&\quad (k_{on}\|u\|^2+k_{off}\|b\|^2)-(D_1\|\nabla u\|^2+D_2\|\nabla b\|^2). \qquad (3.41)
\end{aligned}
$$

Here, we have used the inner products

$$
\begin{aligned}
\langle u, I_{r_n}u\rangle &= W\overline{I_{r_n,u}} \\
\langle b, I_{r_n}b\rangle &= W\overline{I_{r_n,b}} \\
\langle u_0, I_{r_n}u\rangle &= Wu_0\overline{I_{r_n}u} \\
\langle b_0, I_{r_n}u\rangle &= Wb_0\overline{I_{r_n}u} \\
\langle u_0, I_{r_n}u_0\rangle &= Wu_0^2\overline{I_{r_n}} \\
\langle u_0, I_{r_n}b_0\rangle &= \langle b_0, I_{r_n}u_0\rangle = Wu_0b_0\overline{I_{r_n}} \\
\langle u, 1\rangle &= \langle 1, u\rangle = Wu_0 \\
\langle u, b\rangle &= \langle b, u\rangle = W(bu)_0 = W(ub)_0 \\
\langle u, u_0\rangle &= Wu_0^2 \\
\langle u, b_0\rangle &= Wb_0u_0 \\
\langle u_0, b_0\rangle &= Wb_0u_0 \\
\langle u_0, u_0\rangle &= Wu_0^2 \\
\langle u, u\rangle &= \|u\|^2 \\
\langle u, \Delta u\rangle &= -\|\nabla u\|^2. \qquad (3.42)
\end{aligned}
$$

3.3 Approximate Analytical Solution

In this section, we specialize to initial data (1.7), (1.8) from pre-bleach steady states to obtain an approximate analytical solution for sufficiently small t. The terms in the entries of v_{11} and v_{12} that are of lower order in $\|\omega\|$ are neglected.

3.3.1 The $\omega_1 = \omega_2 = 0$ Case

When $\omega_1 = \omega_2 = 0$, our initial block for the component in the direction of $\mathbf{u}_{1,(0,0)}$ is

$$R_0 = \begin{bmatrix} -\frac{u_{22}}{k_{off}(k_{on}-k_{off})} & \frac{k_{off}c_i}{k_{off}+k_{on}} \\ \frac{1}{k_{on}-k_{off}} & \frac{k_{on}c_i}{k_{off}+k_{on}} \end{bmatrix} \tag{3.43}$$

where the QR factorization variables are

$$\begin{aligned}
b_{11} &= \|a\|_2 = \sqrt{W\frac{\frac{u_{22}^2}{k_{off}^2}+1}{(k_{on}-k_{off})^2}} \\
x_{11} &= a/b_{11} = \frac{\begin{bmatrix} -\frac{u_{22}}{k_{off}(k_{on}-k_{off})} \\ \frac{1}{k_{on}-k_{off}} \end{bmatrix}}{\sqrt{W\frac{\frac{u_{22}^2}{k_{off}^2}+1}{(k_{on}-k_{off})^2}}} \\
b_{12} &= x_{11}\cdot b = \frac{\sqrt{W}k_{off}c_i(-u_{22}+k_{on})}{k_{on}+k_{off}\sqrt{u_{22}^2+k_{off}^2}} \\
w &= b - x_{11}b_{12} = \frac{c_i}{k_{on}+k_{off}}\begin{bmatrix} k_{off}-\frac{k_{off}u_{22}^2}{k_{off}^2+u_{22}^2}+\frac{k_{off}k_{on}u_{22}}{k_{off}^2+u_{22}^2} \\ k_{on}+\frac{k_{off}^2u_{22}}{k_{off}^2+u_{22}^2}-\frac{k_{off}^2k_{on}}{k_{off}^2+u_{22}^2} \end{bmatrix} \\
b_{22} &= \|w\|_2 = \sqrt{W\left(\frac{c_i}{k_{on}+k_{off}}\right)^2}\times \\
&\quad \sqrt{\left(k_{off}-\frac{k_{off}u_{22}^2}{k_{off}^2+u_{22}^2}+\frac{k_{off}k_{on}u_{22}}{k_{off}^2+u_{22}^2}\right)^2+\left(k_{on}+\frac{k_{off}^2u_{22}}{k_{off}^2+u_{22}^2}-\frac{k_{off}^2k_{on}}{k_{off}^2+u_{22}^2}\right)^2} \\
x_{12} &= w/b_{22} = \frac{\begin{bmatrix} k_{off}-\frac{k_{off}u_{22}^2}{k_{off}^2+u_{22}^2}+\frac{k_{off}k_{on}u_{22}}{k_{off}^2+u_{22}^2} \\ k_{on}+\frac{k_{off}^2u_{22}}{k_{off}^2+u_{22}^2}-\frac{k_{off}^2k_{on}}{k_{off}^2+u_{22}^2} \end{bmatrix}}{\sqrt{W((k_{off}-k_{on})^2+(k_{on}-k_{off})^2)}}.
\end{aligned} \tag{3.44}$$

Substituting $u_{22} = -k_{off}$ in x_{11} and x_{12}, X_1 becomes

$$X_1 = \begin{bmatrix} \frac{1}{\sqrt{2W}} & \frac{-1}{\sqrt{2W}} \\ \frac{1}{\sqrt{2W}} & \frac{1}{\sqrt{2W}} \end{bmatrix} \tag{3.45}$$

which yields

$$
\begin{aligned}
M_1 &= X_1^H L X_1 = \\
&\left[\begin{array}{cc} \frac{1}{\sqrt{2W}} & \frac{-1}{\sqrt{2W}} \\ \frac{1}{\sqrt{2W}} & \frac{1}{\sqrt{2W}} \end{array} \right]^H \times \\
&\left[\begin{array}{cc} -k_b I_{r_n}(x,y) - k_{on} & k_{off} \\ k_{on} & -k_b I_{r_n}(x,y) - k_{off} \end{array} \right] \times \\
&\left[\begin{array}{cc} \frac{1}{\sqrt{2W}} & \frac{-1}{\sqrt{2W}} \\ \frac{1}{\sqrt{2W}} & \frac{1}{\sqrt{2W}} \end{array} \right] = \\
&\left[\begin{array}{cc} -k_b \overline{I_{r_n}} & 0 \\ k_{on} - k_{off} & -k_b \overline{I_{r_n}} - (k_{on} + k_{off}) \end{array} \right].
\end{aligned} \tag{3.46}
$$

The eigenvalues of M_1 are

$$
\begin{aligned}
\lambda_{1,(0,0)} &= -k_b \overline{I_{r_n}} \\
\lambda_{2,(0,0)} &= -k_b \overline{I_{r_n}} - (k_{on} + k_{off}).
\end{aligned} \tag{3.47}
$$

For the component of the solution in the direction of $\mathbf{u}_{2,(0,0)}$, we use the initial block

$$
\tilde{R}_0 = \left[\begin{array}{cc} \frac{u_{21}}{k_{off}(k_{on} - k_{off})} & \frac{k_{off} c_i}{k_{off} + k_{on}} \\ \frac{-1}{k_{on} - k_{off}} & \frac{k_{on} c_i}{k_{off} + k_{on}} \end{array} \right] \tag{3.48}
$$

where the QR factorization variables obtained by substituting $u_{21} = k_{on}$ are

$$
\begin{aligned}
\tilde{b}_{11} &= \|\tilde{a}\|_2 = \sqrt{W \frac{\frac{u_{21}^2}{k_{off}^2} + 1}{(k_{on} - k_{off})^2}} \\
\tilde{x}_{11} &= \tilde{a}/\tilde{b}_{11} = \frac{\left[\begin{array}{c} \frac{u_{21}}{k_{off}(k_{on} - k_{off})} \\ \frac{-1}{k_{on} - k_{off}} \end{array} \right]}{\sqrt{W \frac{\frac{u_{21}^2}{k_{off}^2} + 1}{(k_{on} - k_{off})^2}}} = \frac{\left[\begin{array}{c} k_{on} \\ -k_{off} \end{array} \right]}{\sqrt{W(k_{on}^2 + k_{off}^2)}} \\
\tilde{b}_{12} &= \tilde{x}_{11} \cdot \tilde{b} = \frac{\sqrt{W} k_{off} c_i (u_{21} - k_{on})}{k_{on} + k_{off} \sqrt{u_{22}^2 + k_{off}^2}} = 0
\end{aligned}
$$

$$
\begin{aligned}
\tilde{w} &= \tilde{b} - \tilde{x}_{11}\tilde{b}_{12} = \tilde{b} = \begin{bmatrix} \frac{k_{off}c_i}{k_{off}+k_{on}} \\ \frac{k_{on}c_i}{k_{off}+k_{on}} \end{bmatrix} \\
\tilde{b}_{22} &= \|\tilde{w}\|_2 = \sqrt{W\left(\frac{c_i}{k_{on}+k_{off}}\right)^2 (k_{on}^2+k_{off}^2)} \\
\tilde{x}_{12} &= \tilde{w}/\tilde{b}_{22} = \frac{\begin{bmatrix} k_{off} \\ k_{on} \end{bmatrix}}{\sqrt{W(k_{on}^2+k_{off}^2)}} \\
\tilde{X}_1 &= \begin{bmatrix} \tilde{x}_{11} & \tilde{x}_{12} \end{bmatrix} = \begin{bmatrix} \frac{k_{on}}{\sqrt{W(k_{on}^2+k_{off}^2)}} & \frac{k_{off}}{\sqrt{W(k_{on}^2+k_{off}^2)}} \\ \frac{-k_{off}}{\sqrt{W(k_{on}^2+k_{off}^2)}} & \frac{k_{on}}{\sqrt{W(k_{on}^2+k_{off}^2)}} \end{bmatrix}. \qquad (3.49)
\end{aligned}
$$

Then

$$
\begin{aligned}
\tilde{M}_1 &= \tilde{X}_1^H L \tilde{X}_1 = \\
&\begin{bmatrix} \frac{k_{on}}{\sqrt{W(k_{on}^2+k_{off}^2)}} & \frac{k_{off}}{\sqrt{W(k_{on}^2+k_{off}^2)}} \\ \frac{-k_{off}}{\sqrt{W(k_{on}^2+k_{off}^2)}} & \frac{k_{on}}{\sqrt{W(k_{on}^2+k_{off}^2)}} \end{bmatrix}^H \times \\
&\begin{bmatrix} -k_b I_{r_n}(x,y) - k_{on} & k_{off} \\ k_{on} & -k_b I_{r_n}(x,y) - k_{off} \end{bmatrix} \times \\
&\begin{bmatrix} \frac{k_{on}}{\sqrt{W(k_{on}^2+k_{off}^2)}} & \frac{k_{off}}{\sqrt{W(k_{on}^2+k_{off}^2)}} \\ \frac{-k_{off}}{\sqrt{W(k_{on}^2+k_{off}^2)}} & \frac{k_{on}}{\sqrt{W(k_{on}^2+k_{off}^2)}} \end{bmatrix} = \\
&\begin{bmatrix} -k_b\overline{I_{r_n}} - (k_{on}+k_{off}) & 0 \\ k_{on}-k_{off} & -k_b\overline{I_{r_n}} \end{bmatrix}. \qquad (3.50)
\end{aligned}
$$

It follows that the eigenvalues of $\tilde{M}_1$ are

$$
\begin{aligned}
\tilde{\lambda}_{1,(0,0)} &= -k_b\overline{I_{r_n}} - (k_{on}+k_{off}) \\
\tilde{\lambda}_{2,(0,0)} &= -k_b\overline{I_{r_n}}. \qquad (3.51)
\end{aligned}
$$

3.3.2 The $\omega \neq 0$ Case

To facilitate analysis of high-frequency components, here we neglect lower-order terms in $\|\omega\|_2$. For the component of the solution in the directions of $\mathbf{u}_{1,\omega}$ and $\mathbf{u}_{2,\omega}$ with $\|\omega\| > 0$,

the initial blocks are

$$
\begin{aligned}
R_0 &= \left[\frac{-1}{(D_1-D_2)\|\omega\|^2+(k_{on}-k_{off})} \left[\begin{array}{c} \frac{u_{22}e^{i\omega\cdot\mathbf{x}}}{k_{off}} \\ -e^{i\omega\cdot\mathbf{x}} \end{array} \right] \left[\begin{array}{c} \frac{k_{off}c_i}{k_{off}+k_{on}} \\ \frac{k_{on}c_i}{k_{off}+k_{on}} \end{array} \right] \right] \\
\tilde{R}_0 &= \left[\frac{-1}{(D_1-D_2)\|\omega\|^2+(k_{on}-k_{off})} \left[\begin{array}{c} -\frac{u_{21}e^{i\omega\cdot\mathbf{x}}}{k_{off}} \\ e^{i\omega\cdot\mathbf{x}} \end{array} \right] \left[\begin{array}{c} \frac{k_{off}c_i}{k_{off}+k_{on}} \\ \frac{k_{on}c_i}{k_{off}+k_{on}} \end{array} \right] \right] \qquad (3.52)
\end{aligned}
$$

where the QR factorization variables for R_0 are

$$
\begin{aligned}
b_{11} &= \|a\|_2 = \sqrt{W\frac{\frac{u_{22}^2}{k_{off}^2}+1}{((D_1-D_2)\|\omega\|^2+(k_{on}-k_{off}))^2}} \\
x_{11} &= a/b_{11} = \frac{\left[\begin{array}{c} -\frac{u_{22}e^{i\omega\cdot\mathbf{x}}}{k_{off}} \\ e^{i\omega\cdot\mathbf{x}} \end{array} \right]}{\sqrt{W\left(\frac{u_{22}^2}{k_{off}^2}+1\right)}} \\
b_{12} &= x_{11}\cdot b = 0 \\
w &= b - x_{11}b_{12} = \left[\begin{array}{c} \frac{c_i}{k_{on}+k_{off}}k_{off} \\ \frac{c_i}{k_{on}+k_{off}}k_{on} \end{array} \right] \\
b_{22} &= \|w\|_2 = \sqrt{W\left(\frac{c_i}{k_{on}+k_{off}}\right)^2(k_{on}^2+k_{off}^2)} \\
x_{12} &= w/b_{22} = \frac{\left[\begin{array}{c} k_{off} \\ k_{on} \end{array} \right]}{\sqrt{W(k_{on}^2+k_{off}^2)}} \\
\tilde{b}_{11} &= \|\tilde{a}\|_2 = \sqrt{W\frac{\frac{u_{21}^2}{k_{off}^2}+1}{((D_1-D_2)\|\omega\|^2+(k_{on}-k_{off}))^2}} \qquad (3.53)
\end{aligned}
$$

and the QR factorization variables for $\tilde{R}_0$ are

$$\begin{aligned}
\tilde{x}_{11} &= \tilde{a}/\tilde{b}_{11} = \frac{\begin{bmatrix} \frac{u_{21}e^{i\omega\cdot\mathbf{x}}}{k_{off}} \\ -e^{i\omega\cdot\mathbf{x}} \end{bmatrix}}{\sqrt{W\left(\frac{u_{21}^2}{k_{off}^2}+1\right)}} \\
\tilde{b}_{12} &= \tilde{x}_{11}\cdot\tilde{b} = 0 \\
\tilde{w} &= \tilde{b}-\tilde{x}_{11}\tilde{b}_{12} = \begin{bmatrix} \frac{c_i}{k_{on}+k_{off}}k_{off} \\ \frac{c_i}{k_{on}+k_{off}}k_{on} \end{bmatrix} \\
\tilde{b}_{22} &= \|\tilde{w}\|_2 = \sqrt{W\left(\frac{c_i}{k_{on}+k_{off}}\right)^2(k_{on}^2+k_{off}^2)} \\
\tilde{x}_{12} &= \tilde{w}/\tilde{b}_{22} = \frac{\begin{bmatrix} k_{off} \\ k_{on} \end{bmatrix}}{\sqrt{W(k_{on}^2+k_{off}^2)}}.
\end{aligned} \tag{3.54}$$

Orthogonalization of these initial blocks yield

$$\begin{aligned}
X_1 &= \begin{bmatrix} \frac{\begin{bmatrix} -u_{22}e^{i\omega\cdot\mathbf{x}} \\ k_{off}e^{i\omega\cdot\mathbf{x}} \end{bmatrix}}{\sqrt{W(u_{22}^2+k_{off}^2)}} & \frac{\begin{bmatrix} k_{off} \\ k_{on} \end{bmatrix}}{\sqrt{W(k_{on}^2+k_{off}^2)}} \end{bmatrix} \\
\tilde{X}_1 &= \begin{bmatrix} \frac{\begin{bmatrix} u_{21}e^{i\omega\cdot\mathbf{x}} \\ -k_{off}e^{i\omega\cdot\mathbf{x}} \end{bmatrix}}{\sqrt{W(u_{21}^2+k_{off}^2)}} & \frac{\begin{bmatrix} k_{off} \\ k_{on} \end{bmatrix}}{\sqrt{W(k_{on}^2+k_{off}^2)}} \end{bmatrix}.
\end{aligned} \tag{3.55}$$

We then compute

$$\begin{aligned}
M_1 &= X_1^H L X_1 = \\
&\begin{bmatrix} \frac{\begin{bmatrix} -u_{22}e^{i\omega\cdot\mathbf{x}} \\ k_{off}e^{i\omega\cdot\mathbf{x}} \end{bmatrix}}{\sqrt{W(u_{22}^2+k_{off}^2)}} & \frac{\begin{bmatrix} k_{off} \\ k_{on} \end{bmatrix}}{\sqrt{W(k_{on}^2+k_{off}^2)}} \end{bmatrix}^H \times \\
&\begin{bmatrix} -k_b I_{r_n}(x,y)-k_{on}+D_1\Delta & k_{off} \\ k_{on} & -k_b I_{r_n}(x,y)-k_{off}+D_2\Delta \end{bmatrix} \times \\
&\begin{bmatrix} \frac{\begin{bmatrix} -u_{22}e^{i\omega\cdot\mathbf{x}} \\ k_{off}e^{i\omega\cdot\mathbf{x}} \end{bmatrix}}{\sqrt{W(u_{22}^2+k_{off}^2)}} & \frac{\begin{bmatrix} k_{off} \\ k_{on} \end{bmatrix}}{\sqrt{W(k_{on}^2+k_{off}^2)}} \end{bmatrix} =
\end{aligned}$$

$$\begin{bmatrix} \frac{n_{21}}{u_{22}^2+k_{off}^2} & \frac{k_b k_{off}\hat{I_{r_n}}(\omega_1,\omega_2)(\overline{u_{22}}-k_{on})}{W\sqrt{u_{22}^2+k_{off}^2}\sqrt{k_{on}^2+k_{off}^2}} \\ \frac{k_b k_{off}\overline{\hat{I_{r_n}}}(\omega_1,\omega_2)(u_{22}-k_{on})}{W\sqrt{u_{22}^2+k_{off}^2}\sqrt{k_{on}^2+k_{off}^2}} & -k_b\overline{I_{r_n}} \end{bmatrix}$$

$$\begin{aligned} n_{21} &= -k_b\overline{I_{r_n}}(u_{22}^2+k_{off}^2) - \|\omega\|^2(D_1u_{22}^2+k_{off}^2D_2) - \\ &\quad (k_{on}u_{22}^2+\overline{u_{22}}k_{off}^2+k_{off}k_{on}u_{22}+k_{off}^3) \\ \tilde{M}_1 &= \tilde{X}_1^H L\tilde{X}_1 = \\ &\quad \begin{bmatrix} \frac{\begin{bmatrix} u_{21}e^{i\omega\cdot\mathbf{x}} \\ -k_{off}e^{i\omega\cdot\mathbf{x}} \end{bmatrix}}{\sqrt{W(u_{21}^2+k_{off}^2)}} & \frac{\begin{bmatrix} k_{off} \\ k_{on} \end{bmatrix}}{\sqrt{W(k_{on}^2+k_{off}^2)}} \end{bmatrix}^H \times \\ &\quad \begin{bmatrix} -k_bI_{r_n}(x,y)-k_{on}+D_1\Delta & k_{off} \\ k_{on} & -k_bI_{r_n}(x,y)-k_{off}+D_2\Delta \end{bmatrix} \times \\ &\quad \begin{bmatrix} \frac{\begin{bmatrix} u_{21}e^{i\omega\cdot\mathbf{x}} \\ -k_{off}e^{i\omega\cdot\mathbf{x}} \end{bmatrix}}{\sqrt{W(u_{21}^2+k_{off}^2)}} & \frac{\begin{bmatrix} k_{off} \\ k_{on} \end{bmatrix}}{\sqrt{W(k_{on}^2+k_{off}^2)}} \end{bmatrix} = \\ &\quad \begin{bmatrix} \frac{n_{22}}{u_{21}^2+k_{off}^2} & \frac{k_b k_{off}\hat{I_{r_n}}(\omega_1,\omega_2)(-\overline{u_{21}}+k_{on})}{W\sqrt{u_{21}^2+k_{off}^2}\sqrt{k_{on}^2+k_{off}^2}} \\ \frac{k_b k_{off}\overline{\hat{I_{r_n}}}(\omega_1,\omega_2)(-u_{21}+k_{on})}{W\sqrt{u_{21}^2+k_{off}^2}\sqrt{k_{on}^2+k_{off}^2}} & -k_b\overline{I_{r_n}} \end{bmatrix} \\ n_{22} &= -k_b\overline{I_{r_n}}(u_{21}^2+k_{off}^2) - \|\omega\|^2(D_1u_{21}^2+k_{off}^2D_2) - \\ &\quad (k_{on}u_{21}^2+\overline{u_{21}}k_{off}^2+k_{off}k_{on}u_{21}+k_{off}^3). \end{aligned} \tag{3.56}$$

One of the eigenvalues is calculated using $\frac{\mathrm{tr}(M_1)-\sqrt{\mathrm{tr}^2(M_1)-4\det(M_1)}}{2}$ and the other calculated by $\frac{2\det(M_1)}{\mathrm{tr}(M_1)-\sqrt{\mathrm{tr}^2(M_1)-4\det(M_1)}}$.

The eigenvalues of M_1 are

$$\begin{aligned}
\lambda_{1,\omega} &= -\frac{1}{2(u_{22}^2+k_{off}^2)}(\|\omega\|^2(D_1u_{22}^2+k_{off}^2D_2)) - \frac{(k_{on}u_{22}^2+\overline{u_{22}}k_{off}^2+k_{off}k_{on}u_{22}+k_{off}^3)}{2(u_{22}^2+k_{off}^2)} - \\
&\quad k_b\overline{I_{r_n}} - \frac{1}{2}\left[\frac{1}{(u_{22}^2+k_{off}^2)^2}\|\omega\|^4(D_1u_{22}^2+k_{off}^2D_2)^2+\right. \\
&\quad \frac{1}{(u_{22}^2+k_{off}^2)^2}(k_{on}u_{22}^2+\overline{u_{22}}k_{off}^2+k_{off}k_{on}u_{22}+k_{off}^3)^2+ \\
&\quad \frac{2}{(u_{22}^2+k_{off}^2)^2}\|\omega\|^2(D_1u_{22}^2+k_{off}^2D_2)(k_{on}u_{22}^2+\overline{u_{22}}k_{off}^2+k_{off}k_{on}u_{22}+k_{off}^3)+ \\
&\quad \left.\frac{4k_b^2k_{off}^2\hat{I_{r_n}}^2(\omega_1,\omega_2)(\overline{u}_{22}-k_{on})(u_{22}-k_{on})}{W^2(k_{on}^2+k_{off}^2)(k_{off}^2+u_{22}^2)}\right]^{1/2} \\
\lambda_{2,\omega} &= \frac{n_{23}}{d_{23}} \\
d_{23} &= \frac{-1}{u_{22}^2+k_{off}^2}\left[\|\omega\|^2(D_1u_{22}^2+k_{off}^2D_2)+(k_{on}u_{22}^2+\overline{u_{22}}k_{off}^2+k_{off}k_{on}u_{22}+k_{off}^3)\right] - \\
&\quad 2k_b\overline{I_{r_n}} - \left[\frac{1}{(u_{22}^2+k_{off}^2)^2}\|\omega\|^4(D_1u_{22}^2+k_{off}^2D_2)^2+\right. \\
&\quad \frac{1}{(u_{22}^2+k_{off}^2)^2}(k_{on}u_{22}^2+\overline{u_{22}}k_{off}^2+k_{off}k_{on}u_{22}+k_{off}^3)^2+ \\
&\quad \frac{2}{(u_{22}^2+k_{off}^2)^2}\|\omega\|^2(D_1u_{22}^2+k_{off}^2D_2)(k_{on}u_{22}^2+\overline{u_{22}}k_{off}^2+k_{off}k_{on}u_{22}+k_{off}^3)+ \\
&\quad \left.\frac{4k_b^2k_{off}^2\hat{I_{r_n}}^2(\omega_1,\omega_2)(\overline{u}_{22}-k_{on})(u_{22}-k_{on})}{W^2(k_{on}^2+k_{off}^2)(k_{off}^2+u_{22}^2)}\right]^{1/2}
\end{aligned}$$

$$\begin{aligned}
n_{23} &= \frac{2}{(u_{22}^2+k_{off}^2)}\left[k_b\overline{I_{r_n}}\|\omega\|^2(D_1u_{22}^2+k_{off}^2D_2)+k_b^2\overline{I_{r_n}}^2(u_{22}^2+k_{off}^2)+\right. \\
&\quad \left.k_b\overline{I_{r_n}}(k_{on}u_{22}^2+\overline{u_{22}}k_{off}^2+k_{off}k_{on}u_{22}+k_{off}^3)\right] - \\
&\quad \frac{2k_b^2k_{off}^2\hat{I_{r_n}}^2(\omega_1,\omega_2)(\overline{u}_{22}-k_{on})(u_{22}-k_{on})}{W^2(k_{on}^2+k_{off}^2)(k_{off}^2+u_{22}^2)}. \qquad (3.57)
\end{aligned}$$

The eigenvalues of $\tilde{M}_1$ are

$$\begin{aligned}
\tilde{\lambda}_{1,\omega} &= -\frac{1}{2(u_{21}^2+k_{off}^2)}(\|\omega\|^2(D_1u_{21}^2+k_{off}^2D_2)) - \frac{(k_{on}u_{21}^2+\overline{u_{21}}k_{off}^2+k_{off}k_{on}u_{21}+k_{off}^3)}{2(u_{21}^2+k_{off}^2)} - \\
&\quad k_b\overline{I_{r_n}} - \frac{1}{2}\left[\frac{1}{(u_{21}^2+k_{off}^2)^2}\|\omega\|^4(D_1u_{21}^2+k_{off}^2D_2)^2+\right. \\
&\quad \frac{1}{(u_{21}^2+k_{off}^2)^2}(k_{on}u_{21}^2+\overline{u_{21}}k_{off}^2+k_{off}k_{on}u_{21}+k_{off}^3)^2+ \\
&\quad \frac{2}{(u_{21}^2+k_{off}^2)^2}\|\omega\|^2(D_1u_{21}^2+k_{off}^2D_2)(k_{on}u_{21}^2+\overline{u_{21}}k_{off}^2+k_{off}k_{on}u_{21}+k_{off}^3)+ \\
&\quad \left.\frac{4k_b^2k_{off}^2\hat{I_{r_n}}^2(\omega_1,\omega_2)(-\overline{u}_{21}+k_{on})(-u_{21}+k_{on})}{W^2(k_{on}^2+k_{off}^2)(k_{off}^2+u_{21}^2)}\right]^{1/2} \\
\tilde{\lambda}_{2,\omega} &= \frac{n_{24}}{d_{24}} \\
d_{24} &= \frac{-1}{u_{21}^2+k_{off}^2}\left[\|\omega\|^2(D_1u_{21}^2+k_{off}^2D_2)+(k_{on}u_{21}^2+\overline{u_{21}}k_{off}^2+k_{off}k_{on}u_{21}+k_{off}^3)\right] - \\
&\quad 2k_b\overline{I_{r_n}} - \left[\frac{1}{(u_{21}^2+k_{off}^2)^2}\|\omega\|^4(D_1u_{21}^2+k_{off}^2D_2)^2+\right. \\
&\quad \frac{1}{(u_{21}^2+k_{off}^2)^2}(k_{on}u_{21}^2+\overline{u_{21}}k_{off}^2+k_{off}k_{on}u_{21}+k_{off}^3)^2+ \\
&\quad \frac{2}{(u_{21}^2+k_{off}^2)^2}\|\omega\|^2(D_1u_{21}^2+k_{off}^2D_2)(k_{on}u_{21}^2+\overline{u_{21}}k_{off}^2+k_{off}k_{on}u_{21}+k_{off}^3)+ \\
&\quad \left.\frac{4k_b^2k_{off}^2\hat{I_{r_n}}^2(\omega_1,\omega_2)(-\overline{u}_{21}+k_{on})(-u_{21}+k_{on})}{W^2(k_{on}^2+k_{off}^2)(k_{off}^2+u_{21}^2)}\right]^{1/2}
\end{aligned}$$

$$\begin{aligned}
n_{24} &= \frac{2}{(u_{21}^2+k_{off}^2)}\left[k_b\overline{I_{r_n}}\|\omega\|^2(D_1u_{21}^2+k_{off}^2D_2)+k_b^2\overline{I_{r_n}}^2(u_{21}^2+k_{off}^2)+\right. \\
&\quad \left.k_b\overline{I_{r_n}}(k_{on}u_{21}^2+\overline{u_{21}}k_{off}^2+k_{off}k_{on}u_{21}+k_{off}^3)\right] - \\
&\quad \frac{2k_b^2k_{off}^2\hat{I_{r_n}}^2(\omega_1,\omega_2)(-\overline{u}_{21}+k_{on})(-u_{21}+k_{on})}{W^2(k_{on}^2+k_{off}^2)(k_{off}^2+u_{21}^2)}
\end{aligned} \tag{3.58}$$

where $\hat{I_{r_n}}^2(\omega_1,\omega_2)$ decays rapidly to zero at higher frequencies. Formulas $\frac{\mathrm{tr}(\tilde{M}_1)-\sqrt{\mathrm{tr}^2(\tilde{M}_1)-4\det(\tilde{M}_1)}}{2}$ and $\frac{2\det(\tilde{M}_1)}{\mathrm{tr}(\tilde{M}_1)-\sqrt{\mathrm{tr}^2(\tilde{M}_1)-4\det(\tilde{M}_1)}}$ are then applied to calculate the eigenvalues of $\tilde{M}_1$.

Finally, the component of the solution in the direction of $\mathbf{u}_{1,\omega}$ is

$$[B_0^H e^{M_1 t} B_0]_{12} = \left\langle \mathbf{v}_{1,\omega} \otimes e^{i\omega\cdot\mathbf{x}}, \rho_{1,\omega}(L) \begin{bmatrix} u(x,y,0) \\ b(x,y,0) \end{bmatrix} \right\rangle \tag{3.59}$$

where $\rho_{1,\omega}$ is a polynomial of degree 1 which interpolates $e^{\lambda t}$ at $\lambda_{1,\omega}$ and $\lambda_{2,\omega}$ given by

$$\rho_{1,\omega}(L) = \frac{e^{\lambda_{1,\omega} t}}{\lambda_{1,\omega} - \lambda_{2,\omega}}[L - \lambda_{2,\omega} I] + \frac{e^{\lambda_{2,\omega} t}}{\lambda_{2,\omega} - \lambda_{1,\omega}}[L - \lambda_{1,\omega} I] \tag{3.60}$$

We conclude that the solution is

$$\begin{aligned}
\begin{bmatrix} u(x,y,t) \\ b(x,y,t) \end{bmatrix} &= \sum_{\omega\in\mathbb{Z}^2} \mathbf{u}_{1,\omega}(x,y) \left\langle \mathbf{v}_{1,\omega}, \rho_{1,\omega}(L) \begin{bmatrix} u(x,y,0) \\ b(x,y,0) \end{bmatrix} \right\rangle + \\
&\quad \sum_{\omega\in\mathbb{Z}^2} \mathbf{u}_{2,\omega}(x,y) \left\langle \mathbf{v}_{2,\omega}, \rho_{2,\omega}(L) \begin{bmatrix} u(x,y,0) \\ b(x,y,0) \end{bmatrix} \right\rangle \\
&= \frac{-1}{(D_1 - D_2)\|\omega\|^2 + (k_{on} - k_{off})} \begin{bmatrix} u_{11}(\omega) e^{i\omega\cdot\mathbf{x}} \\ u_{21}(\omega) e^{i\omega\cdot\mathbf{x}} \end{bmatrix} \times \\
&\quad \begin{bmatrix} \frac{\overline{u_{22}}}{k_{off}} e^{-i\omega\cdot\mathbf{x}} & -e^{-i\omega\cdot\mathbf{x}} \end{bmatrix} \rho_{1,\omega}(L) \begin{bmatrix} \frac{k_{off} c_i}{k_{off} + k_{on}} \\ \frac{k_{on} c_i}{k_{off} + k_{on}} \end{bmatrix} + \\
&\quad \frac{-1}{(D_1 - D_2)\|\omega\|^2 + (k_{on} - k_{off})} \begin{bmatrix} u_{12}(\omega) e^{i\omega\cdot\mathbf{x}} \\ u_{22}(\omega) e^{i\omega\cdot\mathbf{x}} \end{bmatrix} \times \\
&\quad \begin{bmatrix} \frac{-\overline{u_{21}}}{k_{off}} e^{-i\omega\cdot\mathbf{x}} & e^{-i\omega\cdot\mathbf{x}} \end{bmatrix} \rho_{2,\omega}(L) \begin{bmatrix} \frac{k_{off} c_i}{k_{off} + k_{on}} \\ \frac{k_{on} c_i}{k_{off} + k_{on}} \end{bmatrix}.
\end{aligned} \tag{3.61}$$

We used exact basis functions which are valid for all frequencies, while in previous work [5] basis functions were approximated for the constant coefficient problem, which was valid only at high frequencies.

3.4 Analytics in Frequency Space

Computation of M_1 and $\tilde{M}_1$ in frequency space yield

$$M_1 = X_1^H L X_1 =$$

$$
\begin{bmatrix} \frac{\begin{bmatrix} -u_{22}e^{i\omega\cdot\mathbf{x}} \\ k_{off}e^{i\omega\cdot\mathbf{x}} \end{bmatrix}}{\sqrt{W(u_{22}^2+k_{off}^2)}} & \frac{\begin{bmatrix} k_{off} \\ k_{on} \end{bmatrix}}{\sqrt{W(k_{on}^2+k_{off}^2)}} \end{bmatrix}^H \times
$$

$$
\begin{bmatrix} -k_b I_{r_n}(x,y) - k_{on} + D_1\Delta & k_{off} \\ k_{on} & -k_b I_{r_n}(x,y) - k_{off} + D_2\Delta \end{bmatrix} \times
$$

$$
\begin{bmatrix} \frac{\begin{bmatrix} -u_{22}e^{i\omega\cdot\mathbf{x}} \\ k_{off}e^{i\omega\cdot\mathbf{x}} \end{bmatrix}}{\sqrt{W(u_{22}^2+k_{off}^2)}} & \frac{\begin{bmatrix} k_{off} \\ k_{on} \end{bmatrix}}{\sqrt{W(k_{on}^2+k_{off}^2)}} \end{bmatrix} =
$$

$$
\begin{bmatrix} \frac{n_1}{u_{22}^2+k_{off}^2} & \frac{k_b k_{off} I_0 \exp\left(\frac{-{r_n}^2\|\omega\|^2}{8}\right)(\overline{u_{22}}-k_{on})}{4\pi^2\sqrt{u_{22}^2+k_{off}^2}\sqrt{k_{on}^2+k_{off}^2}} \\ \frac{k_b k_{off}\overline{I_0}\exp\left(\frac{-{r_n}^2\|\omega\|^2}{8}\right)(u_{22}-k_{on})}{4\pi^2\sqrt{u_{22}^2+k_{off}^2}\sqrt{k_{on}^2+k_{off}^2}} & -k_b\overline{I_{r_n}} \end{bmatrix}
$$

$$
\begin{aligned}
n_1 &= -k_b\overline{I_{r_n}}(u_{22}^2+k_{off}^2) - \|\omega\|^2(D_1u_{22}^2+k_{off}^2D_2) - \\
&\quad (k_{on}u_{22}^2+\overline{u_{22}}k_{off}^2+k_{off}k_{on}u_{22}+k_{off}^3)
\end{aligned}
$$

$$
\begin{aligned}
\tilde{M}_1 &= \tilde{X}_1^H L \tilde{X}_1 = \\
&\begin{bmatrix} \frac{\begin{bmatrix} u_{21}e^{i\omega\cdot\mathbf{x}} \\ -k_{off}e^{i\omega\cdot\mathbf{x}} \end{bmatrix}}{\sqrt{W(u_{21}^2+k_{off}^2)}} & \frac{\begin{bmatrix} k_{off} \\ k_{on} \end{bmatrix}}{\sqrt{W(k_{on}^2+k_{off}^2)}} \end{bmatrix}^H \times \\
&\begin{bmatrix} -k_b I_{r_n}(x,y) - k_{on} + D_1\Delta & k_{off} \\ k_{on} & -k_b I_{r_n}(x,y) - k_{off} + D_2\Delta \end{bmatrix} \times \\
&\begin{bmatrix} \frac{\begin{bmatrix} u_{21}e^{i\omega\cdot\mathbf{x}} \\ -k_{off}e^{i\omega\cdot\mathbf{x}} \end{bmatrix}}{\sqrt{W(u_{21}^2+k_{off}^2)}} & \frac{\begin{bmatrix} k_{off} \\ k_{on} \end{bmatrix}}{\sqrt{W(k_{on}^2+k_{off}^2)}} \end{bmatrix} = \\
&\begin{bmatrix} \frac{n_2}{u_{21}^2+k_{off}^2} & \frac{k_b k_{off} I_0 \exp\left(\frac{-{r_n}^2\|\omega\|^2}{8}\right)(-\overline{u_{21}}+k_{on})}{4\pi^2\sqrt{u_{21}^2+k_{off}^2}\sqrt{k_{on}^2+k_{off}^2}} \\ \frac{k_b k_{off}\overline{I_0}\exp\left(\frac{-{r_n}^2\|\omega\|^2}{8}\right)(-u_{21}+k_{on})}{\pi^2\sqrt{u_{21}^2+k_{off}^2}\sqrt{k_{on}^2+k_{off}^2}} & -k_b\overline{I_{r_n}} \end{bmatrix} \\
n_2 &= -k_b\overline{I_{r_n}}(u_{21}^2+k_{off}^2) - \|\omega\|^2(D_1u_{21}^2+k_{off}^2D_2) - \\
&\quad (k_{on}u_{21}^2+\overline{u_{21}}k_{off}^2+k_{off}k_{on}u_{21}+k_{off}^3).
\end{aligned} \tag{3.62}
$$

The calculated eigenvalues $\frac{\mathrm{tr}(M_1)-\sqrt{\mathrm{tr}^2(M_1)-4\det(M_1)}}{2}$ and $\frac{2\det(M_1)}{\mathrm{tr}(M_1)-\sqrt{\mathrm{tr}^2(M_1)-4\det(M_1)}}$ are

$$
\begin{aligned}
\lambda_{1,\omega} &= -\frac{1}{2(u_{22}^2+k_{off}^2)}(\|\omega\|^2(D_1u_{22}^2+k_{off}^2D_2)) - \frac{(k_{on}u_{22}^2+\overline{u_{22}}k_{off}^2+k_{off}k_{on}u_{22}+k_{off}^3)}{2(u_{22}^2+k_{off}^2)} - \\
& k_b\overline{I_{r_n}} - \frac{1}{2}\left[\frac{1}{(u_{22}^2+k_{off}^2)^2}\|\omega\|^4(D_1u_{22}^2+k_{off}^2D_2)^2+\right. \\
& \frac{1}{(u_{22}^2+k_{off}^2)^2}(k_{on}u_{22}^2+\overline{u_{22}}k_{off}^2+k_{off}k_{on}u_{22}+k_{off}^3)^2+ \\
& \frac{2}{(u_{22}^2+k_{off}^2)^2}\|\omega\|^2(D_1u_{22}^2+k_{off}^2D_2)(k_{on}u_{22}^2+\overline{u_{22}}k_{off}^2+k_{off}k_{on}u_{22}+k_{off}^3)+ \\
& \left.\frac{\frac{1}{4\pi^4}k_b^2k_{off}^2I_0^2\exp\left(\frac{-r_n^2\|\omega\|^2}{4}\right)(\overline{u}_{22}-k_{on})(u_{22}-k_{on})}{(k_{on}^2+k_{off}^2)(k_{off}^2+u_{22}^2)}\right]^{1/2} \\
\lambda_{2,\omega} &= \frac{n_{23}}{d_{23}} \\
n_{23} &= \frac{2}{(u_{22}^2+k_{off}^2)}\left[k_b\overline{I_{r_n}}\|\omega\|^2(D_1u_{22}^2+k_{off}^2D_2)+k_b^2\overline{I_{r_n}}^2(u_{22}^2+k_{off}^2)+\right. \\
& \left. k_b\overline{I_{r_n}}(k_{on}u_{22}^2+\overline{u_{22}}k_{off}^2+k_{off}k_{on}u_{22}+k_{off}^3)\right] - \\
& \frac{\frac{1}{8\pi^4}k_b^2k_{off}^2I_0^2\exp\left(\frac{-r_n^2\|\omega\|^2}{4}\right)(\overline{u}_{22}-k_{on})(u_{22}-k_{on})}{(k_{on}^2+k_{off}^2)(k_{off}^2+u_{22}^2)} \\
d_{23} &= \frac{-1}{u_{22}^2+k_{off}^2}\left[\|\omega\|^2(D_1u_{22}^2+k_{off}^2D_2)+(k_{on}u_{22}^2+\overline{u_{22}}k_{off}^2+k_{off}k_{on}u_{22}+k_{off}^3)\right] - \\
& 2k_b\overline{I_{r_n}} - \left[\frac{1}{(u_{22}^2+k_{off}^2)^2}\|\omega\|^4(D_1u_{22}^2+k_{off}^2D_2)^2+\right. \\
& \frac{1}{(u_{22}^2+k_{off}^2)^2}(k_{on}u_{22}^2+\overline{u_{22}}k_{off}^2+k_{off}k_{on}u_{22}+k_{off}^3)^2+ \\
& \frac{2}{(u_{22}^2+k_{off}^2)^2}\|\omega\|^2(D_1u_{22}^2+k_{off}^2D_2)(k_{on}u_{22}^2+\overline{u_{22}}k_{off}^2+k_{off}k_{on}u_{22}+k_{off}^3)+ \\
& \left.\frac{\frac{1}{4\pi^4}k_b^2k_{off}^2I_0^2\exp\left(\frac{-r_n^2\|\omega\|^2}{4}\right)(\overline{u}_{22}-k_{on})(u_{22}-k_{on})}{(k_{on}^2+k_{off}^2)(k_{off}^2+u_{22}^2)}\right]^{1/2}. \qquad (3.63)
\end{aligned}
$$

Similarly, the eigenvalues of $\tilde{M}_1$ are

$$\begin{aligned}
\tilde{\lambda}_{1,\omega} &= -\frac{1}{2(u_{21}^2+k_{off}^2)}(\|\omega\|^2(D_1u_{21}^2+k_{off}^2D_2)) - \frac{(k_{on}u_{21}^2+\overline{u_{21}}k_{off}^2+k_{off}k_{on}u_{21}+k_{off}^3)}{2(u_{21}^2+k_{off}^2)} - \\
&\quad k_b\overline{I_{r_n}} - \frac{1}{2}\left[\frac{1}{(u_{21}^2+k_{off}^2)^2}\|\omega\|^4(D_1u_{21}^2+k_{off}^2D_2)^2+\right. \\
&\quad \frac{1}{(u_{21}^2+k_{off}^2)^2}(k_{on}u_{21}^2+\overline{u_{21}}k_{off}^2+k_{off}k_{on}u_{21}+k_{off}^3)^2+ \\
&\quad \frac{2}{(u_{21}^2+k_{off}^2)^2}\|\omega\|^2(D_1u_{21}^2+k_{off}^2D_2)(k_{on}u_{21}^2+\overline{u_{21}}k_{off}^2+k_{off}k_{on}u_{21}+k_{off}^3)+ \\
&\quad \left.\frac{\frac{1}{4\pi^4}k_b^2k_{off}^2I_0^2\exp\left(\frac{-r_n^2\|\omega\|^2}{4}\right)(-\overline{u}_{21}+k_{on})(-u_{21}+k_{on})}{(k_{on}^2+k_{off}^2)(k_{off}^2+u_{21}^2)}\right]^{1/2} \\
\tilde{\lambda}_{2,\omega} &= \frac{n_{24}}{d_{24}} \\
n_{24} &= \frac{2}{(u_{21}^2+k_{off}^2)}\left[k_b\overline{I_{r_n}}\|\omega\|^2(D_1u_{21}^2+k_{off}^2D_2)+k_b^2\overline{I_{r_n}}^2(u_{21}^2+k_{off}^2)+\right. \\
&\quad \left.k_b\overline{I_{r_n}}(k_{on}u_{21}^2+\overline{u_{21}}k_{off}^2+k_{off}k_{on}u_{21}+k_{off}^3)\right] - \\
&\quad \frac{\frac{1}{8\pi^4}k_b^2k_{off}^2I_0^2\exp\left(\frac{-r_n^2\|\omega\|^2}{4}\right)(-\overline{u}_{21}+k_{on})(-u_{21}+k_{on})}{(k_{on}^2+k_{off}^2)(k_{off}^2+u_{21}^2)} \\
d_{24} &= \frac{-1}{u_{21}^2+k_{off}^2}\left[\|\omega\|^2(D_1u_{21}^2+k_{off}^2D_2)+(k_{on}u_{21}^2+\overline{u_{21}}k_{off}^2+k_{off}k_{on}u_{21}+k_{off}^3)\right] - \\
&\quad 2k_b\overline{I_{r_n}} - \left[\frac{1}{(u_{21}^2+k_{off}^2)^2}\|\omega\|^4(D_1u_{21}^2+k_{off}^2D_2)^2+\right. \\
&\quad \frac{1}{(u_{21}^2+k_{off}^2)^2}(k_{on}u_{21}^2+\overline{u_{21}}k_{off}^2+k_{off}k_{on}u_{21}+k_{off}^3)^2+ \\
&\quad \frac{2}{(u_{21}^2+k_{off}^2)^2}\|\omega\|^2(D_1u_{21}^2+k_{off}^2D_2)(k_{on}u_{21}^2+\overline{u_{21}}k_{off}^2+k_{off}k_{on}u_{21}+k_{off}^3)+ \\
&\quad \left.\frac{\frac{1}{4\pi^4}k_b^2k_{off}^2I_0^2\exp\left(\frac{-r_n^2\|\omega\|^2}{4}\right)(-\overline{u}_{21}+k_{on})(-u_{21}+k_{on})}{(k_{on}^2+k_{off}^2)(k_{off}^2+u_{21}^2)}\right]^{1/2}. \qquad (3.64)
\end{aligned}$$

Asymptotic analysis of the above eigenvalues as $\|\omega\| \to \infty$ yields

$$\begin{aligned}
\lambda_{1,\omega} &\approx -\frac{\|\omega\|^2(D_1u_{22}^2+k_{off}^2D_2)}{(u_{22}^2+k_{off}^2)} \\
\lambda_{2,\omega} &\approx -k_b\overline{I_{r_n}} \\
\tilde{\lambda}_{1,\omega} &\approx -\frac{\|\omega\|^2(D_1u_{22}^2+k_{off}^2D_2)}{(u_{22}^2+k_{off}^2)} \\
\tilde{\lambda}_{2,\omega} &\approx -k_b\overline{I_{r_n}}
\end{aligned} \tag{3.65}$$

and when $\|\omega\| \to 0$ we have

$$\begin{aligned}
\lambda_{1,\omega} &\approx -k_b\overline{I_{r_n}} - \left[\frac{\frac{1}{8\pi^4}k_b^2k_{off}^2I_0^2(k_{off}+k_{on})^2}{(k_{on}^2+k_{off}^2)}\right]^{1/2} \\
\lambda_{2,\omega} &\approx \frac{2k_b^2\overline{I_{r_n}}^2 - \frac{\frac{1}{16\pi^4}k_b^2k_{off}^2I_0^2(k_{off}+k_{on})^2}{(k_{on}^2+k_{off}^2)}}{-2k_b\overline{I_{r_n}} - \left[\frac{\frac{1}{8\pi^4}k_b^2k_{off}^2I_0^2(k_{off}+k_{on})^2}{(k_{on}^2+k_{off}^2)}\right]^{1/2}} \\
\tilde{\lambda}_{1,\omega} &\approx -k_b\overline{I_{r_n}} - (k_{on}+k_{off}) \\
\tilde{\lambda}_{2,\omega} &\approx -k_b\overline{I_{r_n}}.
\end{aligned} \tag{3.66}$$

3.5 Efficient Implementation

In this section we show how the KSS method for the first order photobleaching kinetics can be implemented efficiently through vectorized polynomial interpolation. This approach produces the approximate analytical solution that can provide insight into qualitative behavior. We use FFTs that produces frequencies in the range $-\frac{N}{2}+1 \le \omega \le \frac{N}{2}$. The Fourier coefficients of the solution at time t_{n+1} are computed as follows:

$$\begin{aligned}
\begin{bmatrix} \hat{u}(\omega,t_{n+1}) \\ \hat{b}(\omega,t_{n+1}) \end{bmatrix} &= \begin{bmatrix} u_{11}(\omega) \\ u_{21}(\omega) \end{bmatrix} \left\langle \mathbf{v}_{1,\omega}, \rho_{1\omega}(L) \begin{bmatrix} u(x,y,t_n) \\ b(x,y,t_n) \end{bmatrix} \right\rangle + \\
&\quad \begin{bmatrix} u_{12}(\omega) \\ u_{22}(\omega) \end{bmatrix} \left\langle \mathbf{v}_{2,\omega}, \rho_{2\omega}(L) \begin{bmatrix} u(x,y,t_n) \\ b(x,y,t_n) \end{bmatrix} \right\rangle \\
&= \begin{bmatrix} u_{11}(\omega) \\ u_{21}(\omega) \end{bmatrix} [c_{0,\omega}^1(\overline{v_{11}(\omega)}\hat{u}(\omega)+\overline{v_{21}(\omega)}\hat{b}(\omega)) + c_{1,\omega}^1(\overline{v_{11}(\omega)}\hat{p}(\omega)+\overline{v_{21}(\omega)}\hat{q}(\omega))] + \\
&\quad \begin{bmatrix} u_{12}(\omega) \\ u_{22}(\omega) \end{bmatrix} [c_{0,\omega}^2(\overline{v_{12}(\omega)}\hat{u}(\omega)+\overline{v_{22}(\omega)}\hat{b}(\omega)) + c_{1,\omega}^2(\overline{v_{12}(\omega)}\hat{p}(\omega)+\overline{v_{22}(\omega)}\hat{q}(\omega))]
\end{aligned} \tag{3.67}$$

where $\rho_{j,\omega}$ is a polynomial of degree 1 which interpolates $e^{\lambda\Delta t}$ at $\lambda_{1,\omega}^j$ and $\lambda_{2,\omega}^j$, for $j = 1,2$. We have

$$\rho_{j,\omega}(L)\begin{bmatrix} u \\ b \end{bmatrix}_n = c_{0,\omega}^j \begin{bmatrix} u \\ b \end{bmatrix}_n + c_{1,\omega}^j \begin{bmatrix} p \\ q \end{bmatrix}_n \tag{3.68}$$

where

$$\begin{bmatrix} p \\ q \end{bmatrix}_n = L\begin{bmatrix} u \\ b \end{bmatrix}_n. \tag{3.69}$$

The coefficients of $\rho_{j,\omega}(L)$ are given by

$$\begin{aligned} f_{k,\omega}^j &= e^{\lambda_{k,\omega}^j \Delta t} \\ c_{1,\omega}^j &= \frac{f_{2,\omega}^j - f_{1,\omega}^j}{\lambda_{2,\omega}^j - \lambda_{1,\omega}^j}, \quad j = 1,2 \\ c_{0,\omega}^j &= f_{2,\omega}^j - c_{1,\omega}^j \lambda_{2,\omega}^j \end{aligned} \tag{3.70}$$

For $\hat{u}$ and $\hat{b}$, the appropriate matrices of 2-D Fourier coefficients are multiplied component-wise. An inverse FFT yields the solution at time t_{n+1}. The resulting algorithm requires $O(N^2 \log N)$ floating-point operations, where N is the number of grid points per dimension.

3.6 Numerical Results

We now use numerical experiments to validate the formulas of the previous sections. Errors for the solution of first-order photobleaching kinetics by applying a first-order ($K = 1$) KSS method are shown is this section. We present the absolute and relative errors versus number of grid points per dimension (N) and number of time steps ($nsteps$). Errors are computed by comparing the solution at the final time (denoted by t_f) to that obtained by computing the matrix exponential of $L * t_f$ times the initial data. Parameters are $k_b = 1$ and $C_i = 1$ in all cases.

Table 3.1: Execution time, absolute error and relative error for different grid point for $nsteps = 10{,}000$ with parameters $k_{on} = 10^{-0.5}\ s^{-1}$, $k_{off} = 10^{-1}\ s^{-1}$, $D_1 = 30\ \mu m^2/s$, $D_2 = 10^{-4}\ \mu m^2/s$ and $\omega_{r_n} = 0.5\ \mu m$.

	N=8	N=16	N=32	N=64
Execution time	4.4901	7.9654	19.7626	75.9164
Absolute error	0.0026	1.3708e-04	6.2202e-05	3.3702e-06
Relative error	0.0012	1.8657e-05	3.6038e-06	6.9968e-08

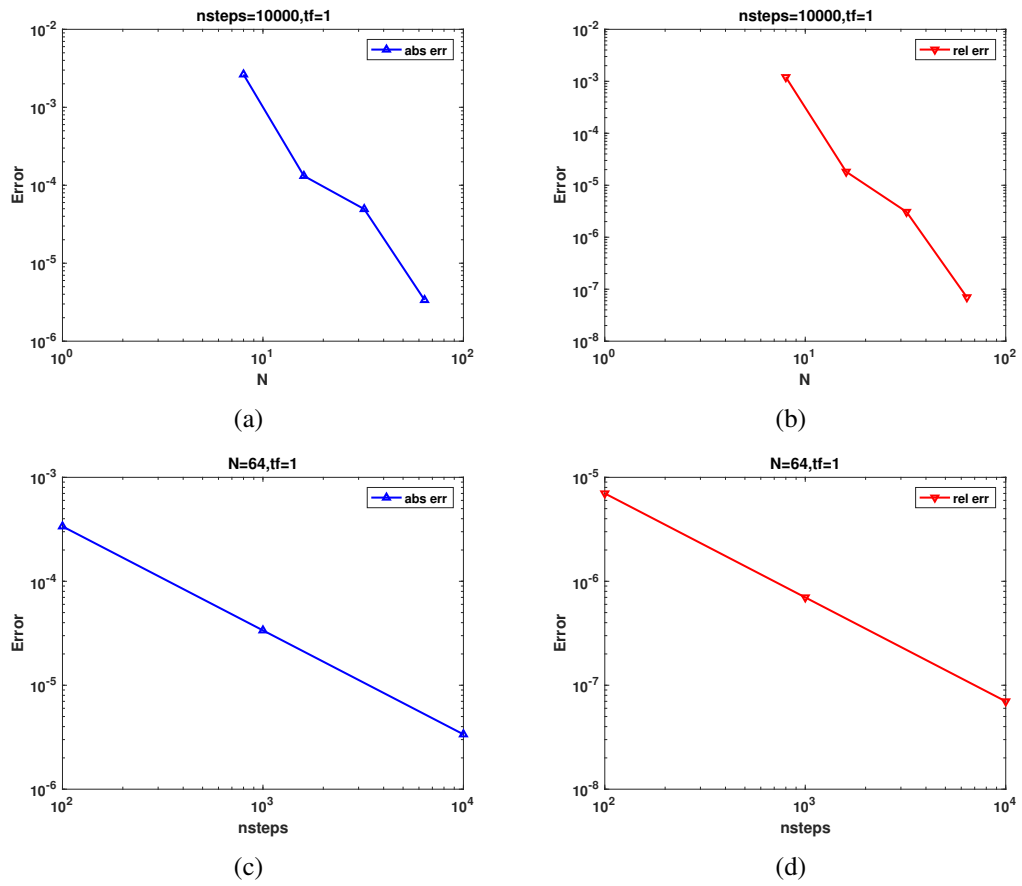

Figure 3.1: a and b: Absolute and relative errors versus grid points (N). c and d: Absolute and relative errors versus time steps. Parameters are $k_{on} = 10^{-0.5}\ s^{-1}$, $k_{off} = 10^{-1}\ s^{-1}$, $D_1 = 30\ \mu m^2/s$, $D_2 = 10^{-4}\ \mu m^2/s$ and $\omega_{r_n} = 0.5\ \mu m$.

Table 3.2: Execution time, absolute error and relative error for different grid point for $N = 64$ with parameters $k_{on} = 10^{-0.5}\ s^{-1}$, $k_{off} = 10^{-1}\ s^{-1}$, $D_1 = 30\ \mu m^2/s$, $D_2 = 10^{-4}\ \mu m^2/s$ and $\omega_{r_n} = 0.5\ \mu m$.

	time steps=100	time steps=1000	time steps=10000
Execution time	0.79309	6.8334	75.9164
Absolute error	3.3739e-04	3.3705e-05	3.3702e-06
Relative error	7.0045e-06	6.9974e-07	6.9968e-08

For our first test case, reaction-dominant parameters that are defined in Chapter 1 are set to be $k_{on} = 10^{-0.5}\ s^{-1}$, $k_{off} = 10^{-1}\ s^{-1}$, $D_1 = 30\ \mu m^2/s$, $D_2 = 10^{-4}\ \mu m^2/s$ and $\omega_{r_n} = 0.5$ μm for Figure 1. These values are taken from [11, 13, 22].

Figures 3.1a and 3.1b show absolute and relative errors versus grid points (N) for $nsteps = 10,000$ (number of time steps) and final time $t_f = 1$. It shows a rapidly decreasing

trend for both absolute and relative errors by increasing N. This is due to each solution being compared to an approximate solution computing using the matrix exponential on a finer grid. Figures 3.1c and 3.1d show absolute and relative errors versus time steps for $N = 64$ and final time $t_f = 1$, corresponding to a time step $\Delta t = 1/nsteps$. It shows first-order accuracy in time, as expected. Table 3.1 shows the execution time, absolute error and relative error for different grid sizes for $nsteps = 10,000$ with parameters $k_{on} = 10^{-0.5}\ s^{-1}$, $k_{off} = 10^{-1}\ s^{-1}$, $D_1 = 30\ \mu m^2/s$, $D_2 = 10^{-4}\ \mu m^2/s$ and $\omega_{r_n} = 0.5\ \mu m$. Table 3.2 shows the execution time, absolute error and relative error for different time step sizes, with $N = 64$, for the same parameters.

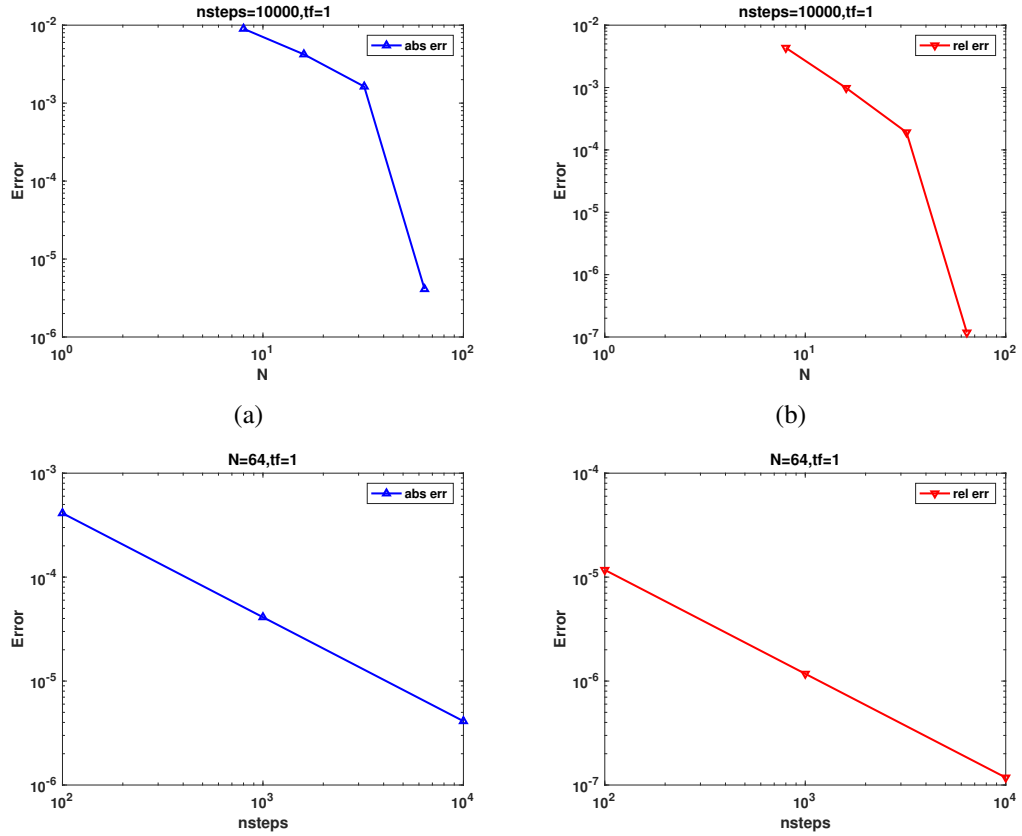

Figure 3.2: a and b: Absolute and relative errors versus grid points (N). c and d: Absolute and relative errors versus time steps. Parameters are $k_{on} = 10^{3.5}\ s^{-1}$, $k_{off} = 1\ s^{-1}$, $D_1 = 30\ \mu m^2/s$, $D_2 = 10^{-4}\ \mu m^2/s$ and $\omega_{r_n} = 0.5\ \mu m$.

For the second case, effective diffusion parameter values are set to be $k_{on} = 10^{3.5}\ s^{-1}$, $k_{off} = 1\ s^{-1}$, $D_1 = 30\ \mu m^2/s$, $D_2 = 10^{-4}\ \mu m^2/s$ and $\omega_{r_n} = 0.5\ \mu m$ for Figure 3.2. Figures 3.2a and 3.2b show absolute and relative errors versus grid points per dimension (N) for $nsteps = 10,000$ and $t_f = 1$. It shows a rapidly decreasing trend for both absolute and

Table 3.3: Execution time, absolute error and relative error for different grid point for $nsteps = 10,000$ with parameters $k_{on} = 10^{3.5}\ s^{-1}$, $k_{off} = 1\ s^{-1}$, $D_1 = 30\ \mu m^2/s$, $D_2 = 10^{-4}\ \mu m^2/s$ and $\omega_{r_n} = 0.5\ \mu m$.

	N=8	N=16	N=32	N=64
Execution time	4.5759	7.9816	19.9623	71.1799
Absolute error	0.0090	0.0042	0.0016	4.1146e-06
Relative error	0.0043	9.8314e-04	1.9172e-04	1.1792e-07

Table 3.4: Execution time, absolute error and relative error for different grid point for $N = 64$ with parameters $k_{on} = 10^{3.5}\ s^{-1}$, $k_{off} = 1\ s^{-1}$, $D_1 = 30\ \mu m^2/s$, $D_2 = 10^{-4}\ \mu m^2/s$ and $\omega_{r_n} = 0.5\ \mu m$.

	time steps=100	time steps=1000	time steps=10000
Execution time	0.77525	6.8763	71.1799
Absolute error	4.1187e-04	4.1145e-05	4.1146e-06
Relative error	1.1729e-05	1.1748e-06	1.1792e-07

relative errors by increasing N. Figures 3.2c and 3.2d show absolute and relative errors versus number of time steps for $N = 64$ and $t_f = 1$. As before, first-order accuracy in time is obtained. Table 3.3 shows the execution time, absolute error and relative error for different grid point for $nsteps = 10,000$ with parameters $k_{on} = 10^{3.5}\ s^{-1}$, $k_{off} = 1\ s^{-1}$, $D_1 = 30\ \mu m^2/s$, $D_2 = 10^{-4}\ \mu m^2/s$ and $\omega_{r_n} = 0.5\ \mu m$. Table 3.4 shows the execution time, absolute error and relative error for different time steps, with $N = 64$, for the same parameters.

For the third case, pure diffusion parameter values are set to be $k_{on} = 10^{-2}\ s^{-1}$, $k_{off} = 10$

Table 3.5: Execution time, absolute error and relative error for different grid point for $nsteps = 10,000$ with parameters $k_{on} = 10^{-2}\ s^{-1}$, $k_{off} = 10\ s^{-1}$, $D_1 = 30\ \mu m^2/s$, $D_2 = 10^{-4}\ \mu m^2/s$ and $\omega_{r_n} = 0.5\ \mu m$.

	N=8	N=16	N=32	N=64
Execution time	4.6127	7.9169	19.9402	70.3547
Absolute error	0.0088	1.4902e-04	3.8141e-05	2.3867e-09
Relative error	0.0021	1.8470e-05	2.4014e-06	7.8543e-11

s^{-1}, $D_1 = 30\ \mu m^2/s$, $D_2 = 10^{-4}\ \mu m^2/s$ and $\omega_{r_n} = 0.5\ \mu m$ for Figure 3.3. Figures 3.3a and 3.3b show absolute and relative errors versus grid points per dimension (N) for $nsteps = 10,000$ and $t_f = 1$. It shows a rapidly decreasing trend for both absolute and relative errors by increasing N. Figures 3.3c and 3.3d show absolute and relative errors versus number

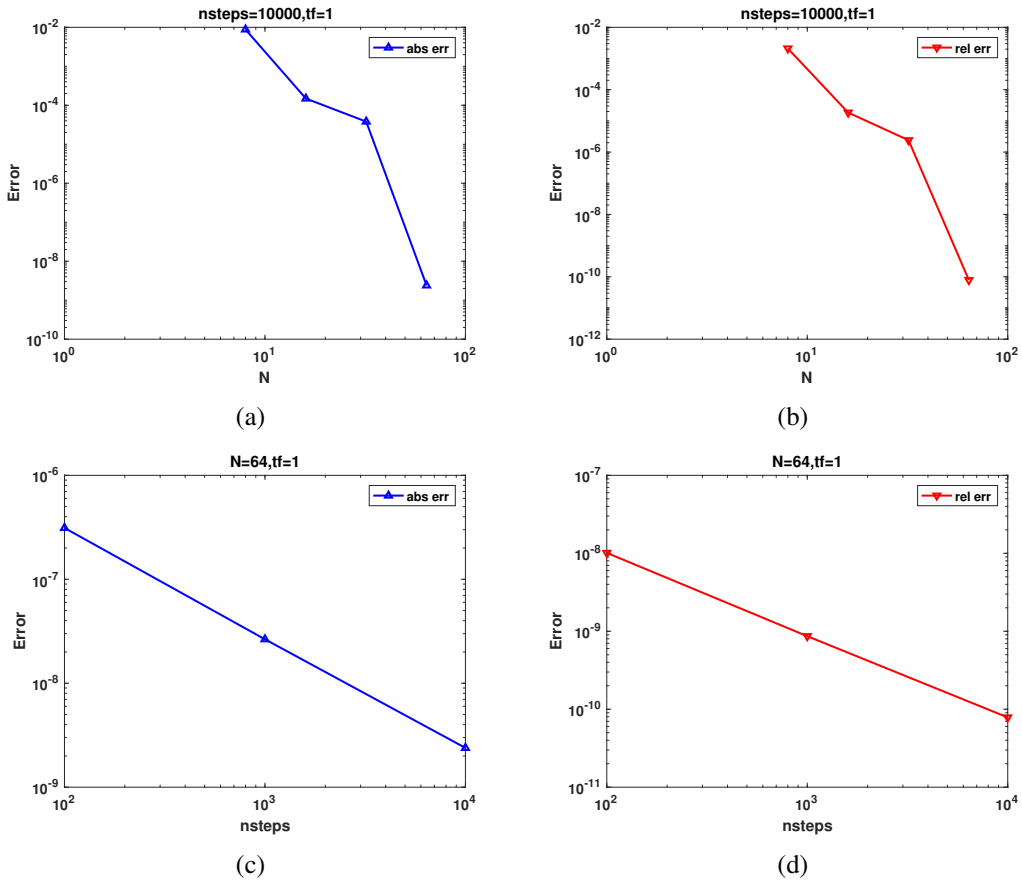

Figure 3.3: a and b: Absolute and relative errors versus grid points (N). c and d: Absolute and relative errors versus time steps. Parameters are $k_{on} = 10^{-2}\ s^{-1}$, $k_{off} = 10\ s^{-1}$, $D_1 = 30\ \mu m^2/s$, $D_2 = 10^{-4}\ \mu m^2/s$ and $\omega_{r_n} = 0.5\ \mu m$.

Table 3.6: Execution time, absolute error and relative error for different grid point for $N = 64$ with parameters $k_{on} = 10^{-2}\ s^{-1}$, $k_{off} = 10\ s^{-1}$, $D_1 = 30\ \mu m^2/s$, $D_2 = 10^{-4}\ \mu m^2/s$ and $\omega_{r_n} = 0.5\ \mu m$.

	time steps=100	time steps=1000	time steps=10000
Execution time	0.81812	6.9748	70.3547
Absolute error	3.1191e-07	2.6479e-08	2.3867e-09
Relative error	1.0130e-08	8.6496e-10	7.8543e-11

of time steps $(timesteps)$ for $N = 64$ and $t_f = 1$. As before, first-order accuracy in time is obtained. Table 3.5 shows the execution time, absolute error and relative error for different grid point for $nsteps = 10{,}000$ with parameters $k_{on} = 10^{-2}\ s^{-1}$, $k_{off} = 10\ s^{-1}$, $D_1 = 30\ \mu m^2/s$, $D_2 = 10^{-4}\ \mu m^2/s$, $\omega_{r_n} = 0.5\ \mu m$. Table 3.6 shows the execution time, absolute error and relative error for different time steps, with $N = 64$, for the same parameters.

For the forth case, diffusion-dominant parameter values are set to be $k_{on} = 255\ s^{-1}$,

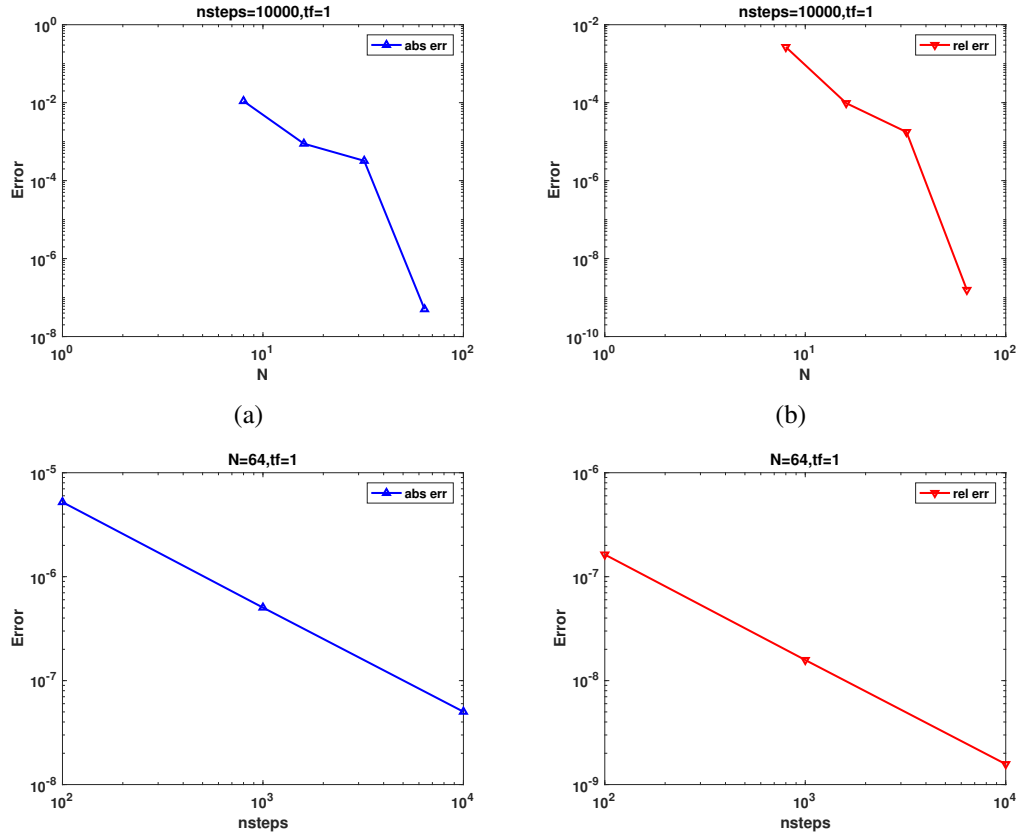

Figure 3.4: a and b: Absolute and relative errors versus grid points (N). c and d: Absolute and relative errors versus time steps. Parameters are $k_{on} = 255\ s^{-1}$, $k_{off} = 31\ s^{-1}$, $D_1 = 45\ \mu m^2/s$, $D_2 = 2.5\ \mu m^2/s$ and $\omega_{r_n} = 0.6\ \mu m$.

Table 3.7: Execution time, absolute error and relative error for different grid point for $nsteps = 10{,}000$ with parameters $k_{on} = 255\ s^{-1}$, $k_{off} = 31\ s^{-1}$, $D_1 = 45\ \mu m^2/s$, $D_2 = 2.5\ \mu m^2/s$ and $\omega_{r_n} = 0.6\ \mu m$.

	N=8	N=16	N=32	N=64
Execution time	4.6111	8.1284	19.9517	70.7699
Absolute error	0.0110	8.8722e-04	3.2260e-04	5.0216e-08
Relative error	0.0027	9.7375e-05	1.7675e-05	1.5728e-09

$k_{off} = 31\ s^{-1}$, $D_1 = 45\ \mu m^2/s$, $D_2 = 2.5\ \mu m^2/s$ and $\omega_{r_n} = 0.6\ \mu m$ for Figure 3.4. Here we consider a diffusion-dominated case. Figures 3.4a and 3.4b show absolute and relative errors versus grid points per dimension (N) for $nsteps = 10{,}000$ and $t_f = 1$. Like other previous cases, it shows a decreasing trend for both absolute and relative errors by increasing N.

Table 3.8: Execution time, absolute error and relative error for different grid point for $N = 64$ with parameters $k_{on} = 255\ s^{-1}$, $k_{off} = 31\ s^{-1}$, $D_1 = 45\ \mu m^2/s$, $D_2 = 2.5\ \mu m^2/s$ and $\omega_{r_n} = 0.6\ \mu m$.

	time steps=100	time steps=1000	time steps=10000
Execution time	0.78513	6.8135	70.7699
Absolute error	5.2135e-06	5.0417e-07	5.0216e-08
Relative error	1.6329e-07	1.5791e-08	1.5728e-09

Figures 3.4c and 3.4d show absolute and relative errors versus time steps for $N = 64$ and $t_f = 1$. First-order accuracy in time is again observed, with the error smaller than in the other cases. Table 3.7 shows the execution time, absolute error and relative error for different grid sizes with $nsteps = 10,000$ and parameters $k_{on} = 255\ s^{-1}$, $k_{off} = 31\ s^{-1}$, $D_1 = 45\ \mu m^2/s$, $D_2 = 2.5\ \mu m^2/s$ and $\omega_{r_n} = 0.6\ \mu m$. Table 3.8 shows the execution time, absolute error and relative error for different time step sizes with $N = 64$ for the same parameters.

Table 3.9: Execution time, absolute error and relative error for different grid point for $nsteps = 10,000$ with parameters $k_{on} = 10^2\ s^{-1}$, $k_{off} = 10^{-1}\ s^{-1}$, $D_1 = 30\ \mu m^2/s$, $D_2 = 10^{-1}\ \mu m^2/s$ and $\omega_{r_n} = 0.5\ \mu m$.

	N=8	N=16	N=32	N=64
Execution time	4.5256	8.0008	20.7176	76.6904
Absolute error	0.0444	0.0113	0.0044	1.2740e-06
Relative error	0.0100	9.6420e-04	1.7973e-04	3.0811e-08

Table 3.10: Execution time, absolute error and relative error for different grid point for $N = 64$ with parameters $k_{on} = 10^2\ s^{-1}$, $k_{off} = 10^{-1}\ s^{-1}$, $D_1 = 30\ \mu m^2/s$, $D_2 = 10^{-1}\ \mu m^2/s$ and $\omega_{r_n} = 0.5\ \mu m$.

	time steps=100	time steps=1000	time steps=10000
Execution time	0.78111	7.6507	76.6904
Absolute error	1.2783e-04	1.2744e-05	1.2740e-06
Relative error	3.0821e-06	3.0810e-07	3.0811e-08

For the fifth case, full model parameter values are set to be $k_{on} = 10^2\ s^{-1}$, $k_{off} = 10^{-1}\ s^{-1}$, $D_1 = 30\ \mu m^2/s$, $D_2 = 10^{-1}\ \mu m^2/s$ and $\omega_{r_n} = 0.5\ \mu m$ for Figure 3.5. Here we consider a diffusion-dominated case. Figures 3.5a and 3.5b show absolute and relative errors versus

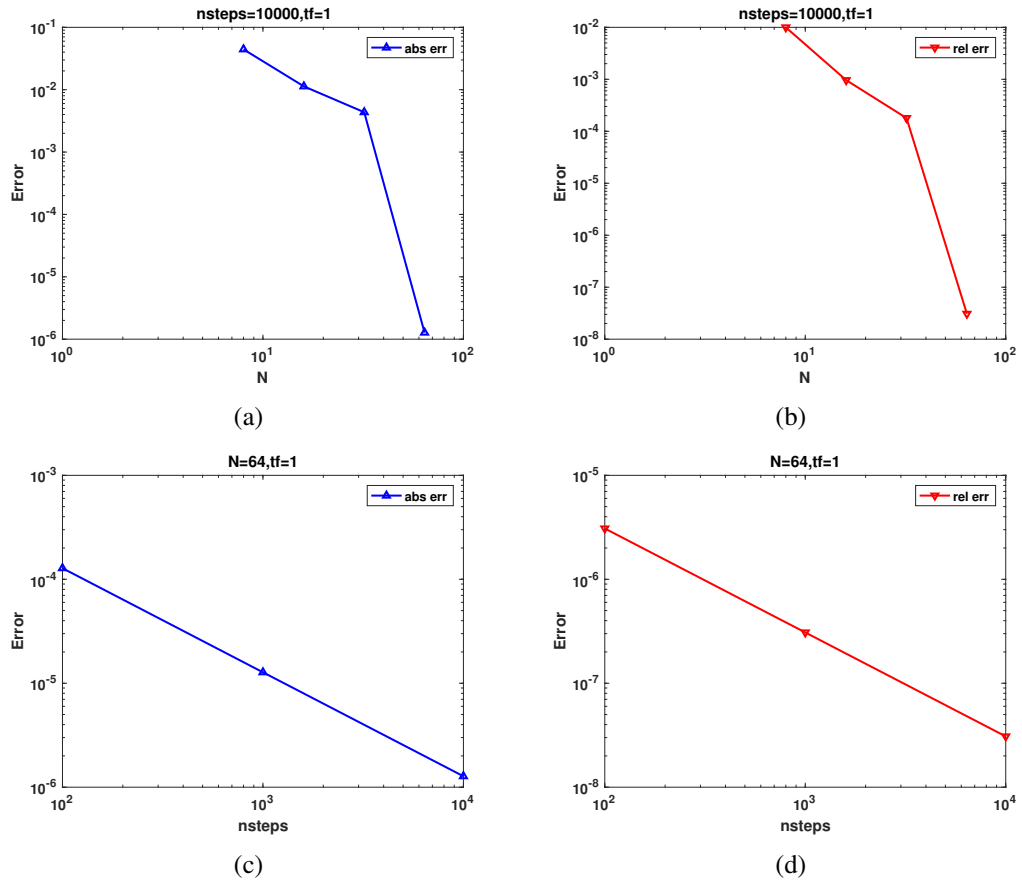

Figure 3.5: a and b: Absolute and relative errors versus grid points (N). c and d: Absolute and relative errors versus time steps. Parameters are $k_{on} = 10^2\ s^{-1}$, $k_{off} = 10\ s^{-1}$, $D_1 = 30\ \mu m^2/s$, $D_2 = 10^{-1}\ \mu m^2/s$ and $\omega_{r_n} = 0.5\ \mu m$.

grid points per dimension (N) for $nsteps = 10,000$ and $t_f = 1$. Like previous cases, it shows a decreasing trend for both absolute and relative errors by increasing N.

Figures 3.5c and 3.5d show absolute and relative errors versus time steps for $N = 64$ and $t_f = 1$. First-order accuracy in time is again observed. Table 3.9 shows the execution time, absolute error and relative error for different grid sizes with $nsteps = 10,000$ and parameters $k_{on} = 10^2\ s^{-1}$, $k_{off} = 10^{-1}\ s^{-1}$, $D_1 = 30\ \mu m^2/s$, $D_2 = 10^{-1}\ \mu m^2/s$ and $\omega_{r_n} = 0.5\ \mu m$. Table 3.10 shows the execution time, absolute error and relative error for different time step sizes with $N = 64$ for the same parameters.

It is particularly interesting to note that in test cases 3 and 4, the Courant-Friedrichs-Lewy (CFL) condition for forward Euler would require more than 9,000 time steps to ensure stability, but this KSS method, an explicit method, is able to not only ensure stability but also high accuracy even when greatly exceeding this CFL limit.

Chapter 4

Analysis Results

4.1 Solutions Analysis Without Time-stepping

The solutions u and b in physical spaces as well as positive frequency spaces without time-stepping for reaction dominant case, diffusion dominant case, effective diffusion case and pure diffusion dominant case, and full model case are shown. By tracking the dependency of solutions u and b in frequency and physical space, we can get a reasonable estimate of the fraction of both mobile and immobile species.

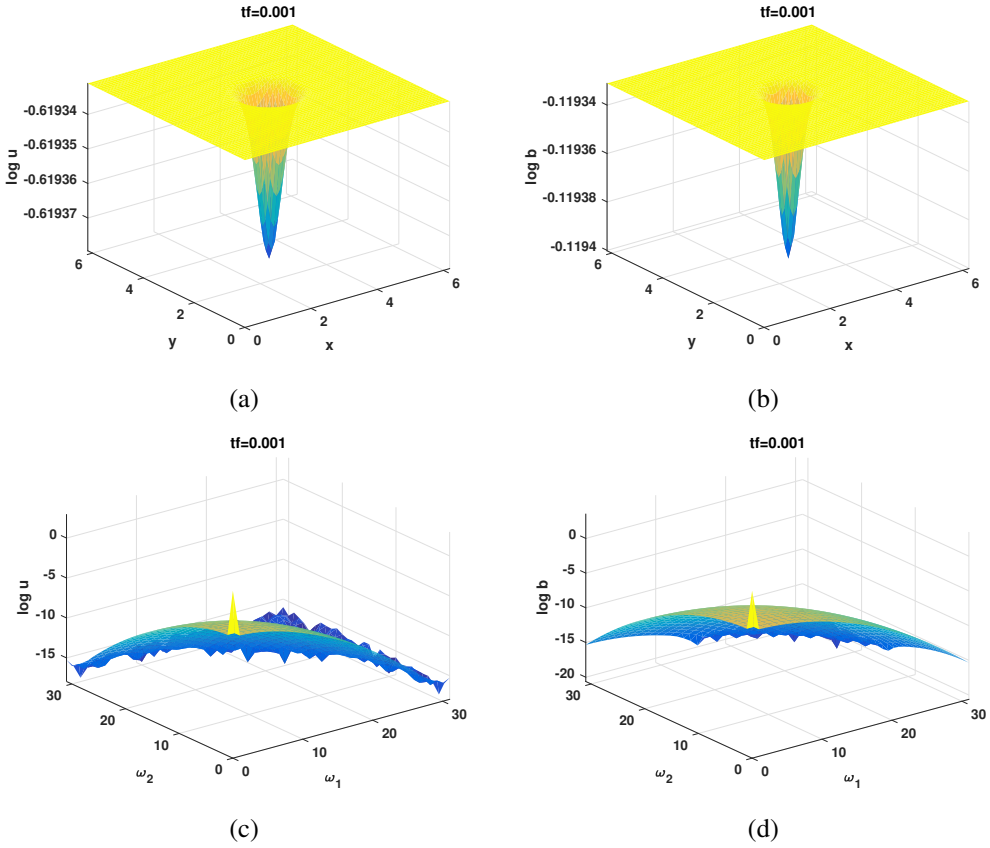

Figure 4.1: a) solution u (unbound) versus (x,y), b) solution b (bound) versus (x,y) with parameters $k_{on} = 10^{-0.5}\ s^{-1}$, $k_{off} = 10^{-1}\ s^{-1}$, $D_1 = 30\ \mu m^2/s$, $D_2 = 10^{-4}\ \mu m^2/s$ and $\omega_{rn} = 0.5\ \mu m$ for reaction-dominant case. c) solution u (unbound) versus frequencies (ω_1, ω_2), d) solution b (bound) versus frequencies. Final time is $tf = 0.001$.

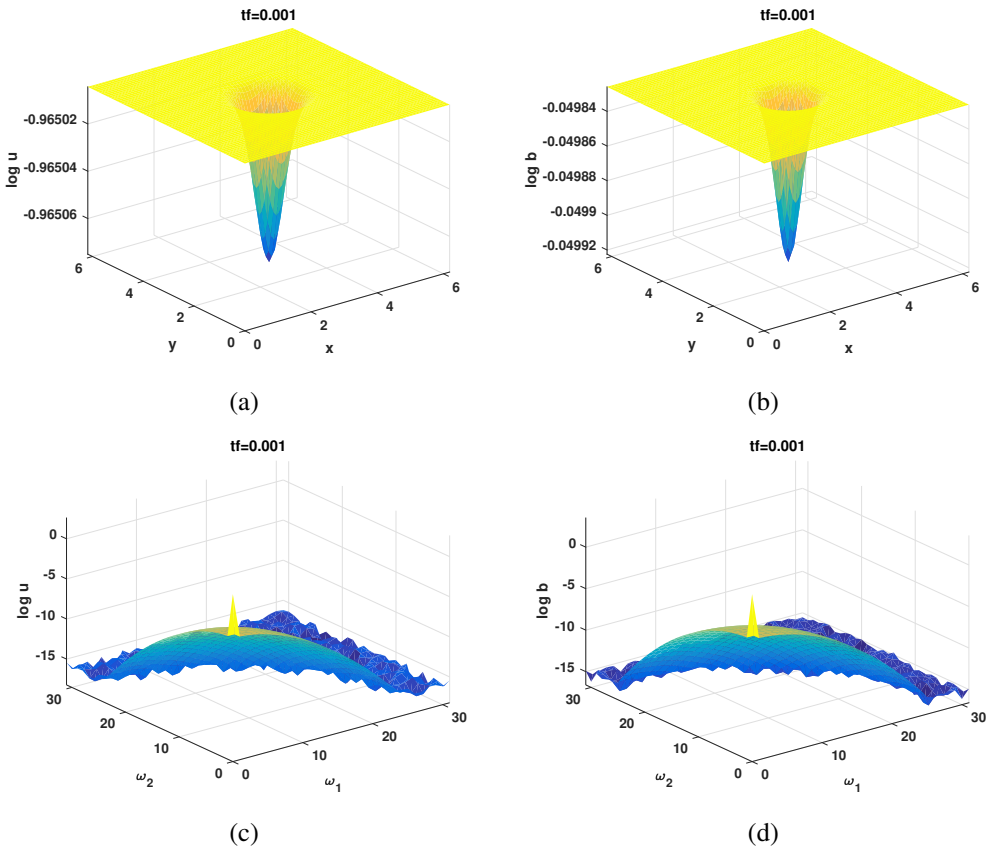

Figure 4.2: a) solution u (unbound) versus (x,y), b) solution b (bound) versus (x,y) with parameters $k_{on} = 255\ s^{-1}$, $k_{off} = 31\ s^{-1}$, $D_1 = 45\ \mu m^2/s$, $D_2 = 2.5\ \mu m^2/s$ and $\omega_{rn} = 0.6$ μm for diffusion-dominant case. c) solution u (unbound) versus frequencies (ω_1, ω_2), d) solution b (bound) versus frequencies. Final time is $tf = 0.001$.

Figures 4.1a and 4.1b show the solution in physical space, u (unbound) and b (bound) versus (x,y). Figures 4.1c and 4.1d show the solution in frequency space, u and b versus frequencies (ω_1, ω_2) for the reaction-dominant case. As shown, the center is located at (π, π) in physical space and the Gaussian solution with its height and width are trackable in physical space. Figures 4.2a and 4.2b show the solution in physical space, u (unbound) and b (bound) versus (x,y). Figures 4.2c and 4.2d show the solution in frequency space, u and b versus frequencies (ω_1, ω_2) for the diffusion-dominant case. Unlike the reaction dominant case, solutions are smoother in frequency space and the rate of decay is faster. Figures 4.3a and 4.3b show the solution in physical space, u (unbound) and b (bound) versus (x,y). Figures 4.3c and 4.3d show the solution in frequency space, u and b versus frequencies (ω_1, ω_2) for the effective diffusion case. Solutions show almost constant behavior in frequency space. Figures 4.4a and 4.4b show the solution in physical space, u (unbound) and b (bound) versus (x,y). Figures 4.4c and 4.4d show the solution in frequency space, u and b versus

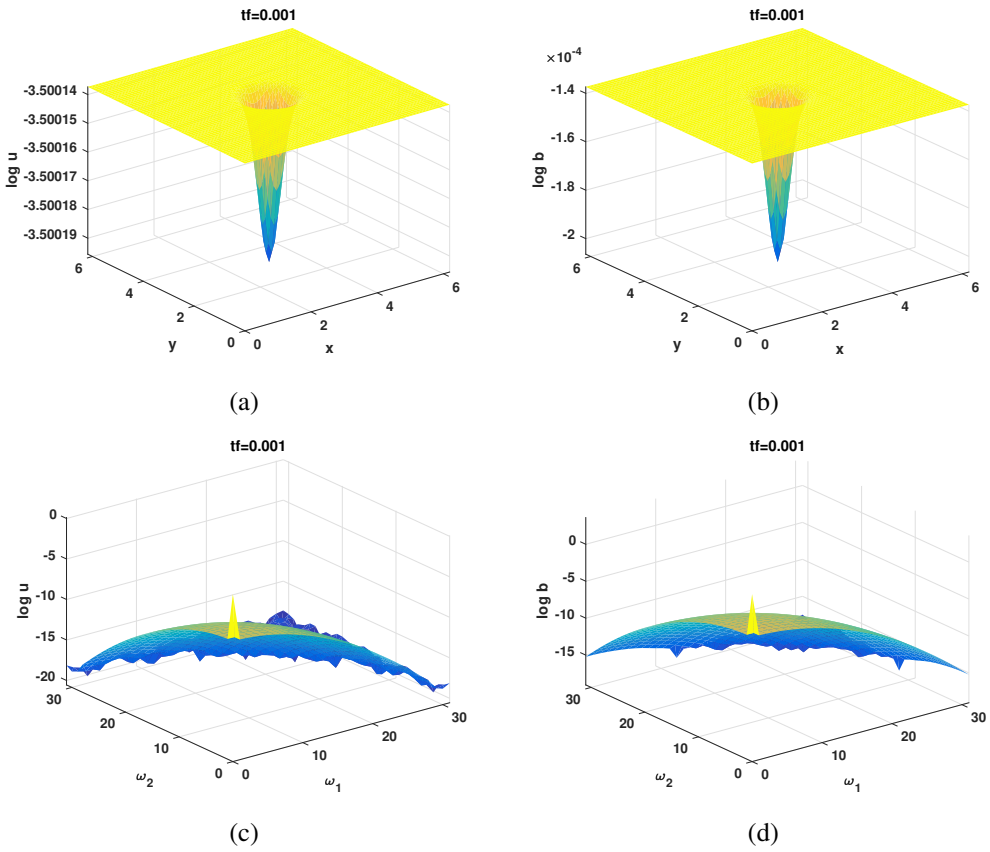

Figure 4.3: a) solution u (unbound) versus (x,y), b) solution b (bound) versus (x,y) with parameters $k_{on} = 10^{3.5}\ s^{-1}$, $k_{off} = 1\ s^{-1}$, $D_1 = 30\ \mu m^2/s$, $D_2 = 10^{-4}\ \mu m^2/s$ and $\omega_{rn} = 0.5$ μm for effective diffusion case. c) solution u (unbound) versus frequencies (ω_1, ω_2), d) solution b (bound) versus frequencies. Final time is $tf = 0.001$.

frequencies (ω_1, ω_2) for the pure diffusion case. We see similar behaviors with different values for solutions in both physical and frequency space. Figures 4.5a and 4.5b show the solution in physical space, u (unbound) and b (bound) versus (x,y). Figures 4.5c and 4.5d show the solution in frequency space, u and b versus frequencies (ω_1, ω_2) for the full model case. Like other cases we can track the heigh and width corresponding to both bound and unbound solutions.

4.2 Component Analysis

We plotted different variables in positive frequency space for different cases such as the reaction dominant, diffusion dominant, effective diffusion, pure diffusion dominant and full model case. Solutions u (unbound) and b (bound) are plotted in both frequencies and physical space for different time steps. The same figures are shown for the total solution

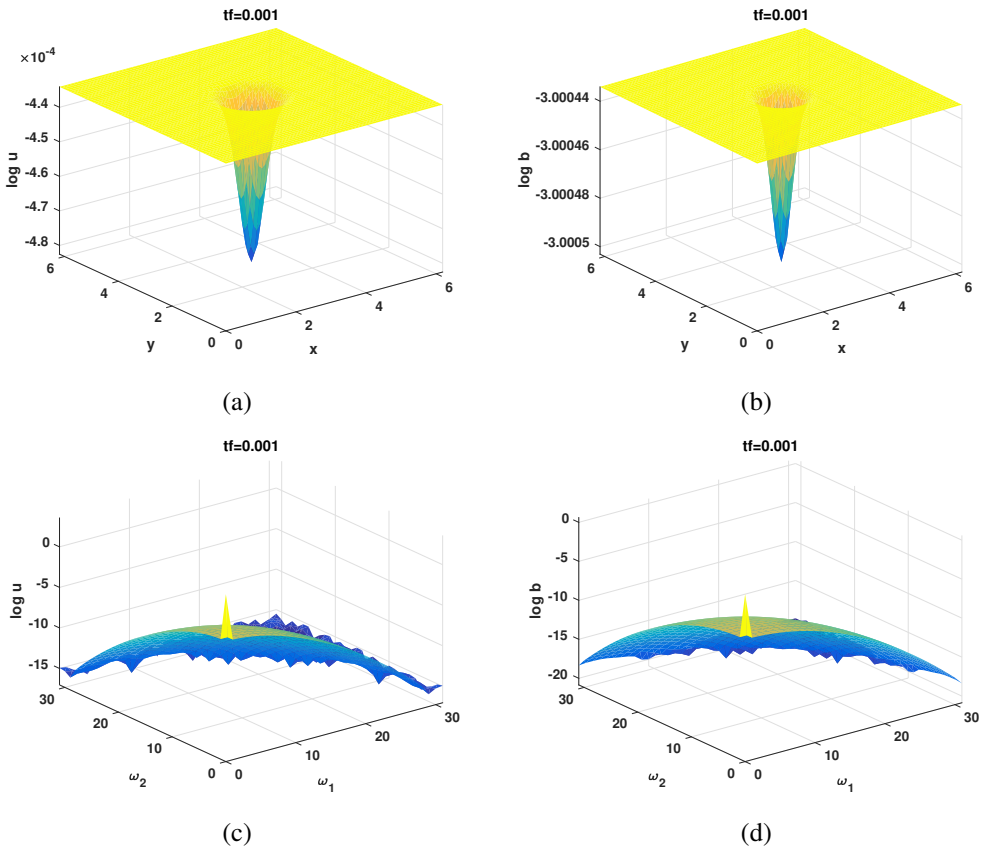

Figure 4.4: a) solution u (unbound) versus (x,y), b) solution b (bound) versus (x,y) with parameters $k_{on} = 10^{-2}\ s^{-1}$, $k_{off} = 10\ s^{-1}$, $D_1 = 30\ \mu m^2/s$, $D_2 = 10^{-4}\ \mu m^2/s$ and $\omega_{rn} = 0.5$ μm for pure diffusion case. c) solution u (unbound) versus frequencies (ω_1, ω_2), d) solution b (bound) versus frequencies. Final time is $tf = 0.001$.

$u+b$. In this chapter variables started with R refers to the first Arnoldi block which was described in chapter 3. Variables without R refer to the second Arnoldi block which was shown with $\tilde{}$ notation.

4.2.1 Reaction Dominant Case

Figure 4.6 shows eigenvalues of M_1 and $\tilde{M}_1$ versus frequencies (ω_1, ω_2) for parameters $k_{on} = 10^{-0.5}\ s^{-1}$, $k_{off} = 10^{-1}\ s^{-1}$, $D_1 = 30\ \mu m^2/s$, $D_2 = 10^{-4}\ \mu m^2/s$ and $\omega_{rn} = 0.5$ μm with $nsteps = 10,000$ and $tf = 1$. Figure 4.6a indicates the non-frequency-dependent eigenvalue since it is constant in frequency space. Figure 4.6b indicates the strongly frequency-dependent eigenvalue since its value varies in frequency space. Also, Figure 4.6c shows the non-frequency-dependent eigenvalue since it is constant in frequency space. Finally, Figure 4.6d shows the frequency-dependent eigenvalue since its value varies in frequency space.

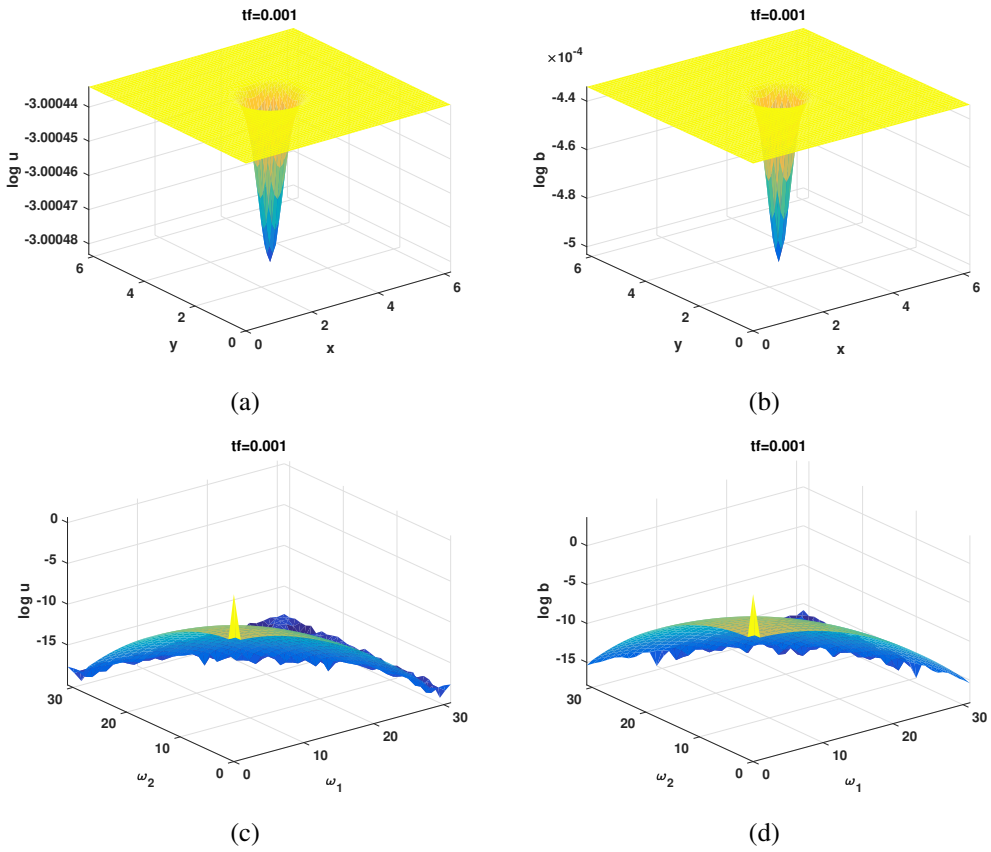

Figure 4.5: a) solution u (unbound) versus (x,y), b) solution b (bound) versus (x,y) with parameters $k_{on} = 10^2\ s^{-1}$, $k_{off} = 10^{-1}\ s^{-1}$, $D_1 = 30\ \mu m^2/s$, $D_2 = 10^{-1}\ \mu m^2/s$ and $\omega_{rn} = 0.5\ \mu m$ for full model case. c) solution u (unbound) versus frequencies (ω_1, ω_2), d) solution b (bound) versus frequencies. Final time is $tf = 0.001$.

Figure 4.7 shows the components of the M_1 versus frequencies (ω_1, ω_2) for parameters $k_{on} = 10^{-0.5}\ s^{-1}$, $k_{off} = 10^{-1}\ s^{-1}$, $D_1 = 30\ \mu m^2/s$, $D_2 = 10^{-4}\ \mu m^2/s$ and $\omega_{rn} = 0.5\ \mu m$ with $nsteps = 10,000$ and $tf = 1$. Figures 4.7a and 4.7d show components of M_1 which correspond to the eigenvalues of M_1 in Figures 4.6a and 4.6b. Figures 4.7b and 4.7c indicate that off-diagonal components of M_1 can be ignored for high frequencies.

Figure 4.8 shows the components of $\tilde{M}_1$ versus frequencies (ω_1, ω_2) for parameters $k_{on} = 10^{-0.5}\ s^{-1}$, $k_{off} = 10^{-1}\ s^{-1}$, $D_1 = 30\ \mu m^2/s$, $D_2 = 10^{-4}\ \mu m^2/s$ and $\omega_{rn} = 0.5\ \mu m$ with $nsteps = 10,000$ and $tf = 1$. Figures 4.8a and 4.8d show components of $\tilde{M}_1$ which correspond to the eigenvalues of $\tilde{M}_1$ in Figures 4.6c and 4.6d. Figures 4.8b and 4.8c indicate that off-diagonal components of $\tilde{M}_1$ can be ignored for high frequencies. Figure 4.9 shows the components of basis functions shown as u_{11}, u_{12}, u_{21} and u_{22} versus frequencies (ω_1, ω_2) for parameters $k_{on} = 10^{-0.5}\ s^{-1}$, $k_{off} = 10^{-1}\ s^{-1}$, $D_1 = 30\ \mu m^2/s$, $D_2 = 10^{-4}\ \mu m^2/s$ and $\omega_{rn} = 0.5\ \mu m$ with $nsteps = 10,000$ and $tf = 1$. Figures 4.9a and 4.9b show

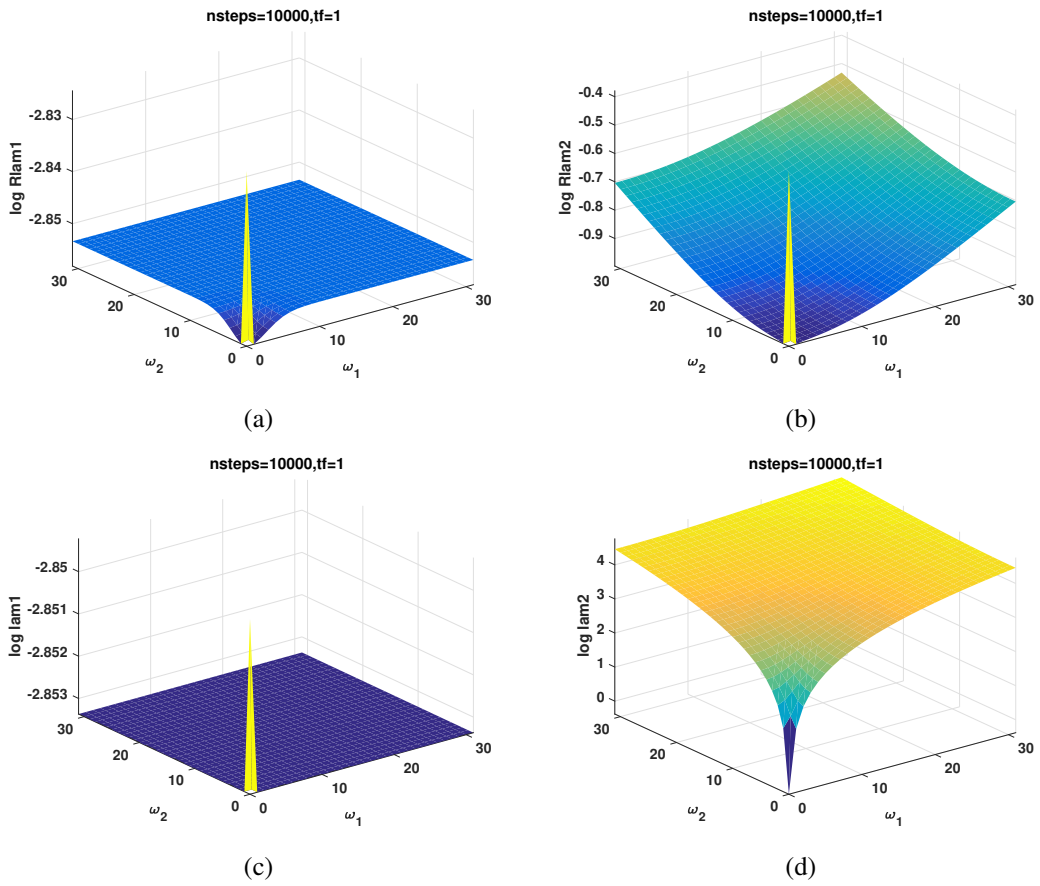

(a) (b)

(c) (d)

Figure 4.6: Eigenvalues versus frequencies (ω_1, ω_2) are shown with $nsteps = 10,000$ and $tf = 1$. Parameters are $k_{on} = 10^{-0.5}\ s^{-1}$, $k_{off} = 10^{-1}\ s^{-1}$, $D_1 = 30\ \mu m^2/s$ and $D_2 = 10^{-4}\ \mu m^2/s$.

the constant basis functions in frequency space. The absolute values of these basis functions are the constant k_{off}. Figures 4.9c and 4.9d show the other basis functions which vary in frequency space. Figure 4.9c shows stronger frequency dependence compared to Figure 4.9d.

Figure 4.10 shows the solutions u (unbound) and b (bound) in physical space (x,y) and frequency space (ω_1, ω_2) for parameters $k_{on} = 10^{-0.5}\ s^{-1}$, $k_{off} = 10^{-1}\ s^{-1}$, $D_1 = 30\ \mu m^2/s$, $D_2 = 10^{-4}\ \mu m^2/s$ and $\omega_{rn} = 0.5\ \mu m$ with $nsteps = 100$ and $tf = 1$. Figure 4.11 shows the solutions u (unbound) and b (bound) in physical space (x,y) and frequency space (ω_1, ω_2) for the same parameters with $nsteps = 10,000$ and $tf = 1$. Figure 4.12 shows the solutions u (unbound) and b (bound) in physical space (x,y) and frequency space (ω_1, ω_2) for the same parameters with $nsteps = 10,000$ and $tf = 1$. Comparison between Figures 4.10, 4.11 and 4.12 gives insight into the behavior of the solutions u (unbound) and b (bound) in both physical and frequency space over evolution of 100, 1,000 and 10,000 time steps.

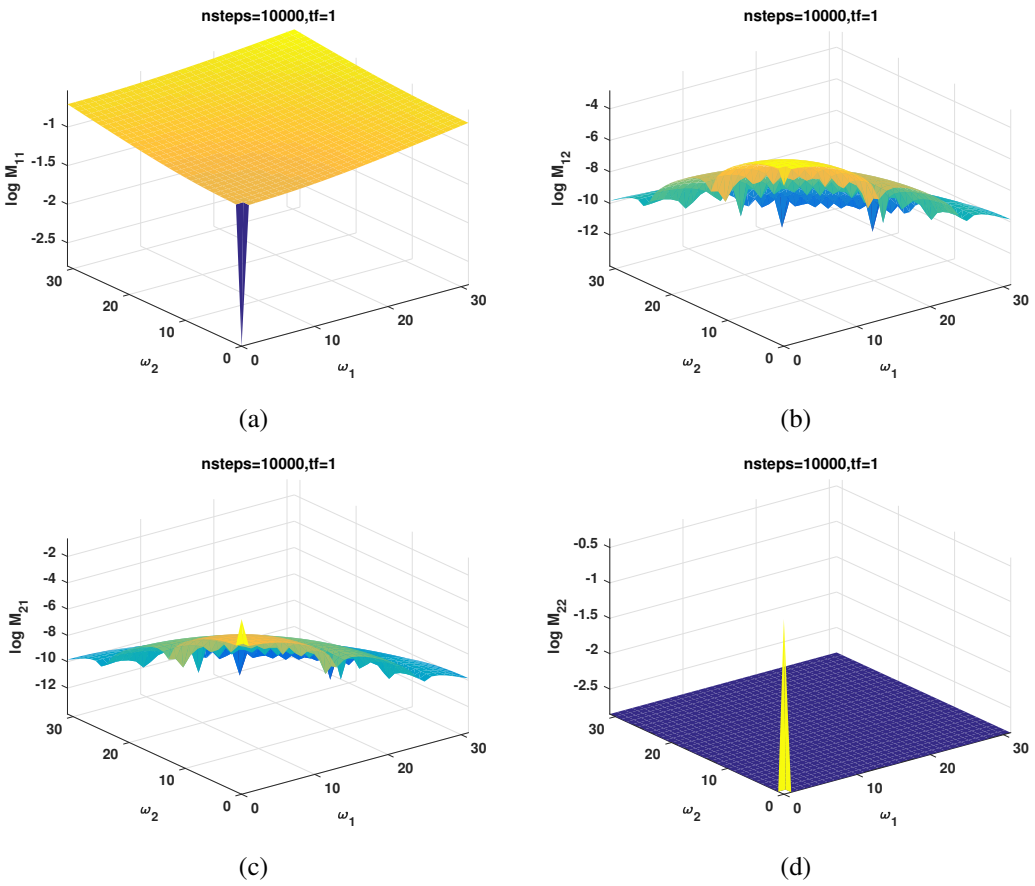

Figure 4.7: M_1 components versus frequencies (ω_1, ω_2) are shown with $nsteps = 10,000$ and $tf = 1$. Parameters are $k_{on} = 10^{-0.5}\ s^{-1}$, $k_{off} = 10^{-1}\ s^{-1}$, $D_1 = 30\ \mu m^2/s$ and $D_2 = 10^{-4}\ \mu m^2/s$.

These 3 sets of Figures provide us a comparison between solutions in both physical and frequency space at different time scales. Also, by tracking the dependence of solutions u (unbound) and b (bound) on the frequency and physical space variables, we can get a reasonable estimate of the fraction of both mobile and immobile species.

Figure 4.13 shows the total solution $u+b$ in physical space (x,y) for parameters $k_{on} = 10^{-0.5}\ s^{-1}$, $k_{off} = 10^{-1}\ s^{-1}$, $D_1 = 30\ \mu m^2/s$, $D_2 = 10^{-4}\ \mu m^2/s$ and $\omega_{rn} = 0.5\ \mu m$ with $nsteps = 100, 1,000, 10,000$ and $tf = 1$. It shows the evolution of the total solution $u+b$ on physical space for different time steps. Figure 4.14 shows the total solution $u+b$ in frequency space (ω_1, ω_2) for parameters $k_{on} = 10^{-0.5}\ s^{-1}$, $k_{off} = 10^{-1}\ s^{-1}$, $D_1 = 30\ \mu m^2/s$, $D_2 = 10^{-4}\ \mu m^2/s$ and $\omega_{rn} = 0.5\ \mu m$ with $nsteps = 100, 1,000, 10,000$ and $tf = 1$. It shows the evolution of the total solution $u+b$ in frequency space for different time steps.

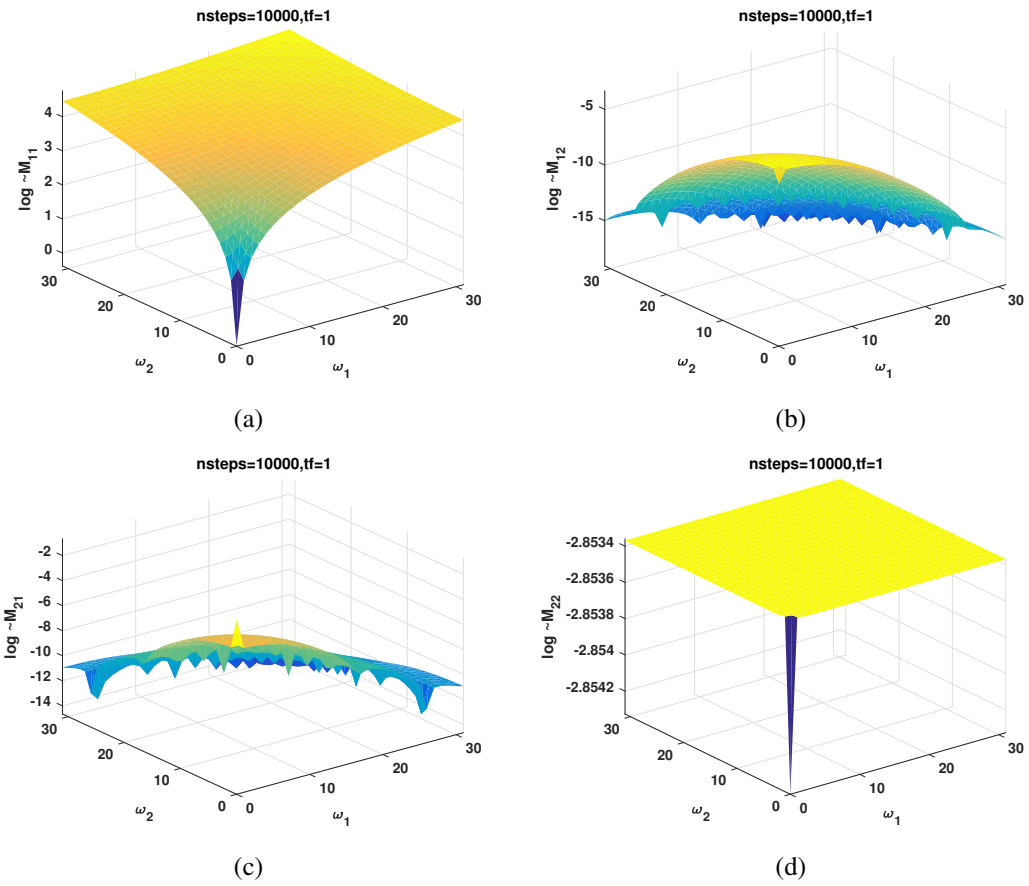

Figure 4.8: $\tilde{M}_1$ components versus frequencies (ω_1, ω_2) are shown with $nsteps = 10,000$ and $tf = 1$. Parameters are $k_{on} = 10^{-0.5}\ s^{-1}$, $k_{off} = 10^{-1}\ s^{-1}$, $D_1 = 30\ \mu m^2/s$ and $D_2 = 10^{-4}\ \mu m^2/s$.

4.2.2 Effective Diffusion Case

Figure 4.15 shows eigenvalues of M_1 and $\tilde{M}_1$ versus frequencies (ω_1, ω_2) for parameters $k_{on} = 10^{3.5}\ s^{-1}$, $k_{off} = 1\ s^{-1}$, $D_1 = 30\ \mu m^2/s$ and $\omega_{rn} = 0.5\ \mu m$ with $nsteps = 10,000$ and $tf = 1$. Figure 4.15a indicates the non-frequency-dependent eigenvalue since it is constant in frequency space. Figure 4.15b indicates the non-frequency-dependent eigenvalue since its value is constant in frequency space. Also, Figure 4.15c shows the non-frequency-dependent eigenvalue since it is constant in frequency space. Finally, Figure 4.15d shows the frequency-dependent eigenvalue since its value varies in frequency space. Figures 4.15a and 4.15c show more variation near the low frequencies compare to the previous case.

Figure 4.16 shows the components of the M_1 versus frequencies (ω_1, ω_2) for parameters $k_{on} = 10^{3.5}\ s^{-1}$, $k_{off} = 1\ s^{-1}$, $D_1 = 30\ \mu m^2/s$ and $\omega_{rn} = 0.5\ \mu m$ with $nsteps = 10,000$ and $tf = 1$. Figures 4.16a and 4.16d show components of M_1 which correspond to the

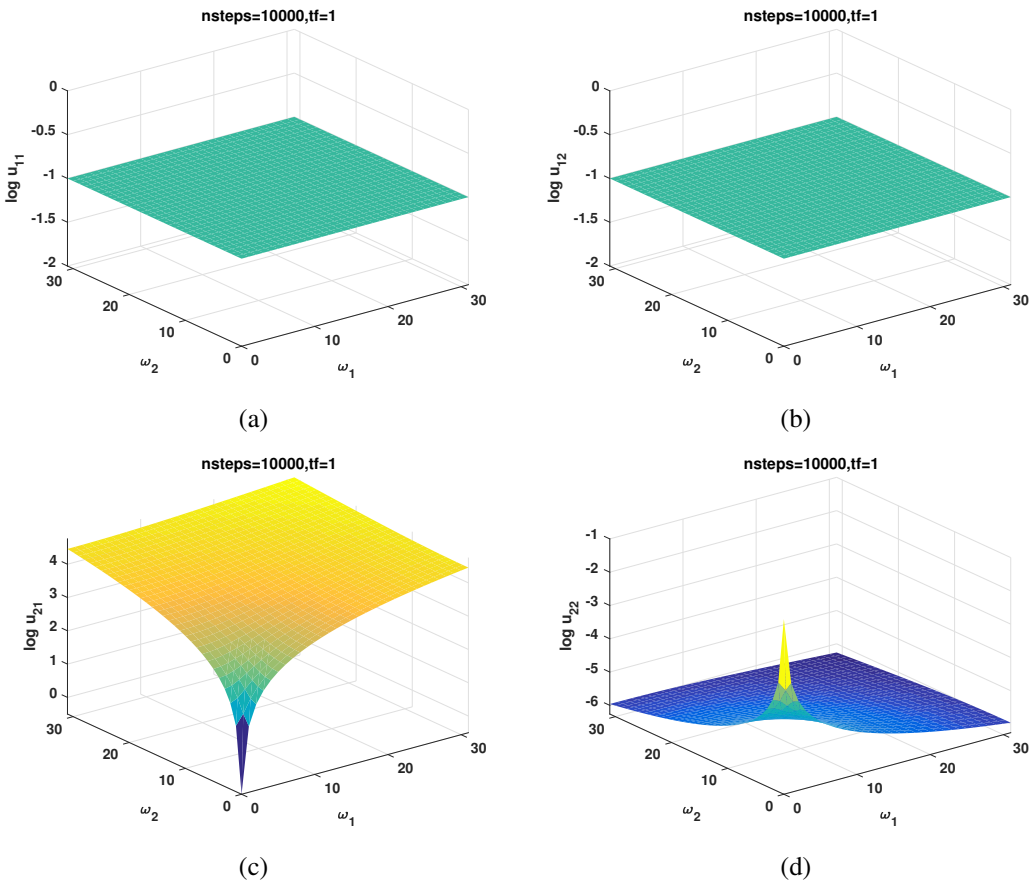

Figure 4.9: Basis function components versus frequencies (ω_1, ω_2) are shown with $nsteps = 10,000$ and $tf = 1$. Parameters are $k_{on} = 10^{-0.5}\ s^{-1}$, $k_{off} = 10^{-1}\ s^{-1}$, $D_1 = 30\ \mu m^2/s$ and $D_2 = 10^{-4}\ \mu m^2/s$.

eigenvalues of M_1 in Figures 4.15a and 4.15b. Figures 4.16b and 4.16c indicate that off-diagonal components of M_1 can be ignored for high frequencies.

Figure 4.17 shows the components of $\tilde{M}_1$ versus frequencies (ω_1, ω_2) for parameters $k_{on} = 10^{3.5}\ s^{-1}$, $k_{off} = 1\ s^{-1}$, $D_1 = 30\ \mu m^2/s$ and $\omega_{rn} = 0.5\ \mu m$ with $nsteps = 10,000$ and $tf = 1$. Figures 4.17a and 4.17d show components of $\tilde{M}_1$ which correspond to the eigenvalues of $\tilde{M}_1$ in Figures 4.15c and 4.15d. Figures 4.17b and 4.17c indicate that off-diagonal components of $\tilde{M}_1$ can be ignored for high frequencies. Figure 4.18 shows the components of basis functions shown as u_{11}, u_{12}, u_{21} and u_{22} versus frequencies (ω_1, ω_2) for parameters $k_{on} = 10^{3.5}\ s^{-1}$, $k_{off} = 1\ s^{-1}$, $D_1 = 30\ \mu m^2/s$ and $\omega_{rn} = 0.5\ \mu m$ with $nsteps = 10,000$ and $tf = 1$. Figures 4.18a and 4.18b show the constant basis functions in frequency space. The absolute values of these basis functions are the constant k_{off}. Figures 4.18c and 4.18d show the other basis functions which vary in frequency space. Figure 4.19 shows the solutions u (unbound) and b (bound) in physical space (x, y) and

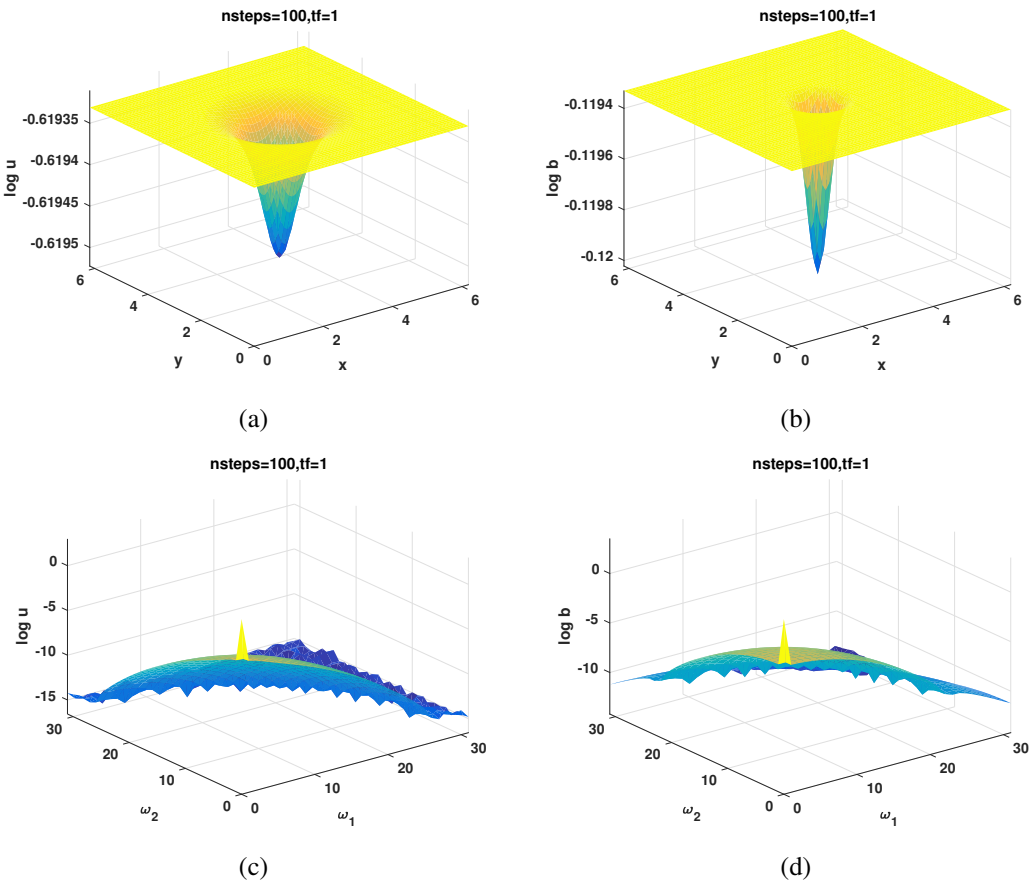

Figure 4.10: (a) and (b) solutions: u (unbound) and b (bound) versus coordinates (x,y) are shown with $nsteps = 100$ and $tf = 1$. (c) and (d) solutions: u (unbound) and b (bound) versus frequencies (ω_1, ω_2) are shown with $nsteps = 100$ and $tf = 1$. Parameters are $k_{on} = 10^{-0.5}\ s^{-1}$, $k_{off} = 10^{-1}\ s^{-1}$, $D_1 = 30\ \mu m^2/s$ and $D_2 = 10^{-4}\ \mu m^2/s$.

frequency space (ω_1, ω_2) for parameters $k_{on} = 10^{3.5}\ s^{-1}$, $k_{off} = 1\ s^{-1}$, $D_1 = 30\ \mu m^2/s$ and $\omega_{rn} = 0.5\ \mu m$ with $nsteps = 100$ and $tf = 1$. Figure 4.20 shows the solutions u (unbound) and b (bound) in physical space (x,y) and frequency space (ω_1, ω_2) for the same parameters with $nsteps = 10,000$ and $tf = 1$. Figure 4.21 shows the solutions u (unbound) and b (bound) in physical space (x,y) and frequency space (ω_1, ω_2) for the same parameters with $nsteps = 10,000$ and $tf = 1$. Comparison between Figures 4.19, 4.20 and 4.21 gives insight into the behavior of the solutions u (unbound) and b (bound) in both physical and frequency space over evolution of 100, 1,000 and 10,000 time steps. These 3 sets of Figures provide us a comparison between solutions in both physical and frequency space at different time scales. Also, by tracking the dependence of solutions u (unbound) and b (bound) on the frequency and physical space variables, we can get a reasonable estimate of the fraction of both mobile and immobile species.

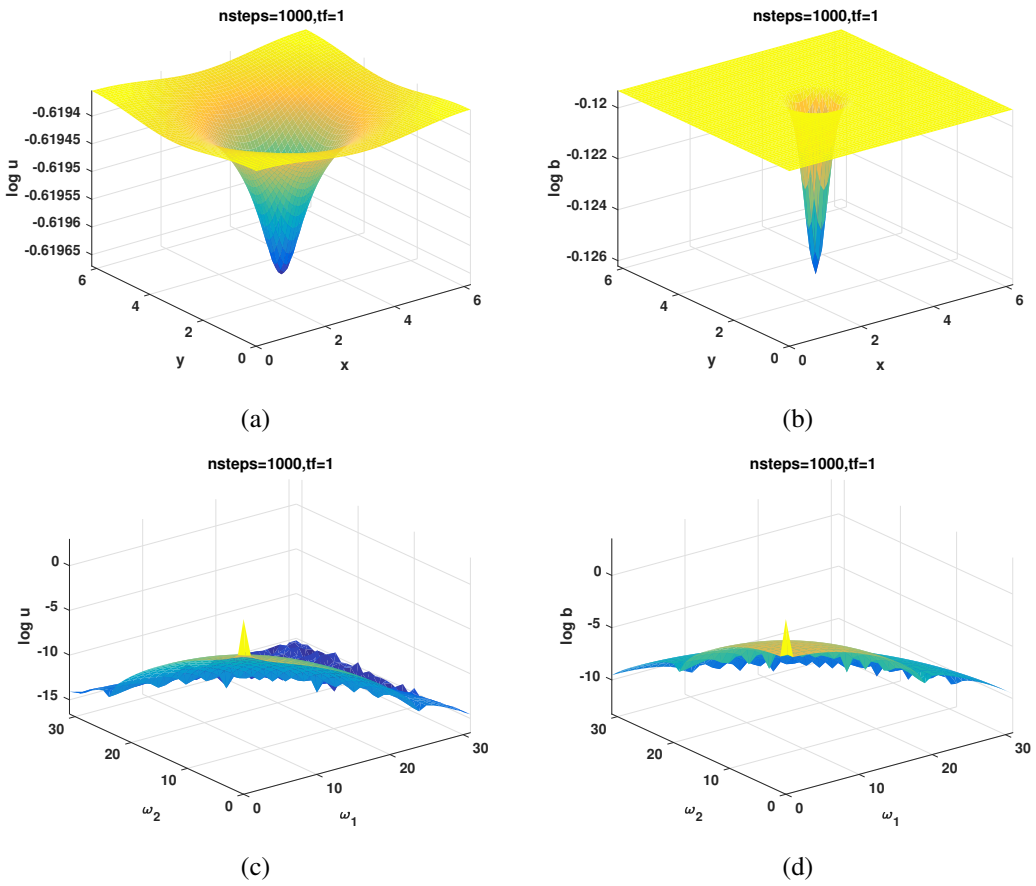

Figure 4.11: (a) and (b) solutions: u (unbound) and b (bound) versus coordinates (x,y) are shown with $nsteps = 1,000$ and $tf = 1$. (c) and (d) solutions: u (unbound) and b (bound) versus frequencies (ω_1, ω_2) are shown with $nsteps = 1,000$ and $tf = 1$. Parameters are $k_{on} = 10^{-0.5}\ s^{-1}$, $k_{off} = 10^{-1}\ s^{-1}$, $D_1 = 30\ \mu m^2/s$ and $D_2 = 10^{-4}\ \mu m^2/s$.

Figure 4.22 shows the total solution $u+b$ in physical space (x,y) for parameters $k_{on} = 10^{3.5}\ s^{-1}$, $k_{off} = 1\ s^{-1}$, $D_1 = 30\ \mu m^2/s$ and $\omega_{rn} = 0.5\ \mu m$ with $nsteps = 100, 1,000, 10,000$ and $tf = 1$. It shows the evolution of the total solution $u+b$ on physical space for different time steps. Figure 4.23 shows the total solution $u+b$ in frequency space (ω_1, ω_2) for parameters $k_{on} = 10^{3.5}\ s^{-1}$, $k_{off} = 1\ s^{-1}$, $D_1 = 30\ \mu m^2/s$ and $\omega_{rn} = 0.5\ \mu m$ with $nsteps = 100, 1,000, 10,000$ and $tf = 1$. It shows the evolution of the total solution $u+b$ in frequency space for different time steps.

4.2.3 Pure Diffusion Dominant Case

Figure 4.24 shows eigenvalues of M_1 and $\tilde{M}_1$ versus frequencies (ω_1, ω_2) for parameters $k_{on} = 10^{-2}\ s^{-1}$, $k_{off} = 10\ s^{-1}$, $D_1 = 30\ \mu m^2/s$ and $\omega_{rn} = 0.5\ \mu m$ with $nsteps = 10,000$ and $tf = 1$. Figure 4.24a indicates the non-frequency-dependent eigenvalue since it is constant

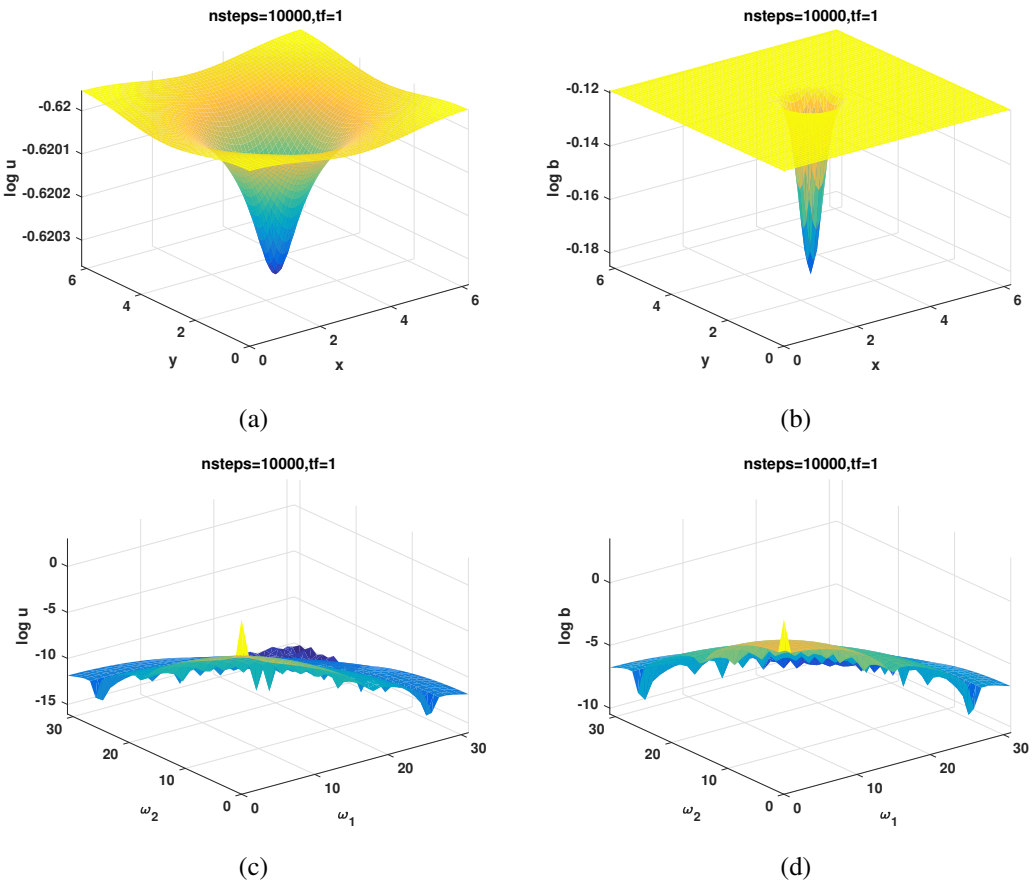

Figure 4.12: (a) and (b) solutions: u (unbound) and b (bound) versus coordinates (x,y) are shown with $nsteps = 10,000$ and $tf = 1$. (c) and (d) solutions: u (unbound) and b (bound) versus frequencies (ω_1, ω_2) are shown with $nsteps = 10,000$ and $tf = 1$. Parameters are $k_{on} = 10^{-0.5}\ s^{-1}$, $k_{off} = 10^{-1}\ s^{-1}$, $D_1 = 30\ \mu m^2/s$ and $D_2 = 10^{-4}\ \mu m^2/s$.

in frequency space. Figure 4.24b indicates the frequency-dependent eigenvalue since its value varies in frequency space. Also, Figure 4.24c shows the non-frequency-dependent eigenvalue since it is constant in frequency space with few oscillations near low frequencies. Finally, Figure 4.24d shows the frequency-dependent eigenvalue since its value varies in frequency space.

Figure 4.25 shows the components of the M_1 versus frequencies (ω_1, ω_2) for parameters $k_{on} = 10^{-2}\ s^{-1}$, $k_{off} = 10\ s^{-1}$, $D_1 = 30\ \mu m^2/s$ and $\omega_{rn} = 0.5\ \mu m$ with $nsteps = 10,000$ and $tf = 1$. Figures 4.25a and 4.25d show components of M_1 which correspond to the eigenvalues of M_1 in Figures 4.24a and 4.24b. Figures 4.25b and 4.25c indicate that off-diagonal components of M_1 can be ignored for high frequencies.

Figure 4.26 shows the components of $\tilde{M}_1$ versus frequencies (ω_1, ω_2) for parameters $k_{on} = 10^{-2}\ s^{-1}$, $k_{off} = 10\ s^{-1}$, $D_1 = 30\ \mu m^2/s$ and $\omega_{rn} = 0.5\ \mu m$ with $nsteps = 10,000$

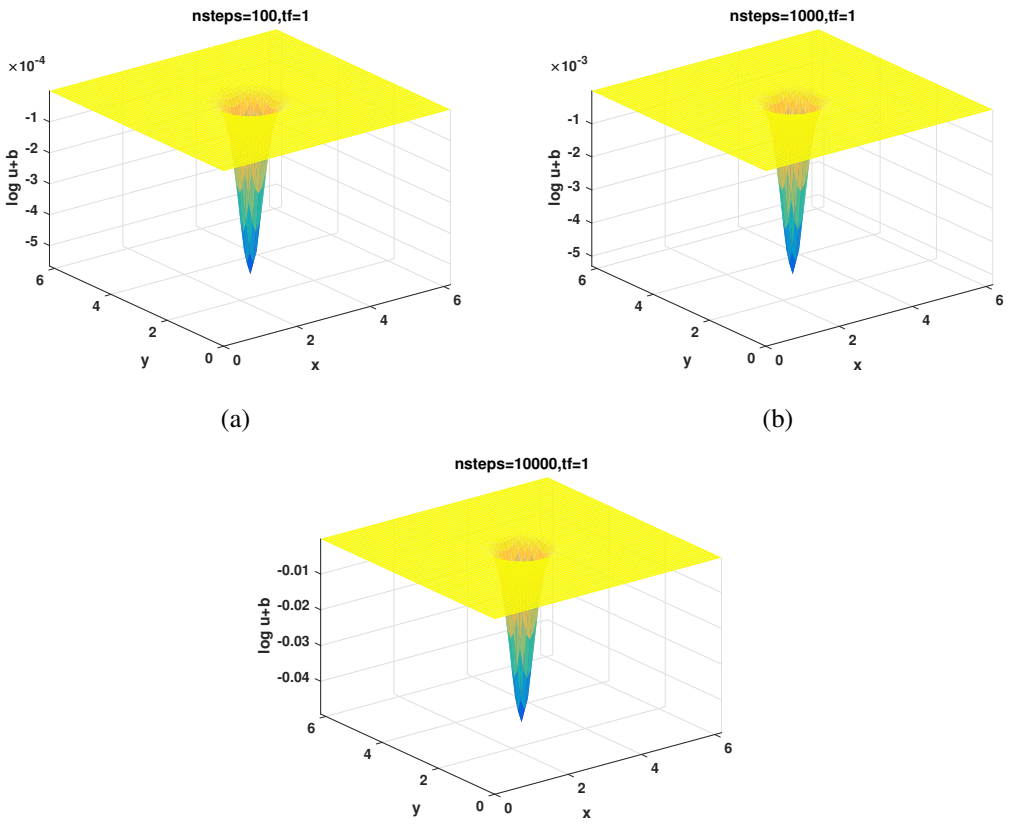

(a) (b)

(c)

Figure 4.13: Solutions $u+b$ versus coordinates (x,y) are shown with $nsteps = 100,1,000,10,000$ and $tf = 1$. Parameters are $k_{on} = 10^{-0.5}\ s^{-1}$, $k_{off} = 10^{-1}\ s^{-1}$, $D_1 = 30\ \mu m^2/s$ and $D_2 = 10^{-4}\ \mu m^2/s$.

and $tf = 1$. Figures 4.26a and 4.26d show components of $\tilde{M}_1$ which correspond to the eigenvalues of $\tilde{M}_1$ in Figures 4.24c and 4.24d. Figures 4.26b and 4.26c indicate that off-diagonal components of $\tilde{M}_1$ can be ignored for high frequencies. Figure 4.27 shows the components of basis functions shown as u_{11}, u_{12}, u_{21} and u_{22} versus frequencies (ω_1,ω_2) for parameters $k_{on} = 10^{-2}\ s^{-1}$, $k_{off} = 10\ s^{-1}$, $D_1 = 30\ \mu m^2/s$ and $\omega_{rn} = 0.5\ \mu m$ with $nsteps = 10,000$ and $tf = 1$. Figures 4.27a and 4.27b show the constant basis functions in frequency space. The absolute values of these basis functions are the constant k_{off}. Figures 4.27c and 4.27d show the other basis functions which vary in frequency space. Figure 4.27c shows stronger frequency dependence compared to Figure 4.27d. Figure 4.28 shows the solutions u (unbound) and b (bound) in physical space (x,y) and frequency space (ω_1,ω_2) for parameters $k_{on} = 10^{-2}\ s^{-1}$, $k_{off} = 10\ s^{-1}$, $D_1 = 30\ \mu m^2/s$ and $\omega_{rn} = 0.5$ μm with $nsteps = 100$ and $tf = 1$. Figure 4.29 shows the solutions u (unbound) and b (bound) in physical space (x,y) and frequency space (ω_1,ω_2) for the same parameters

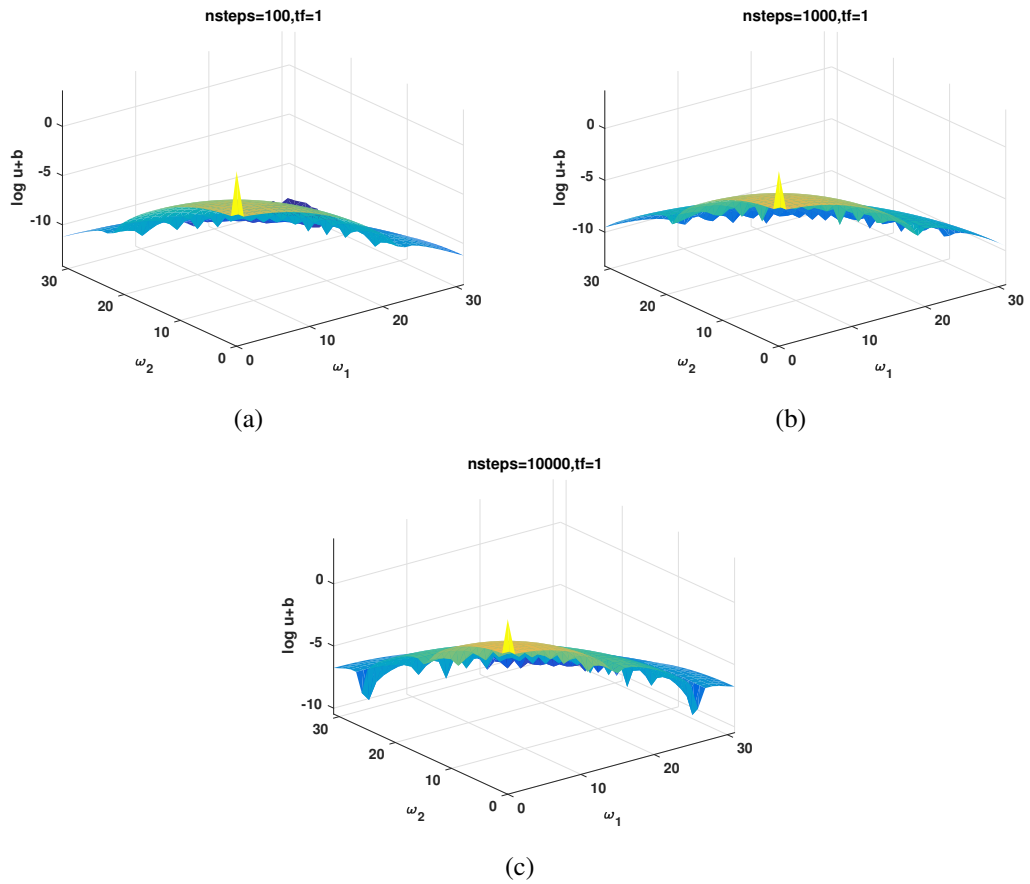

Figure 4.14: Solutions $u+b$ versus frequencies ω_1 and ω_2 are shown with $nsteps = 100, 1,000, 10,000$ and $tf = 1$. Parameters are $k_{on} = 10^{-0.5}\ s^{-1}$, $k_{off} = 10^{-1}\ s^{-1}$, $D_1 = 30\ \mu m^2/s$ and $D_2 = 10^{-4}\ \mu m^2/s$.

with $nsteps = 10,000$ and $tf = 1$. Figure 4.30 shows the solutions u (unbound) and b (bound) in physical space (x,y) and frequency space (ω_1, ω_2) for the same parameters with $nsteps = 10,000$ and $tf = 1$. Comparison between Figures 4.28, 4.29 and 4.30 gives insight into the behavior of the solutions u (unbound) and b (bound) in both physical and frequency space over evolution of 100, 1,000 and 10,000 time steps. These 3 sets of Figures provide us a comparison between solutions in both physical and frequency space at different time scales. Also, by tracking the dependence of solutions u (unbound) and b (bound) on the frequency and physical space variables, we can get a reasonable estimate of the fraction of both mobile and immobile species.

Figure 4.31 shows the total solution $u+b$ in physical space (x,y) for parameters $k_{on} = 10^{-2}\ s^{-1}$, $k_{off} = 10\ s^{-1}$, $D_1 = 30\ \mu m^2/s$ and $\omega_{rn} = 0.5\ \mu m$ with $nsteps = 100, 1,000, 10,000$ and $tf = 1$. It shows the evolution of the total solution $u+b$ on physical space for different time steps. Figure 4.32 shows the total solution $u+b$ in frequency space (ω_1, ω_2)

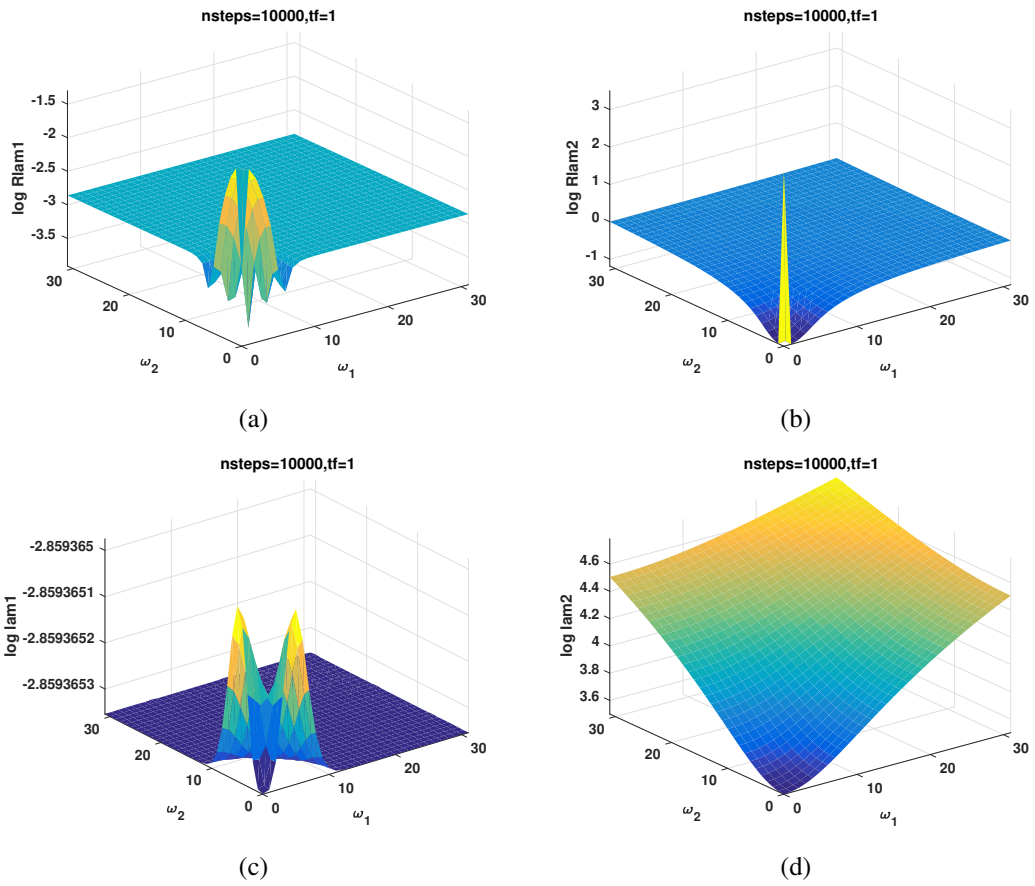

Figure 4.15: Eigenvalues versus frequencies (ω_1, ω_2) are shown with $nsteps = 10,000$ and $tf = 1$. Parameters are $k_{on} = 10^{3.5}\ s^{-1}$, $k_{off} = 1\ s^{-1}$, $D_1 = 30\ \mu m^2/s$ and $D_2 = 10^{-4}\ \mu m^2/s$.

for parameters $k_{on} = 10^{-2}\ s^{-1}$, $k_{off} = 10\ s^{-1}$, $D_1 = 30\ \mu m^2/s$ and $\omega_{rn} = 0.5\ \mu m$ with $nsteps = 100, 1,000, 10,000$ and $tf = 1$. It shows the evolution of the total solution $u + b$ in frequency space for different time steps.

4.2.4 Diffusion Dominant Case

Figure 4.33 shows eigenvalues of M_1 and $\tilde{M}_1$ versus frequencies (ω_1, ω_2) for parameters $k_{on} = 255\ s^{-1}$, $k_{off} = 31\ s^{-1}$, $D_1 = 45\ \mu m^2/s$ and $D_2 = 2.5\ \mu m^2/s$ and $\omega_{rn} = 0.6\ \mu m$ with $nsteps = 10,000$ and $tf = 1$. Figure 4.33a indicates the non-frequency-dependent eigenvalue since it is constant in frequency space. Figure 4.33b indicates the frequency-dependent eigenvalue since its value varies in frequency space. Also, Figure 4.33c shows the non-frequency-dependent eigenvalue since it is constant in frequency space. Finally, Figure 4.33d shows the frequency-dependent eigenvalue since its value varies in frequency space. Figures 4.33a and 4.33c have few oscillations near low frequencies.

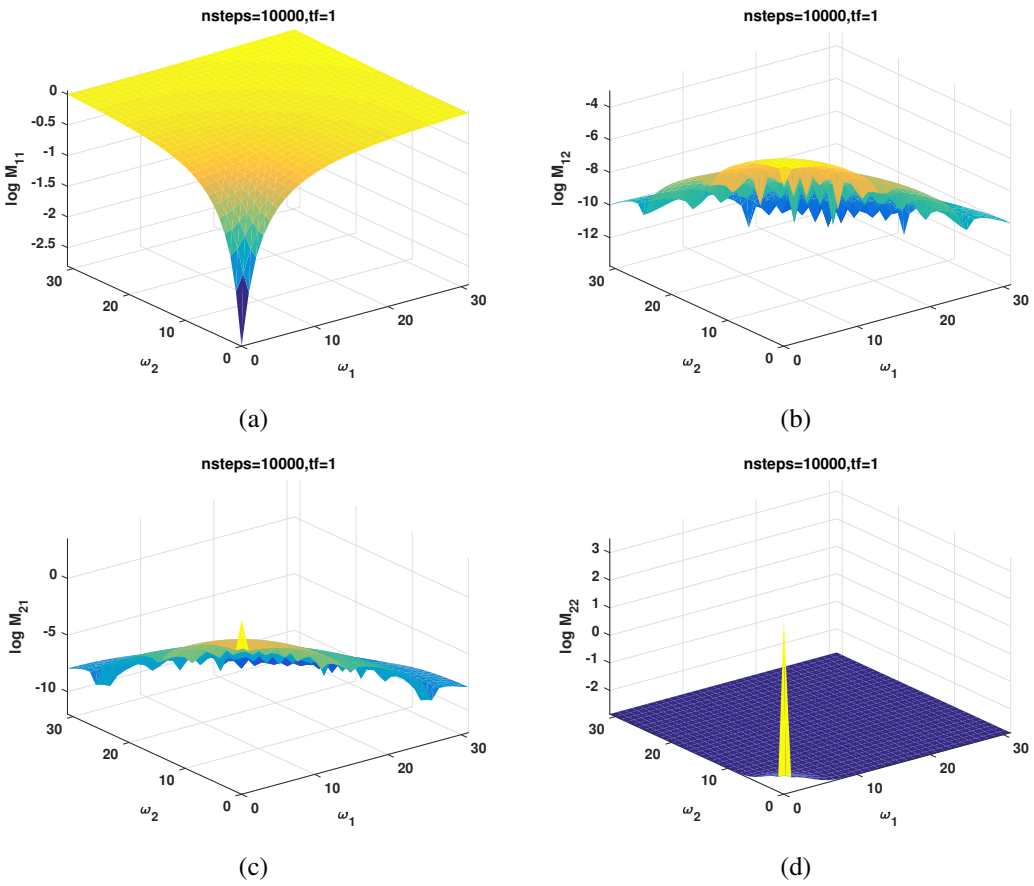

Figure 4.16: M_1 components versus frequencies (ω_1, ω_2) are shown with $nsteps = 10,000$ and $tf = 1$. Parameters are $k_{on} = 10^{3.5}\ s^{-1}$, $k_{off} = 1\ s^{-1}$, $D_1 = 30\ \mu m^2/s$ and $D_2 = 10^{-4}\ \mu m^2/s$.

Figure 4.34 shows the components of the M_1 versus frequencies (ω_1, ω_2) for parameters $k_{on} = 255\ s^{-1}$, $k_{off} = 31\ s^{-1}$, $D_1 = 45\ \mu m^2/s$ and $D_2 = 2.5\ \mu m^2/s$ and $\omega_{rn} = 0.6\ \mu m$ with $nsteps = 10,000$ and $tf = 1$. Figures 4.34a and 4.34d show components of M_1 which correspond to the eigenvalues of M_1 in Figures 4.33a and 4.33b. Figures 4.34b and 4.34c indicate that off-diagonal components of M_1 can be ignored for high frequencies.

Figure 4.35 shows the components of $\tilde{M}_1$ versus frequencies (ω_1, ω_2) for parameters $k_{on} = 255\ s^{-1}$, $k_{off} = 31\ s^{-1}$, $D_1 = 45\ \mu m^2/s$ and $D_2 = 2.5\ \mu m^2/s$ and $\omega_{rn} = 0.6\ \mu m$ with $nsteps = 10,000$ and $tf = 1$. Figures 4.35a and 4.35d show components of $\tilde{M}_1$ which correspond to the eigenvalues of $\tilde{M}_1$ in Figures 4.33c and 4.33d. Figures 4.35b and 4.35c indicate that off-diagonal components of $\tilde{M}_1$ can be ignored for high frequencies. Figure 4.36 shows the components of basis functions shown as u_{11}, u_{12}, u_{21} and u_{22} versus frequencies (ω_1, ω_2) for parameters $k_{on} = 255\ s^{-1}$, $k_{off} = 31\ s^{-1}$, $D_1 = 45\ \mu m^2/s$ and $D_2 = 2.5\ \mu m^2/s$ and $\omega_{rn} = 0.6\ \mu m$ with $nsteps = 10,000$ and $tf = 1$. Figures 4.36a and 4.36b show the

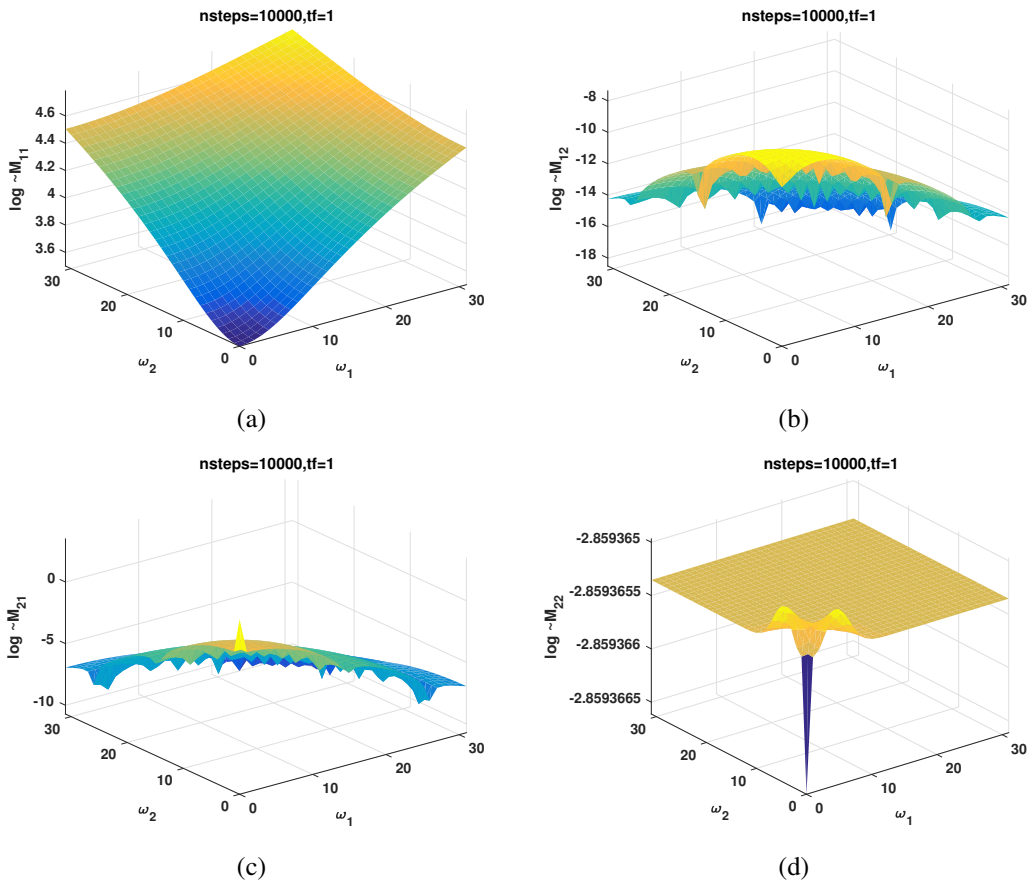

Figure 4.17: $\tilde{M}_1$ components versus frequencies (ω_1, ω_2) are shown with $nsteps = 10,000$ and $tf = 1$. Parameters are $k_{on} = 10^{3.5}\ s^{-1}$, $k_{off} = 1\ s^{-1}$, $D_1 = 30\ \mu m^2/s$ and $D_2 = 10^{-4}\ \mu m^2/s$.

constant basis functions in frequency space. The absolute values of these basis functions are the constant k_{off}. Figures 4.36c and 4.36d show the other basis functions which vary in frequency space. Figure 4.36c shows stronger frequency dependence compared to Figure 4.36d. Figure 4.37 shows the solutions u (unbound) and b (bound) in physical space (x,y) and frequency space (ω_1, ω_2) for parameters $k_{on} = 255\ s^{-1}$, $k_{off} = 31\ s^{-1}$, $D_1 = 45\ \mu m^2/s$ and $D_2 = 2.5\ \mu m^2/s$ and $\omega_{rn} = 0.6\ \mu m$ with $nsteps = 100$ and $tf = 1$. Figure 4.38 shows the solutions u (unbound) and b (bound) in physical space (x,y) and frequency space (ω_1, ω_2) for the same parameters with $nsteps = 10,000$ and $tf = 1$. Figure 4.39 shows the solutions u (unbound) and b (bound) in physical space (x,y) and frequency space (ω_1, ω_2) for the same parameters with $nsteps = 10,000$ and $tf = 1$. Comparison between Figures 4.37, 4.38 and 4.39 gives insight into the behavior of the solutions u (unbound) and b (bound) in both physical and frequency space over evolution of 100, 1,000 and 10,000 time steps. These 3 sets of Figures provide us a comparison between solutions in both physical and frequency

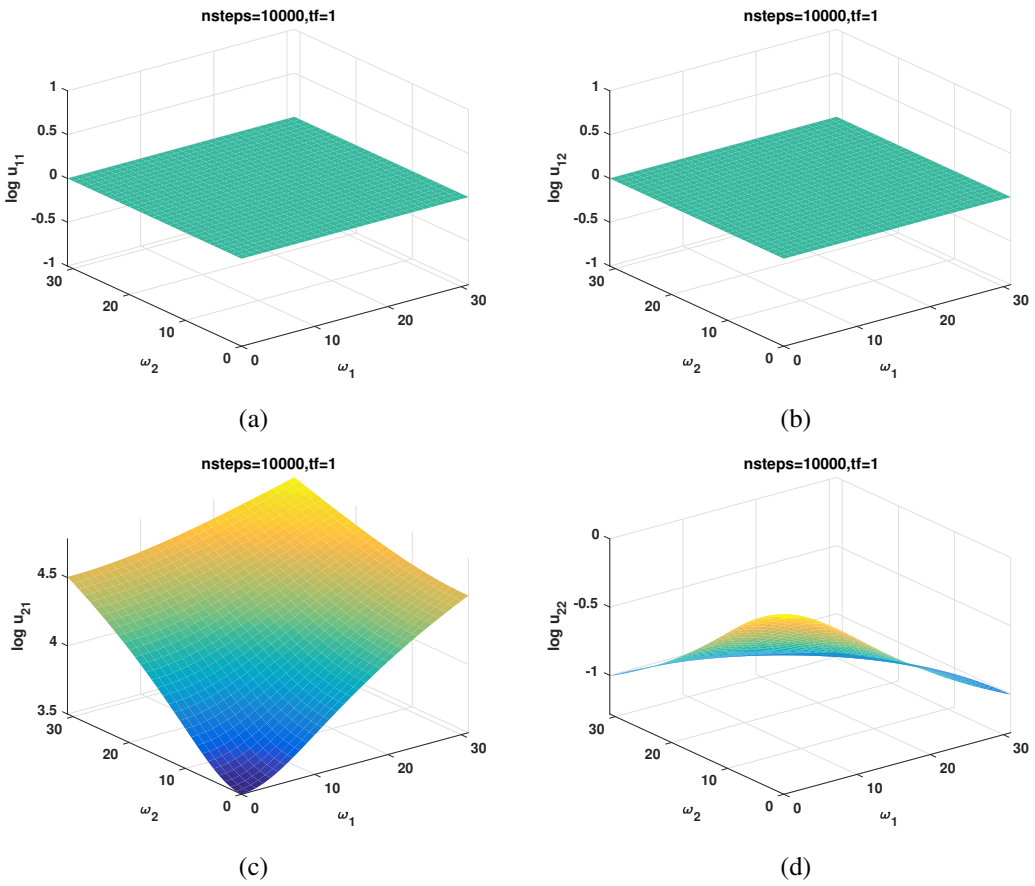

Figure 4.18: Basis function components versus frequencies (ω_1, ω_2) are shown with $nsteps = 10,000$ and $tf = 1$. Parameters are $k_{on} = 10^{3.5}\ s^{-1}$, $k_{off} = 1\ s^{-1}$, $D_1 = 30\ \mu m^2/s$ and $D_2 = 10^{-4}\ \mu m^2/s$.

space at different time scales. Also, by tracking the dependence of solutions u (unbound) and b (bound) on the frequency and physical space variables, we can get a reasonable estimate of the fraction of both mobile and immobile species.

Figure 4.40 shows the total solution $u+b$ in physical space (x,y) for parameters $k_{on} = 255\ s^{-1}$, $k_{off} = 31\ s^{-1}$, $D_1 = 45\ \mu m^2/s$ and $D_2 = 2.5\ \mu m^2/s$ and $\omega_{rn} = 0.6\ \mu m$ with $nsteps = 100, 1,000, 10,000$ and $tf = 1$. It shows the evolution of the total solution $u+b$ on physical space for different time steps. Figure 4.41 shows the total solution $u+b$ in frequency space (ω_1, ω_2) for parameters $k_{on} = 255\ s^{-1}$, $k_{off} = 31\ s^{-1}$, $D_1 = 45\ \mu m^2/s$ and $D_2 = 2.5\ \mu m^2/s$ and $\omega_{rn} = 0.6\ \mu m$ with $nsteps = 100, 1,000, 10,000$ and $tf = 1$. It shows the evolution of the total solution $u+b$ in frequency space for different time steps.

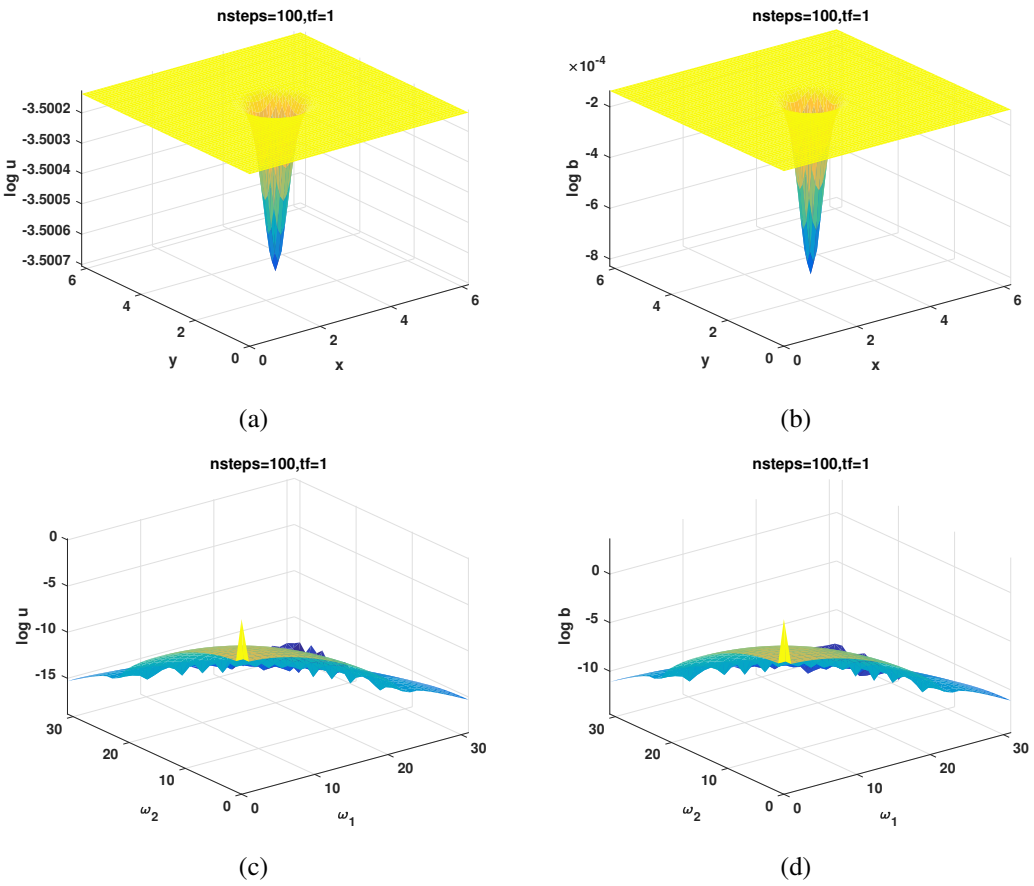

Figure 4.19: (a) and (b) solutions: u (unbound) and b (bound) versus coordinates (x,y) are shown with $nsteps = 100$ and $tf = 1$. (c) and (d) solutions: u (unbound) and b (bound) versus frequencies (ω_1, ω_2) are shown with $nsteps = 100$ and $tf = 1$. Parameters are $k_{on} = 10^{3.5}\ s^{-1}$, $k_{off} = 1\ s^{-1}$, $D_1 = 30\ \mu m^2/s$ and $D_2 = 10^{-4}\ \mu m^2/s$.

4.2.5 Full Model Case

Figure 4.42 shows eigenvalues of M_1 and $\tilde{M}_1$ versus frequencies (ω_1, ω_2) for parameters $k_{on} = 10^2\ s^{-1}$, $k_{off} = 10^{-1}\ s^{-1}$, $D_1 = 30\ \mu m^2/s$ and $D_2 = 10^{-1}\ \mu m^2/s$ and $\omega_{rn} = 0.5\ \mu m$ with $nsteps = 10,000$ and $tf = 1$. Figure 4.42a indicates the non-frequency-dependent eigenvalue since it is constant in frequency space. Figure 4.42b indicates the frequency-dependent eigenvalue since its value varies in frequency space. Figure 4.42c indicates the non-frequency-dependent eigenvalue since it is constant in frequency space. Finally, Figure 4.42d shows the frequency-dependent eigenvalue since its value varies in frequency space. Figures 4.42a and 4.42c have few oscillations near to low frequencies.

Figure 4.43 shows the components of the M_1 versus frequencies (ω_1, ω_2) for parameters $k_{on} = 10^2\ s^{-1}$, $k_{off} = 10^{-1}\ s^{-1}$, $D_1 = 30\ \mu m^2/s$ and $D_2 = 10^{-1}\ \mu m^2/s$ and $\omega_{rn} = 0.5\ \mu m$ with $nsteps = 10,000$ and $tf = 1$. Figures 4.43a and 4.43d show components of M_1 which

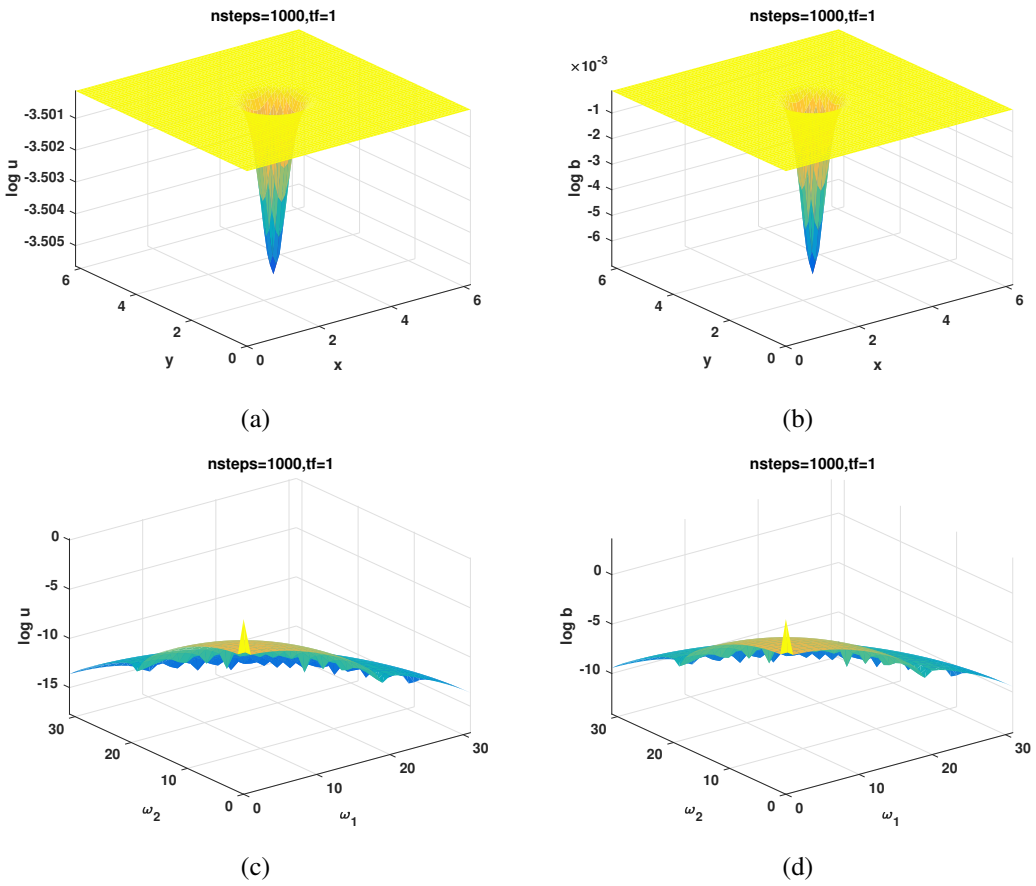

Figure 4.20: (a) and (b) solutions: u (unbound) and b (bound) versus coordinates (x,y) are shown with $nsteps = 1,000$ and $tf = 1$. (c) and (d) solutions: u (unbound) and b (bound) versus frequencies (ω_1, ω_2) are shown with $nsteps = 1,000$ and $tf = 1$. Parameters are $k_{on} = 10^{3.5}\ s^{-1}$, $k_{off} = 1\ s^{-1}$, $D_1 = 30\ \mu m^2/s$ and $D_2 = 10^{-4}\ \mu m^2/s$.

correspond to the eigenvalues of M_1 in Figures 4.42a and 4.42b. Figures 4.43b and 4.43c indicate that off-diagonal components of M_1 can be ignored for high frequencies.

Figure 4.44 shows the components of $\tilde{M}_1$ versus frequencies (ω_1, ω_2) for parameters $k_{on} = 10^2\ s^{-1}$, $k_{off} = 10^{-1}\ s^{-1}$, $D_1 = 30\ \mu m^2/s$ and $D_2 = 10^{-1}\ \mu m^2/s$ and $\omega_{rn} = 0.5\ \mu m$ with $nsteps = 10,000$ and $tf = 1$. Figures 4.44a and 4.44d show components of $\tilde{M}_1$ which correspond to the eigenvalues of $\tilde{M}_1$ in Figures 4.42c and 4.42d. Figures 4.44b and 4.44c indicate that off-diagonal components of $\tilde{M}_1$ can be ignored for high frequencies.

Figure 4.45 shows the components of basis functions shown as u_{11}, u_{12}, u_{21} and u_{22} versus frequencies (ω_1, ω_2) for parameters $k_{on} = 10^2\ s^{-1}$, $k_{off} = 10^{-1}\ s^{-1}$, $D_1 = 30\ \mu m^2/s$ and $D_2 = 10^{-1}\ \mu m^2/s$ and $\omega_{rn} = 0.5\ \mu m$ with $nsteps = 10,000$ and $tf = 1$. Figures 4.45a and 4.45b show the constant basis functions in frequency space. The absolute values of these basis functions are the constant k_{off}. Figures 4.45c and 4.45d show the other basis functions

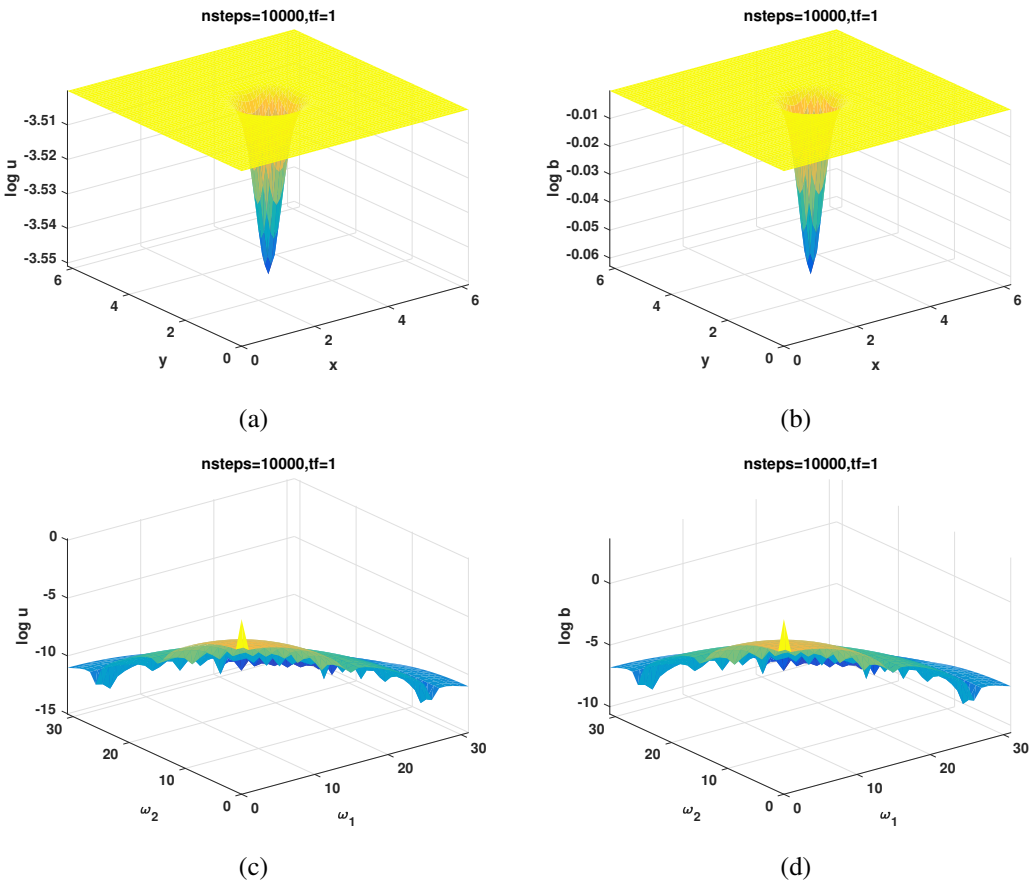

Figure 4.21: (a) and (b) solutions: u (unbound) and b (bound) versus coordinates (x,y) are shown with $nsteps = 10,000$ and $tf = 1$. (c) and (d) solutions: u (unbound) and b (bound) versus frequencies (ω_1, ω_2) are shown with $nsteps = 10,000$ and $tf = 1$. Parameters are $k_{on} = 10^{3.5}\ s^{-1}$, $k_{off} = 1\ s^{-1}$, $D_1 = 30\ \mu m^2/s$ and $D_2 = 10^{-4}\ \mu m^2/s$.

which vary in frequency space. Figure 4.45c shows stronger frequency dependence compared to Figure 4.45d. Figure 4.46 shows the solutions u (unbound) and b (bound) in physical space (x,y) and frequency space (ω_1, ω_2) for parameters $k_{on} = 10^2\ s^{-1}$, $k_{off} = 10^{-1}\ s^{-1}$, $D_1 = 30\ \mu m^2/s$ and $D_2 = 10^{-1}\ \mu m^2/s$ and $\omega_{rn} = 0.5\ \mu m$ with $nsteps = 100$ and $tf = 1$. Figure 4.47 shows the solutions u (unbound) and b (bound) in physical space (x,y) and frequency space (ω_1, ω_2) for the same parameters with $nsteps = 10,000$ and $tf = 1$. Figure 4.48 shows the solutions u (unbound) and b (bound) in physical space (x,y) and frequency space (ω_1, ω_2) for the same parameters with $nsteps = 10,000$ and $tf = 1$. Comparison between Figures 4.46, 4.47 and 4.48 gives insight into the behavior of the solutions u (unbound) and b (bound) in both physical and frequency space over evolution of 100, 1,000 and 10,000 time steps. These 3 sets of Figures provide us a comparison between solutions in both physical and frequency space at different time scales. Also, by tracking the dependence

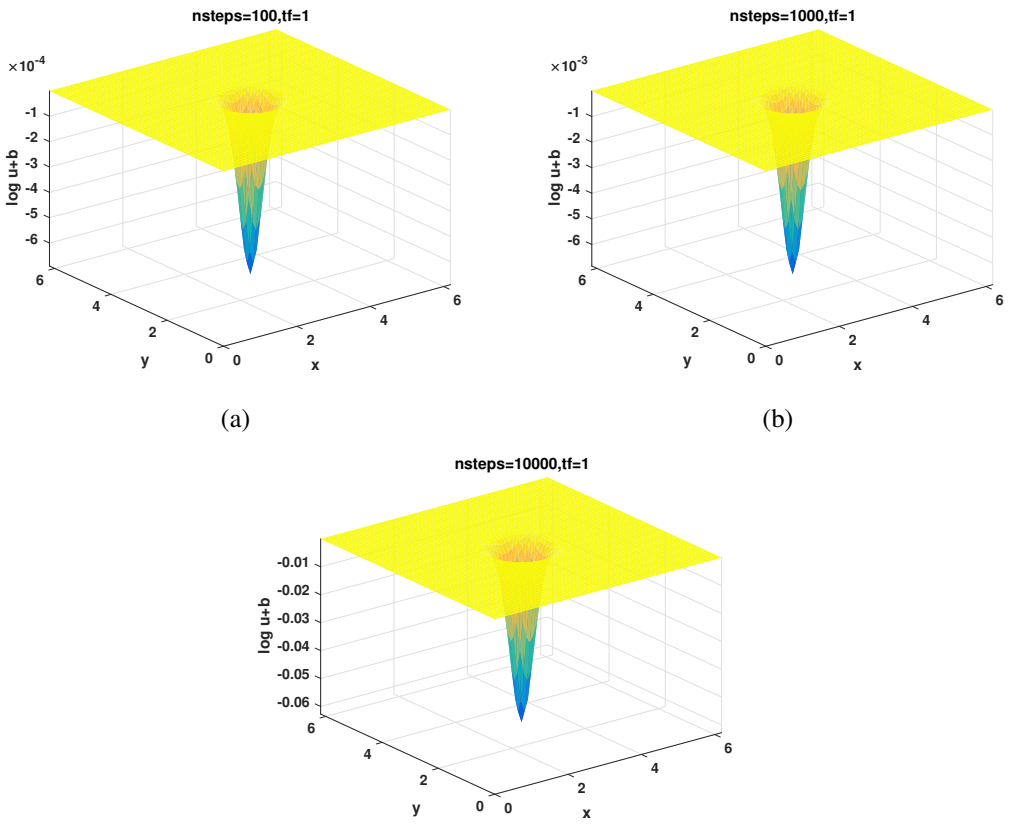

Figure 4.22: Solutions $u+b$ versus coordinates (x,y) are shown with $nsteps = 100, 1,000, 10,000$ and $tf = 1$. Parameters are $k_{on} = 10^{3.5}\ s^{-1}$, $k_{off} = 1\ s^{-1}$, $D_1 = 30\ \mu m^2/s$ and $D_2 = 10^{-4}\ \mu m^2/s$.

of solutions u (unbound) and b (bound) on the frequency and physical space variables, we can get a reasonable estimate of the fraction of both mobile and immobile species.

Figure 4.49 shows the total solution $u+b$ in physical space (x,y) for parameters $k_{on} = 10^2\ s^{-1}$, $k_{off} = 10^{-1}\ s^{-1}$, $D_1 = 30\ \mu m^2/s$ and $D_2 = 10^{-1}\ \mu m^2/s$ and $\omega_{rn} = 0.5\ \mu m$ with $nsteps = 100, 1,000, 10,000$ and $tf = 1$. It shows the evolution of the total solution $u+b$ on physical space for different time steps. Figure 4.50 shows the total solution $u+b$ in frequency space (ω_1, ω_2) for parameters $k_{on} = 10^2\ s^{-1}$, $k_{off} = 10^{-1}\ s^{-1}$, $D_1 = 30\ \mu m^2/s$ and $D_2 = 10^{-1}\ \mu m^2/s$ and $\omega_{rn} = 0.5\ \mu m$ with $nsteps = 100, 1,000, 10,000$ and $tf = 1$. It shows the evolution of the total solution $u+b$ in frequency space for different time steps.

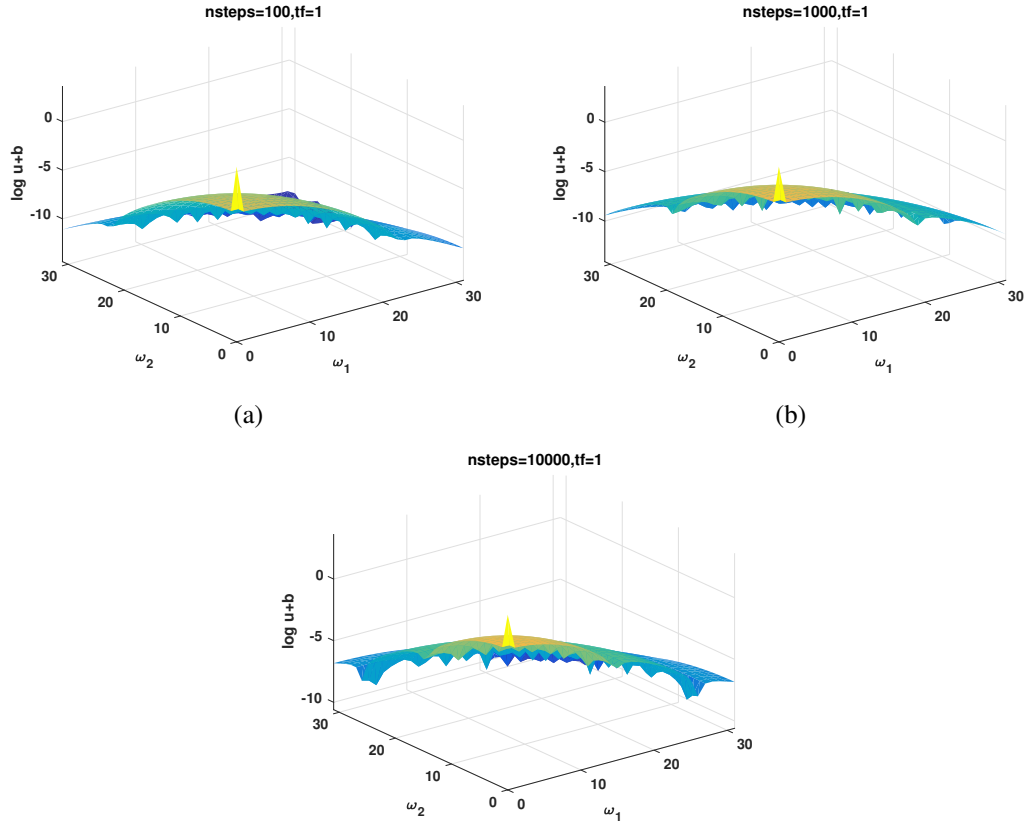

Figure 4.23: Solutions $u+b$ versus frequencies ω_1 and ω_2 are shown with $nsteps = 100, 1,000, 10,000$ and $tf = 1$. Parameters are $k_{on} = 10^{3.5}\ s^{-1}$, $k_{off} = 1\ s^{-1}$, $D_1 = 30\ \mu m^2/s$ and $D_2 = 10^{-4}\ \mu m^2/s$.

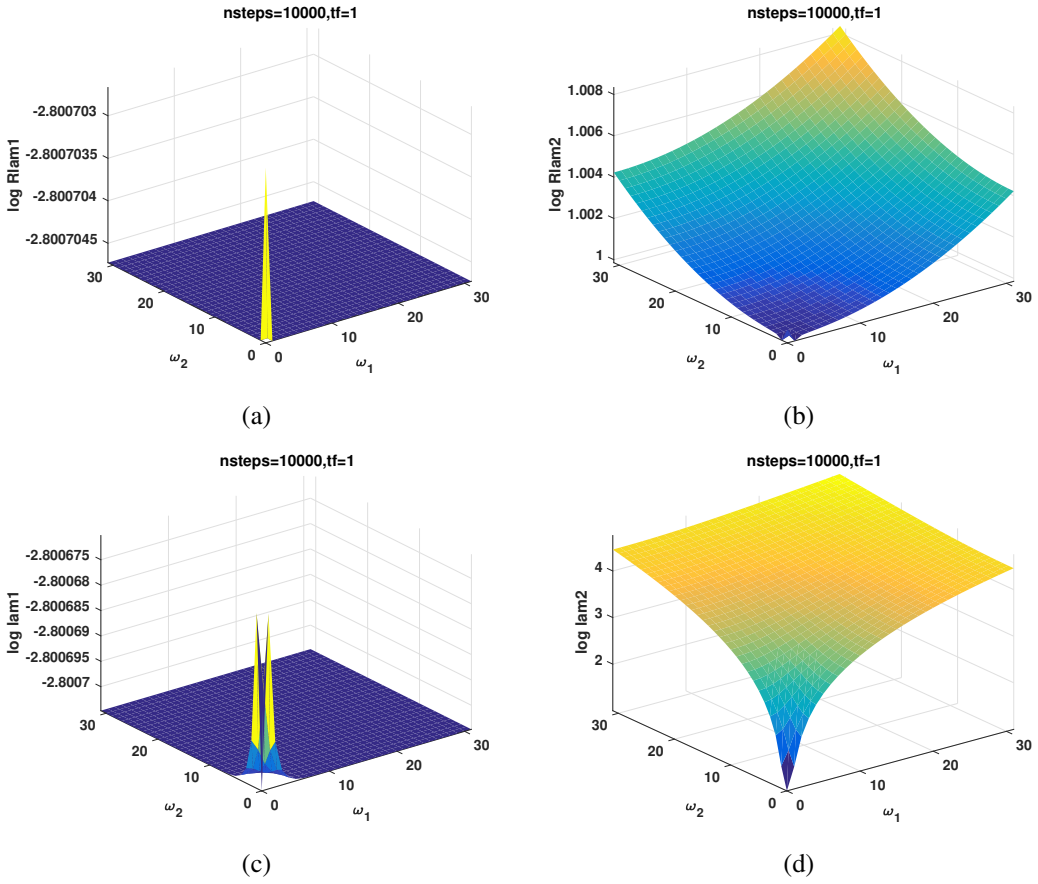

(a) (b)

(c) (d)

Figure 4.24: Eigenvalues versus frequencies (ω_1, ω_2) are shown with $nsteps = 10,000$ and $tf = 1$. Parameters are $k_{on} = 10^{-2}\ s^{-1}$, $k_{off} = 10\ s^{-1}$, $D_1 = 30\ \mu m^2/s$ and $D_2 = 10^{-4}\ \mu m^2/s$.

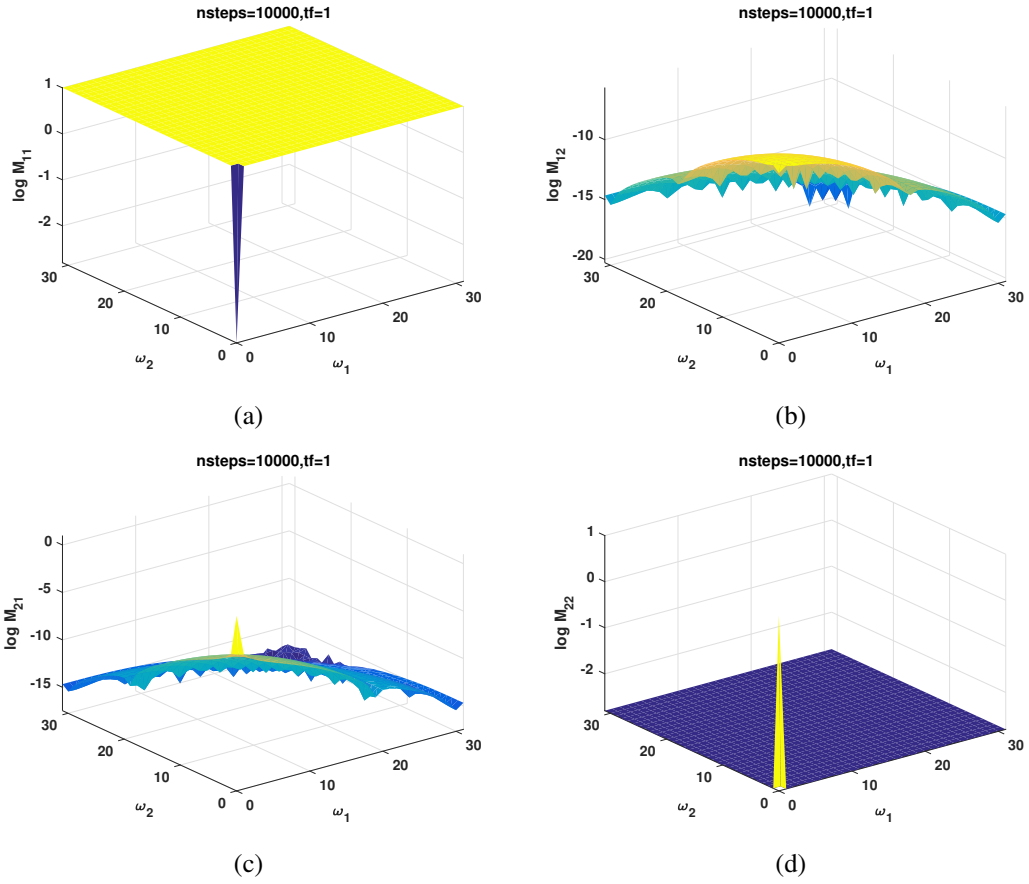

Figure 4.25: M_1 components versus frequencies (ω_1, ω_2) are shown with $nsteps = 10{,}000$ and $tf = 1$. Parameters are $k_{on} = 10^{-2}\ s^{-1}$, $k_{off} = 10\ s^{-1}$, $D_1 = 30\ \mu m^2/s$ and $D_2 = 10^{-4}\ \mu m^2/s$.

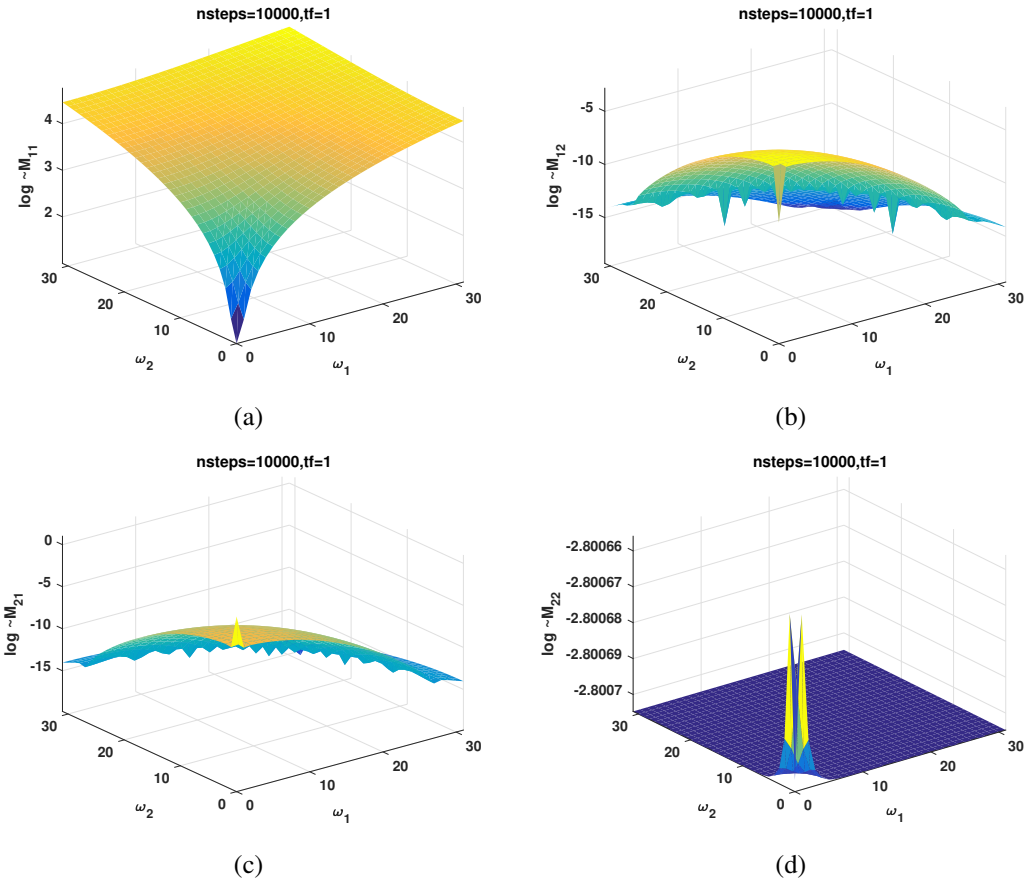

Figure 4.26: $\tilde{M}_1$ components versus frequencies (ω_1, ω_2) are shown with $nsteps = 10{,}000$ and $tf = 1$. Parameters are $k_{on} = 10^{-2}\ s^{-1}$, $k_{off} = 10\ s^{-1}$, $D_1 = 30\ \mu m^2/s$ and $D_2 = 10^{-4}\ \mu m^2/s$.

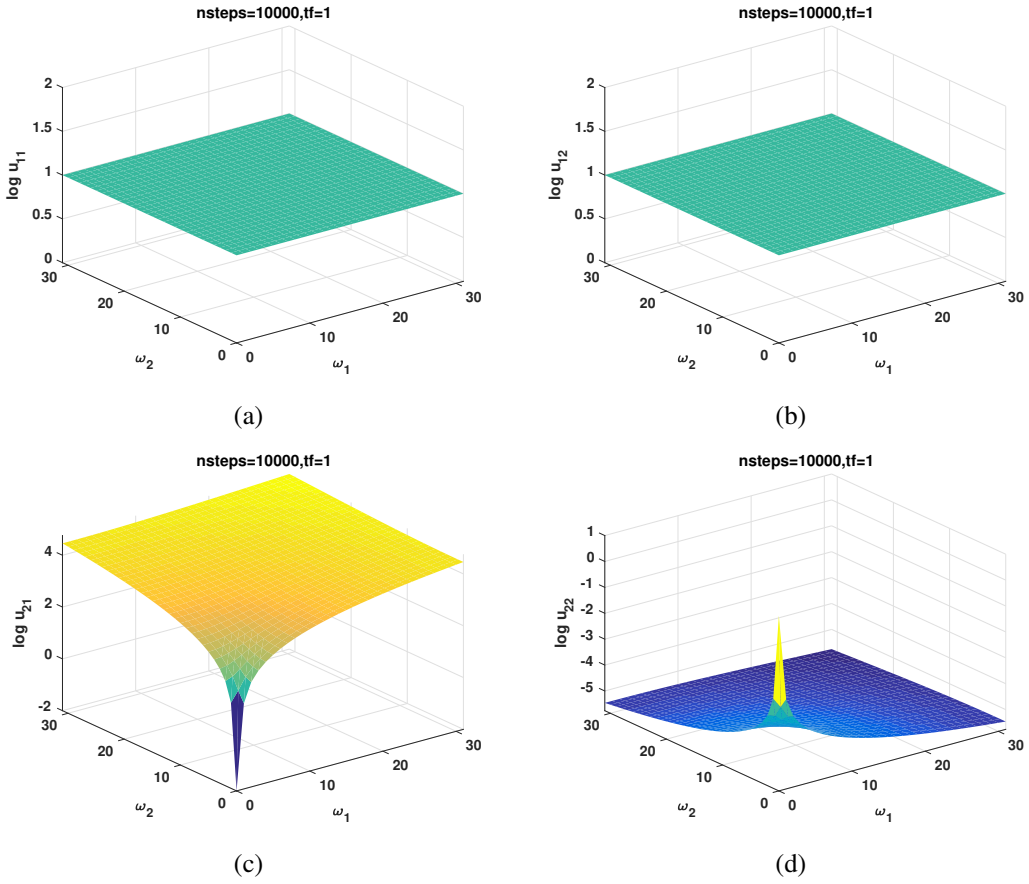

Figure 4.27: Basis function components versus frequencies (ω_1, ω_2) are shown with $nsteps = 10{,}000$ and $tf = 1$. Parameters are $k_{on} = 10^{-2}\ s^{-1}$, $k_{off} = 10\ s^{-1}$, $D_1 = 30\ \mu m^2/s$ and $D_2 = 10^{-4}\ \mu m^2/s$.

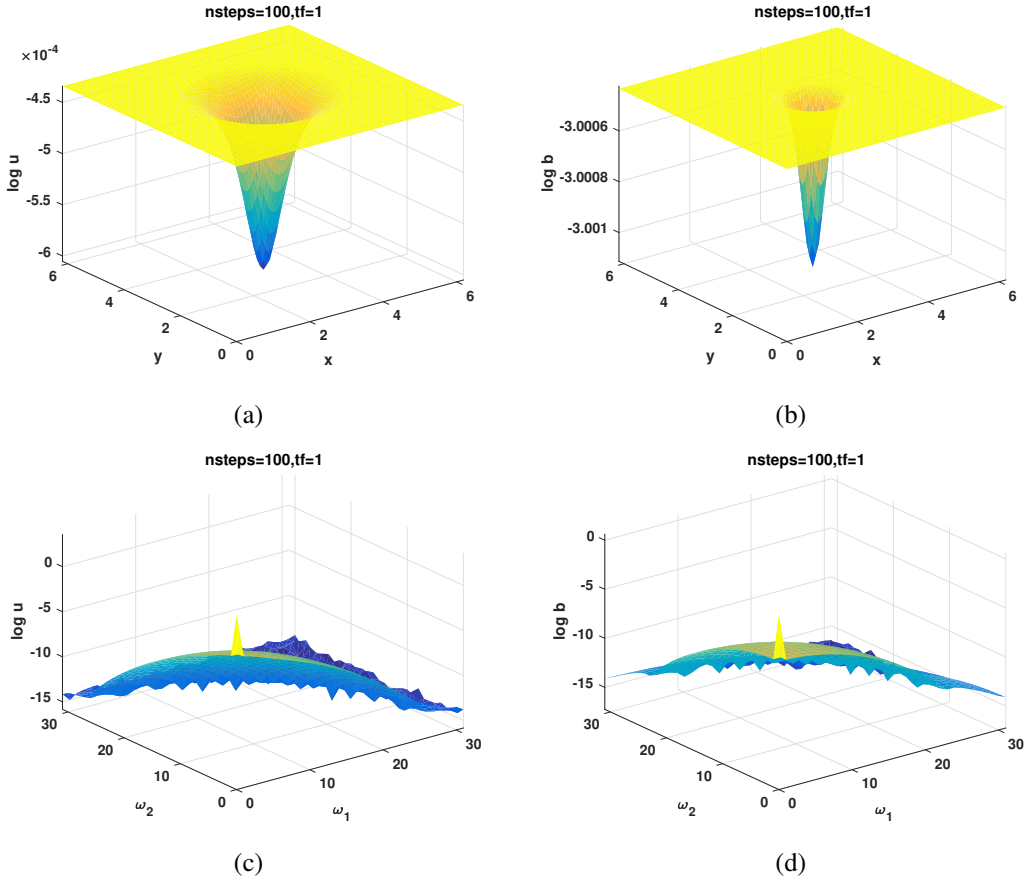

Figure 4.28: (a) and (b) solutions: u (unbound) and b (bound) versus coordinates (x,y) are shown with $nsteps = 100$ and $tf = 1$. (c) and (d) solutions: u (unbound) and b (bound) versus frequencies (ω_1, ω_2) are shown with $nsteps = 100$ and $tf = 1$. Parameters are $k_{on} = 10^{-2}\ s^{-1}$, $k_{off} = 10\ s^{-1}$, $D_1 = 30\ \mu m^2/s$ and $D_2 = 10^{-4}\ \mu m^2/s$.

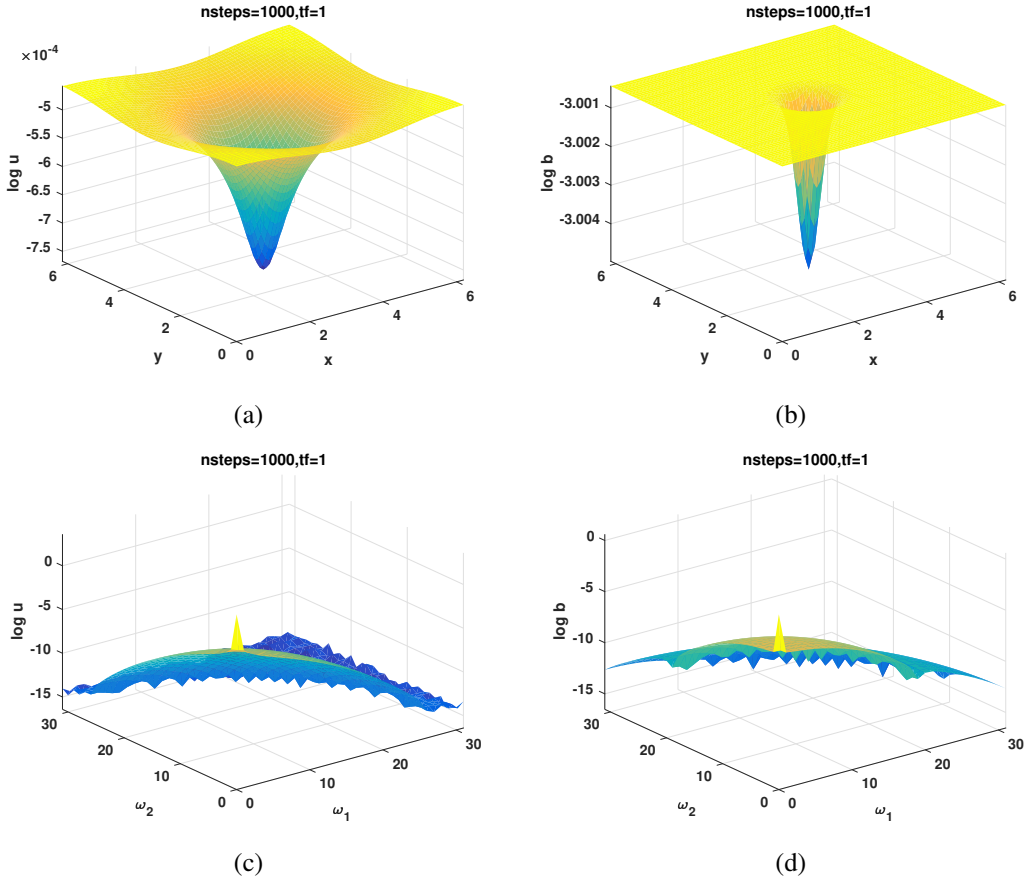

Figure 4.29: (a) and (b) solutions: u (unbound) and b (bound) versus coordinates (x,y) are shown with $nsteps = 1,000$ and $tf = 1$. (c) and (d) solutions: u (unbound) and b (bound) versus frequencies (ω_1, ω_2) are shown with $nsteps = 1,000$ and $tf = 1$. Parameters are $k_{on} = 10^{-2}\ s^{-1}$, $k_{off} = 10\ s^{-1}$, $D_1 = 30\ \mu m^2/s$ and $D_2 = 10^{-4}\ \mu m^2/s$.

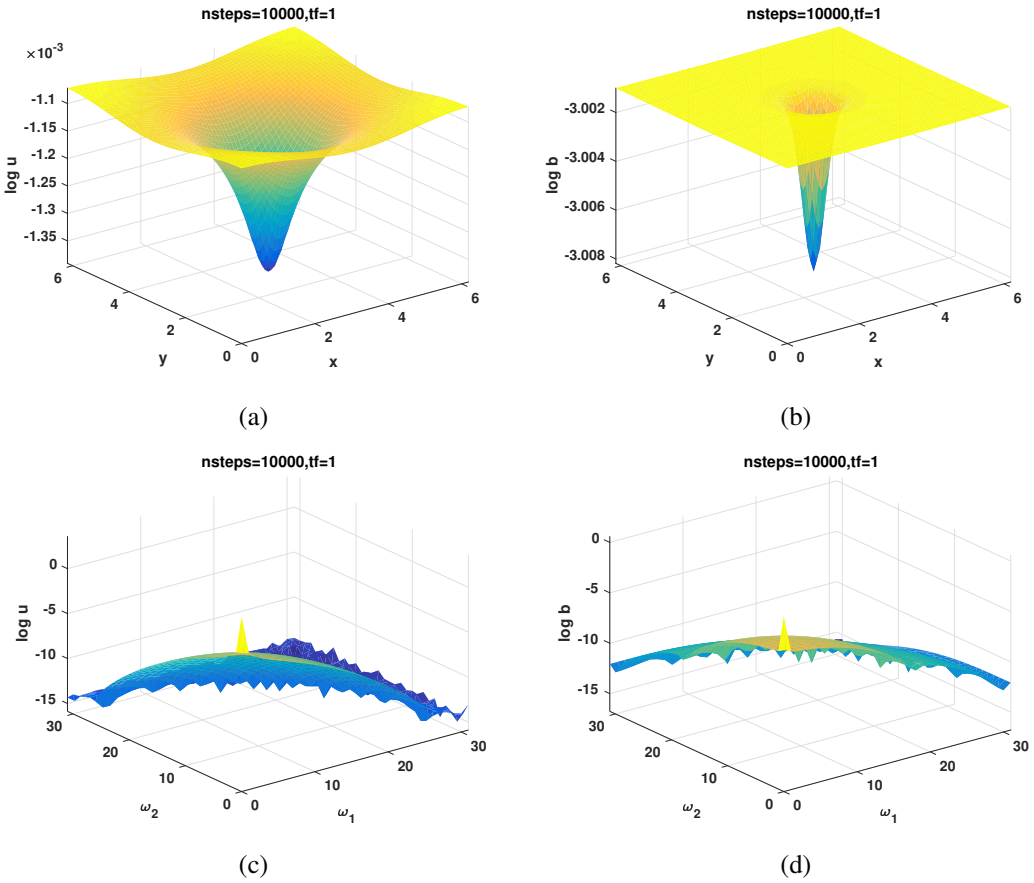

Figure 4.30: (a) and (b) solutions: u (unbound) and b (bound) versus coordinates (x,y) are shown with $nsteps = 10,000$ and $tf = 1$. (c) and (d) solutions: u (unbound) and b (bound) versus frequencies (ω_1, ω_2) are shown with $nsteps = 10,000$ and $tf = 1$. Parameters are $k_{on} = 10^{-2}\ s^{-1}$, $k_{off} = 10\ s^{-1}$, $D_1 = 30\ \mu m^2/s$ and $D_2 = 10^{-4}\ \mu m^2/s$.

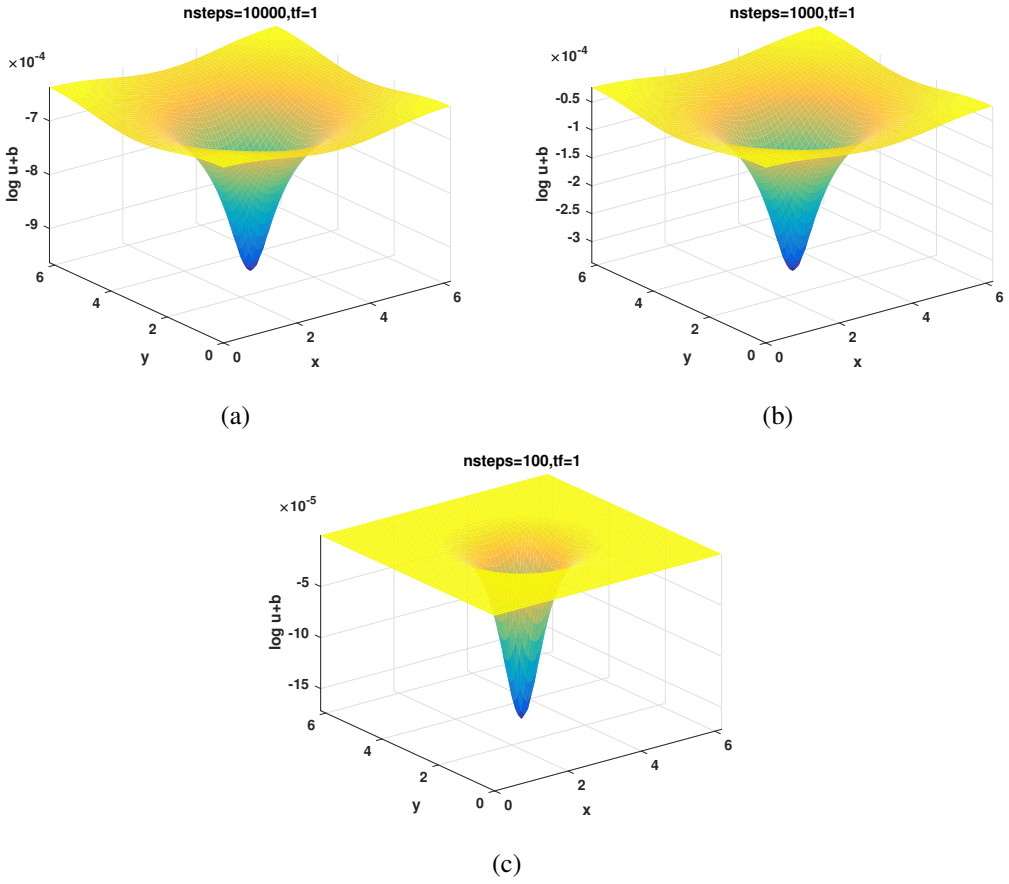

Figure 4.31: Solutions $u+b$ versus coordinates (x,y) are shown with $nsteps = 100, 1,000, 10,000$ and $tf = 1$. Parameters are $k_{on} = 10^{-2}\ s^{-1}$, $k_{off} = 10\ s^{-1}$, $D_1 = 30\ \mu m^2/s$ and $D_2 = 10^{-4}\ \mu m^2/s$.

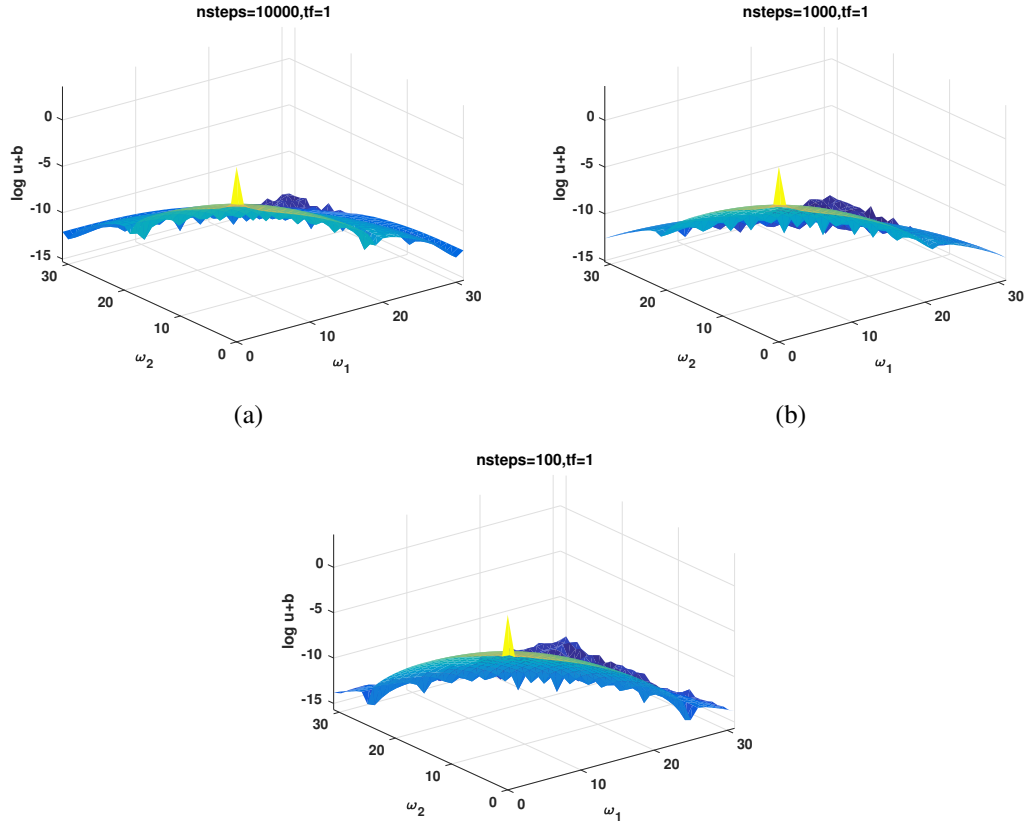

Figure 4.32: Solutions $u+b$ versus frequencies ω_1 and ω_2 are shown with $nsteps = 100, 1,000, 10,000$ and $tf = 1$. Parameters are $k_{on} = 10^{-2}\ s^{-1}$, $k_{off} = 10\ s^{-1}$, $D_1 = 30\ \mu m^2/s$ and $D_2 = 10^{-4}\ \mu m^2/s$.

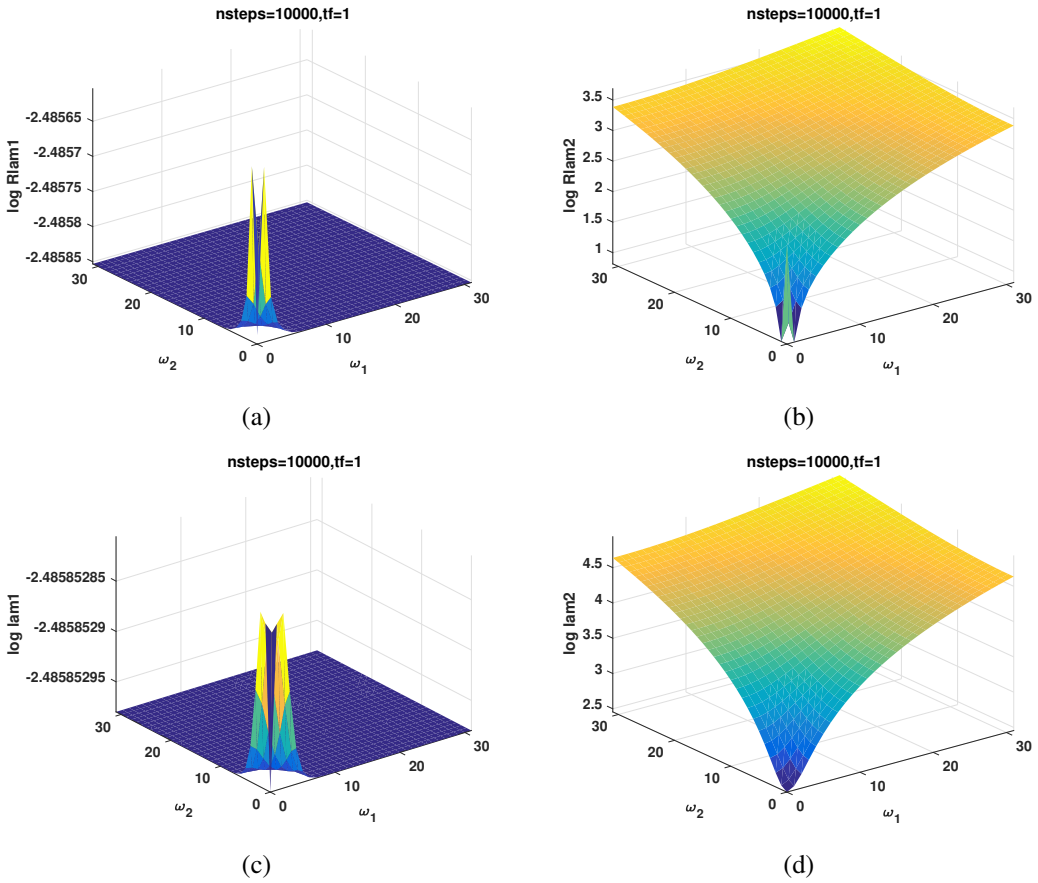

Figure 4.33: Eigenvalues versus frequencies (ω_1, ω_2) are shown with $nsteps = 10{,}000$ and $tf = 1$. Parameters are $k_{on} = 255\ s^{-1}$, $k_{off} = 31\ s^{-1}$, $D_1 = 45\ \mu m^2/s$ and $D_2 = 2.5\ \mu m^2/s$.

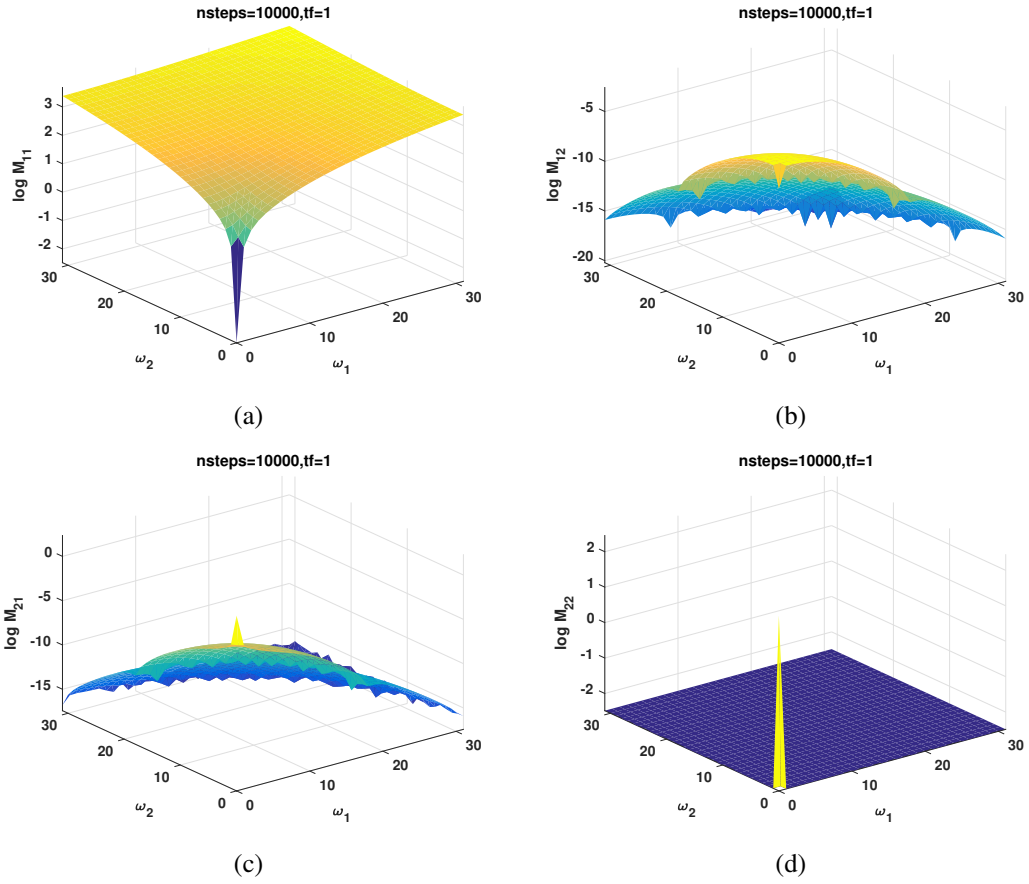

Figure 4.34: M_1 components versus frequencies (ω_1, ω_2) are shown with $nsteps = 10,000$ and $tf = 1$. Parameters are $k_{on} = 255\ s^{-1}$, $k_{off} = 31\ s^{-1}$, $D_1 = 45\ \mu m^2/s$ and $D_2 = 2.5\ \mu m^2/s$.

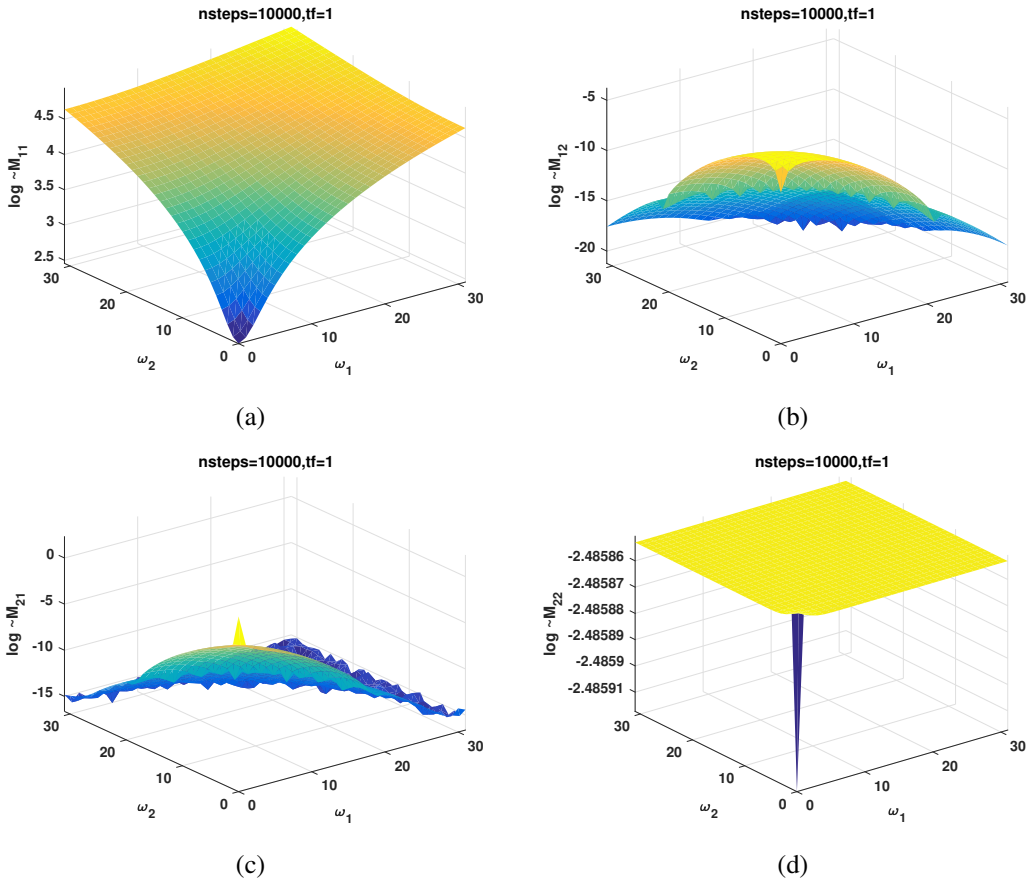

Figure 4.35: $\tilde{M}_1$ components versus frequencies (ω_1, ω_2) are shown with $nsteps = 10,000$ and $tf = 1$. Parameters are $k_{on} = 255\ s^{-1}$, $k_{off} = 31\ s^{-1}$, $D_1 = 45\ \mu m^2/s$ and $D_2 = 2.5\ \mu m^2/s$.

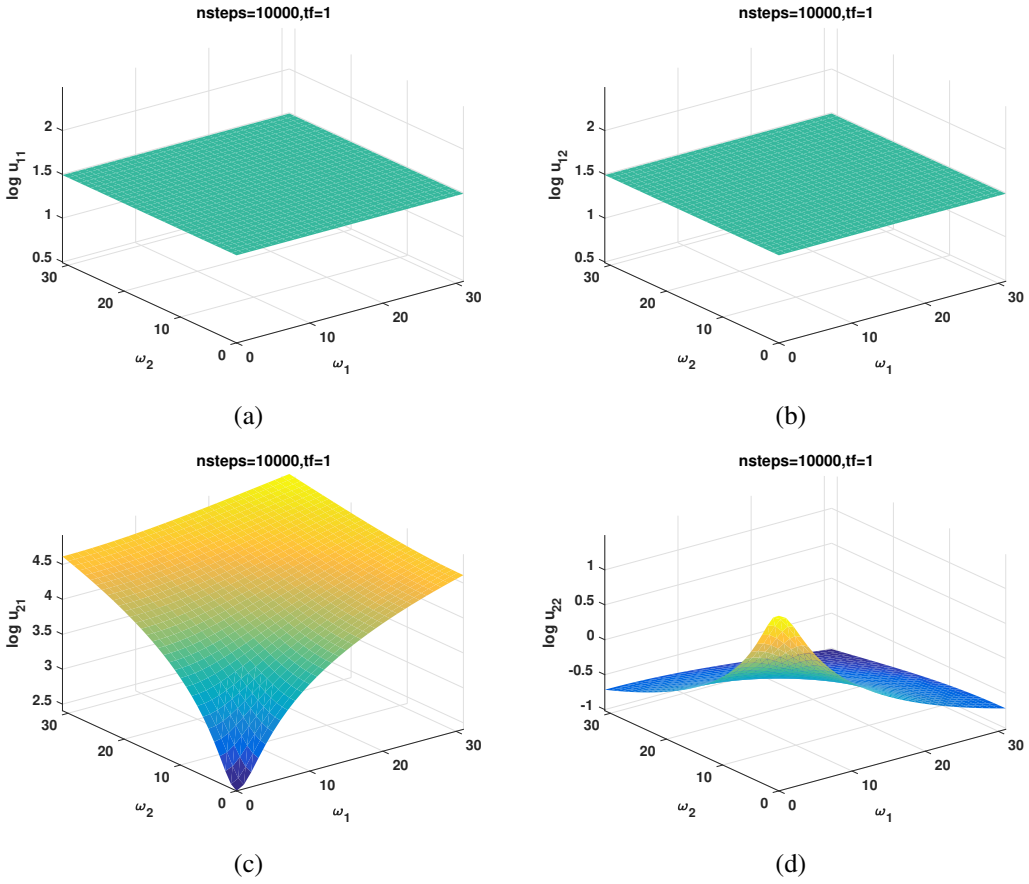

Figure 4.36: Basis function components versus frequencies (ω_1, ω_2) are shown with $nsteps = 10,000$ and $tf = 1$. Parameters are $k_{on} = 255\ s^{-1}$, $k_{off} = 31\ s^{-1}$, $D_1 = 45\ \mu m^2/s$ and $D_2 = 2.5\ \mu m^2/s$.

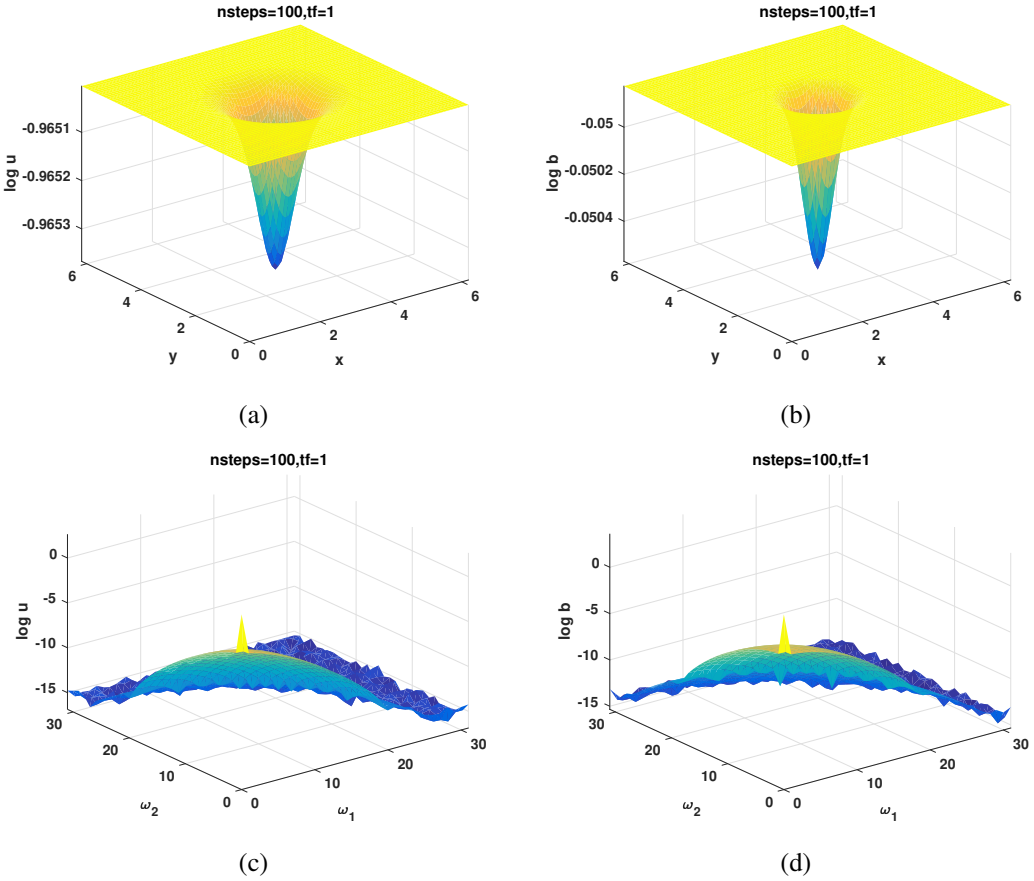

Figure 4.37: (a) and (b) solutions: u (unbound) and b (bound) versus coordinates (x,y) are shown with $nsteps = 100$ and $tf = 1$. (c) and (d) solutions: u (unbound) and b (bound) versus frequencies (ω_1, ω_2) are shown with $nsteps = 100$ and $tf = 1$. Parameters are $k_{on} = 255\ s^{-1}$, $k_{off} = 31\ s^{-1}$, $D_1 = 45\ \mu m^2/s$ and $D_2 = 2.5\ \mu m^2/s$.

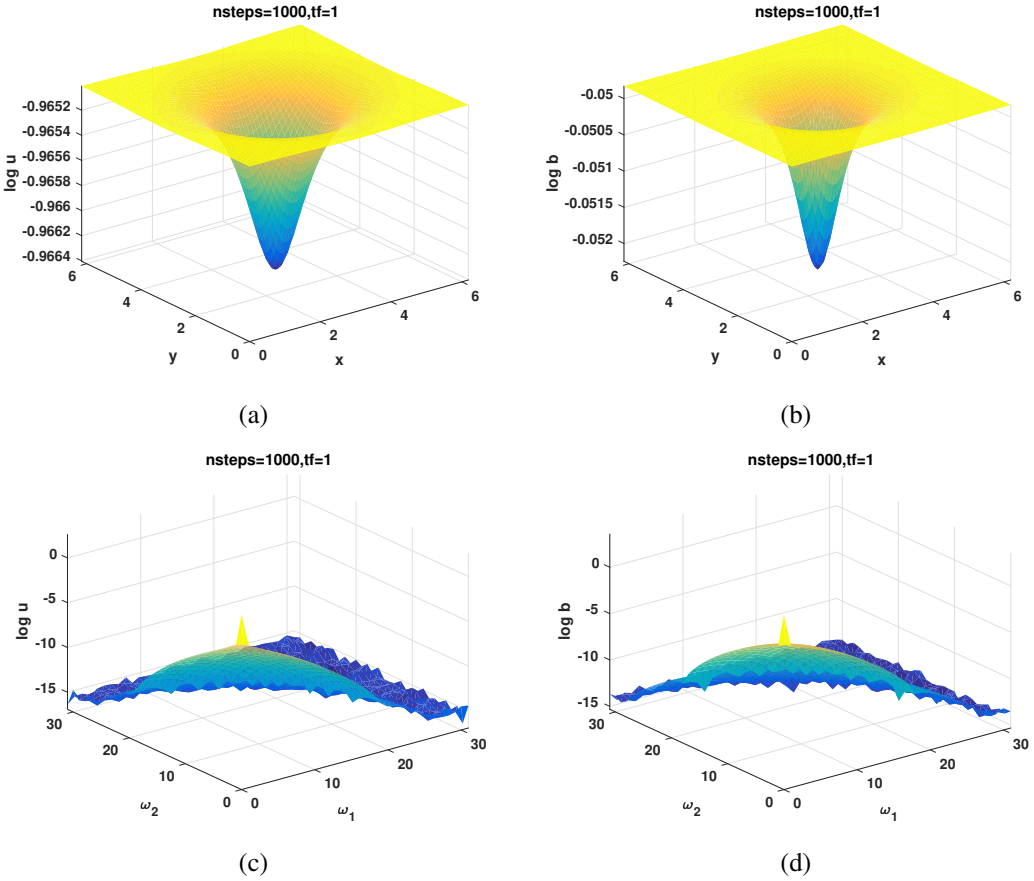

Figure 4.38: (a) and (b) solutions: u (unbound) and b (bound) versus coordinates (x,y) are shown with $nsteps = 1{,}000$ and $tf = 1$. (c) and (d) solutions: u (unbound) and b (bound) versus frequencies (ω_1, ω_2) are shown with $nsteps = 1{,}000$ and $tf = 1$. Parameters are $k_{on} = 255\ s^{-1}$, $k_{off} = 31\ s^{-1}$, $D_1 = 45\ \mu m^2/s$ and $D_2 = 2.5\ \mu m^2/s$.

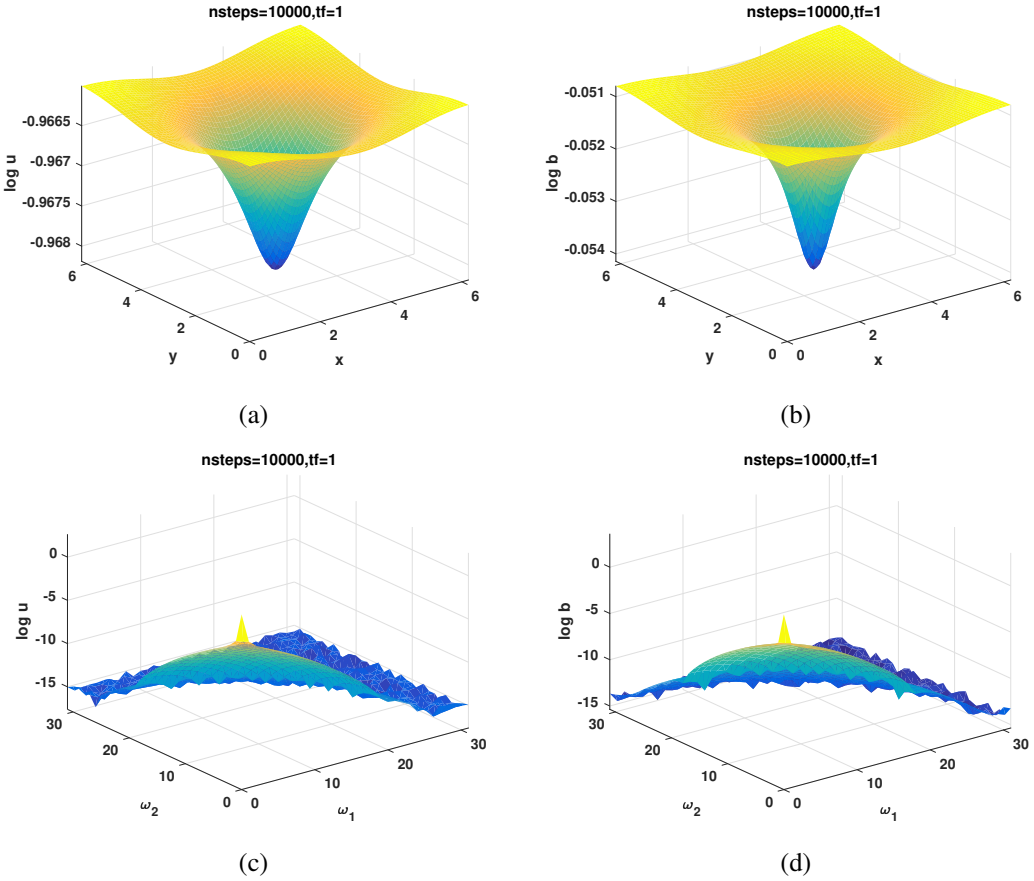

Figure 4.39: (a) and (b) solutions: u (unbound) and b (bound) versus coordinates (x,y) are shown with $nsteps = 10,000$ and $tf = 1$. (c) and (d) solutions: u (unbound) and b (bound) versus frequencies (ω_1, ω_2) are shown with $nsteps = 10,000$ and $tf = 1$. Parameters are $k_{on} = 255\ s^{-1}$, $k_{off} = 31\ s^{-1}$, $D_1 = 45\ \mu m^2/s$ and $D_2 = 2.5\ \mu m^2/s$.

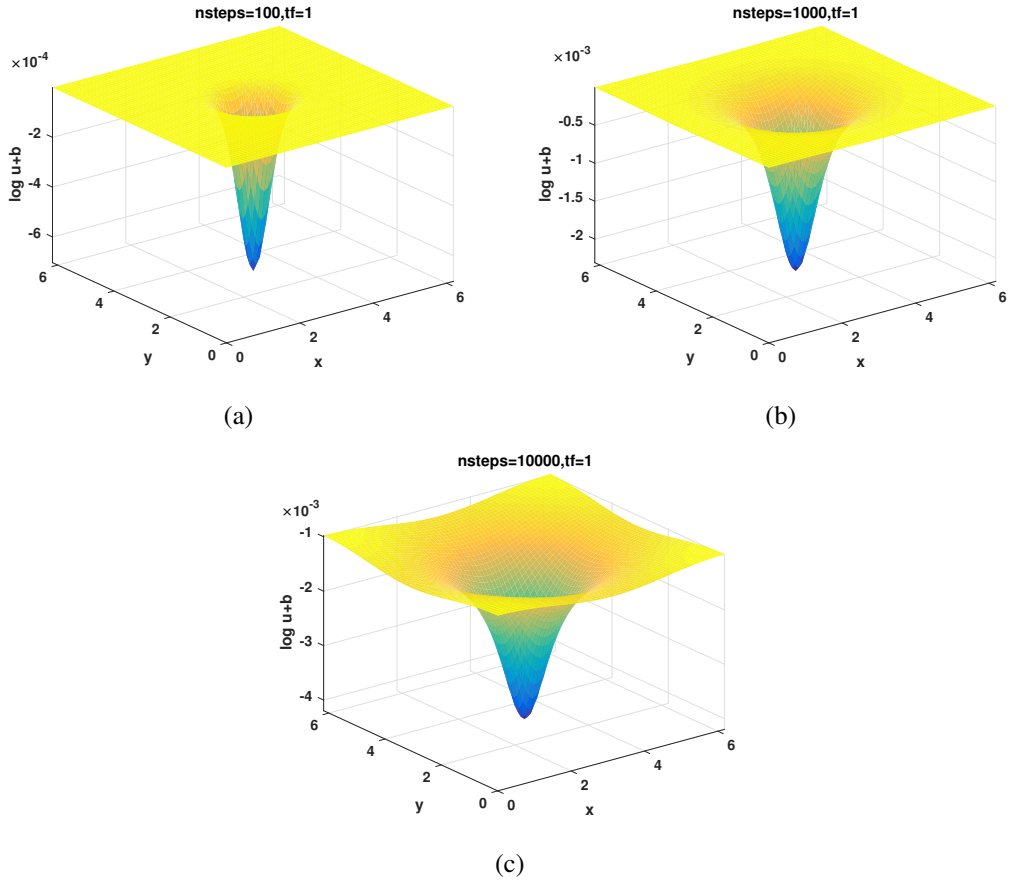

Figure 4.40: Solutions $u+b$ versus coordinates (x,y) are shown with $nsteps = 100, 1,000, 10,000$ and $tf = 1$. Parameters are $k_{on} = 255\ s^{-1}$, $k_{off} = 31\ s^{-1}$, $D_1 = 45\ \mu m^2/s$ and $D_2 = 2.5\ \mu m^2/s$.

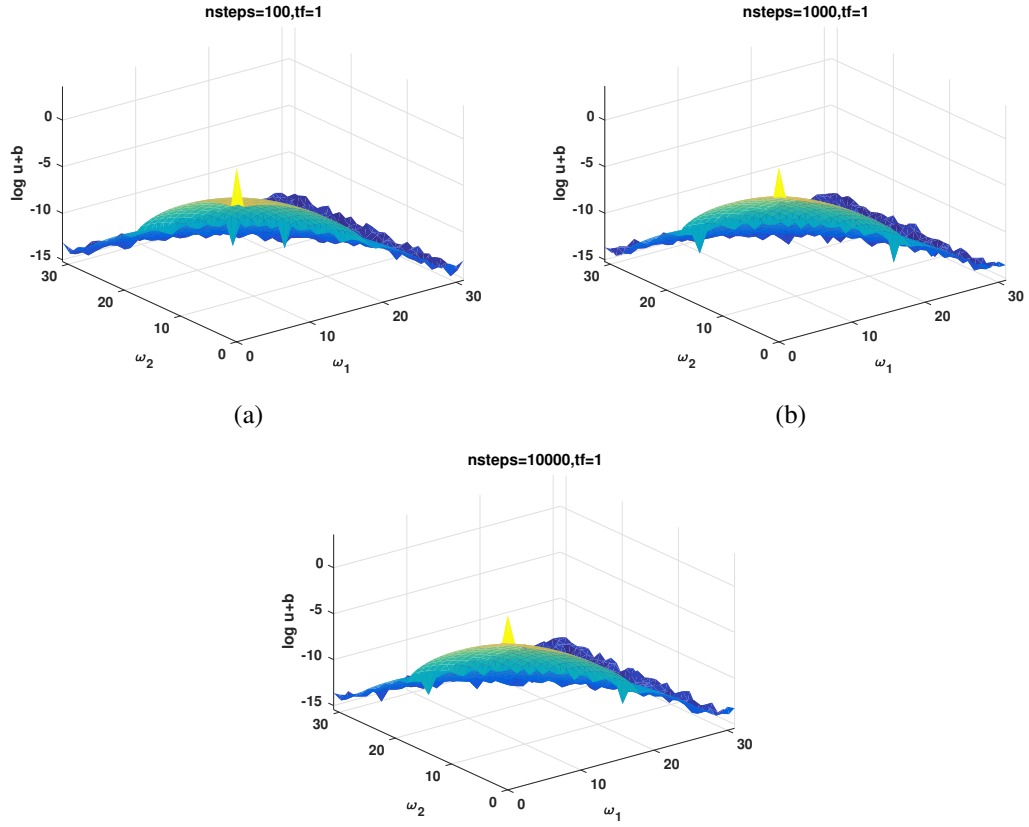

Figure 4.41: Solutions $u+b$ versus frequencies ω_1 and ω_2 are shown with $nsteps = 100, 1,000, 10,000$ and $tf = 1$. Parameters are $k_{on} = 255\ s^{-1}$, $k_{off} = 31\ s^{-1}$, $D_1 = 45\ \mu m^2/s$ and $D_2 = 2.5\ \mu m^2/s$.

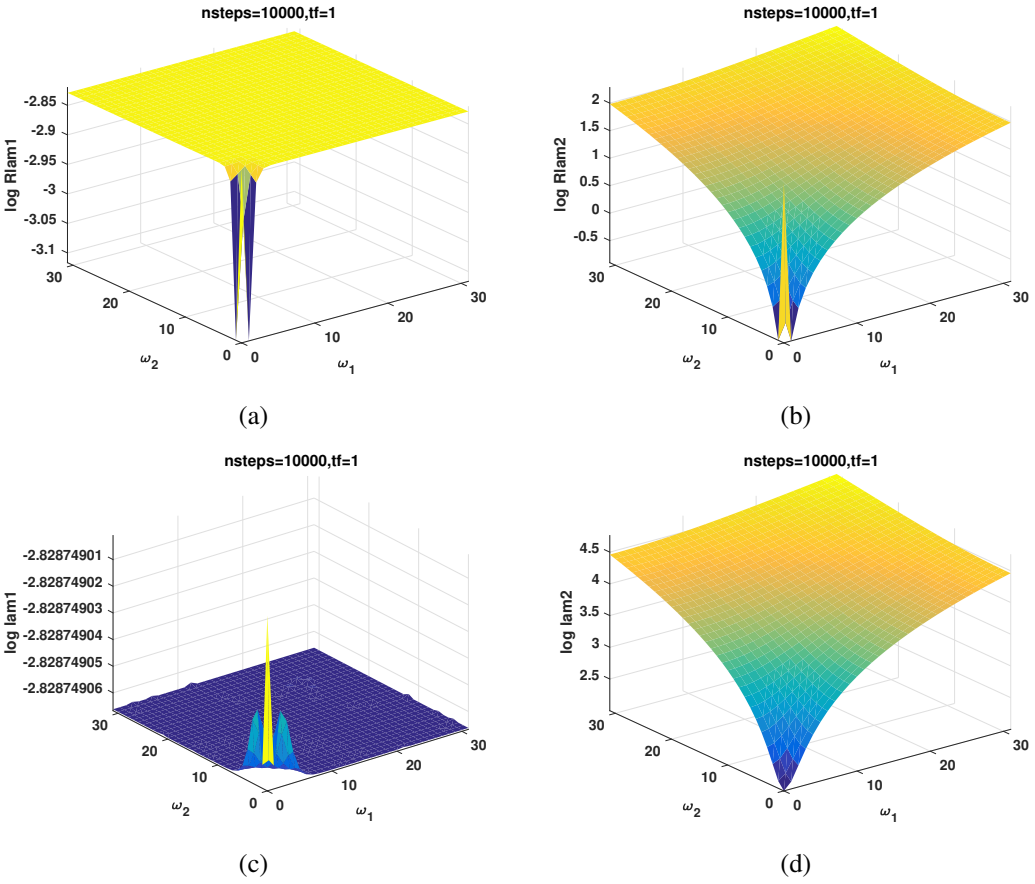

Figure 4.42: Eigenvalues versus frequencies (ω_1, ω_2) are shown with $nsteps = 10,000$ and $tf = 1$. Parameters are $k_{on} = 10^2\ s^{-1}$, $k_{off} = 10^{-1}\ s^{-1}$, $D_1 = 30\ \mu m^2/s$ and $D_2 = 10^{-1}\ \mu m^2/s$.

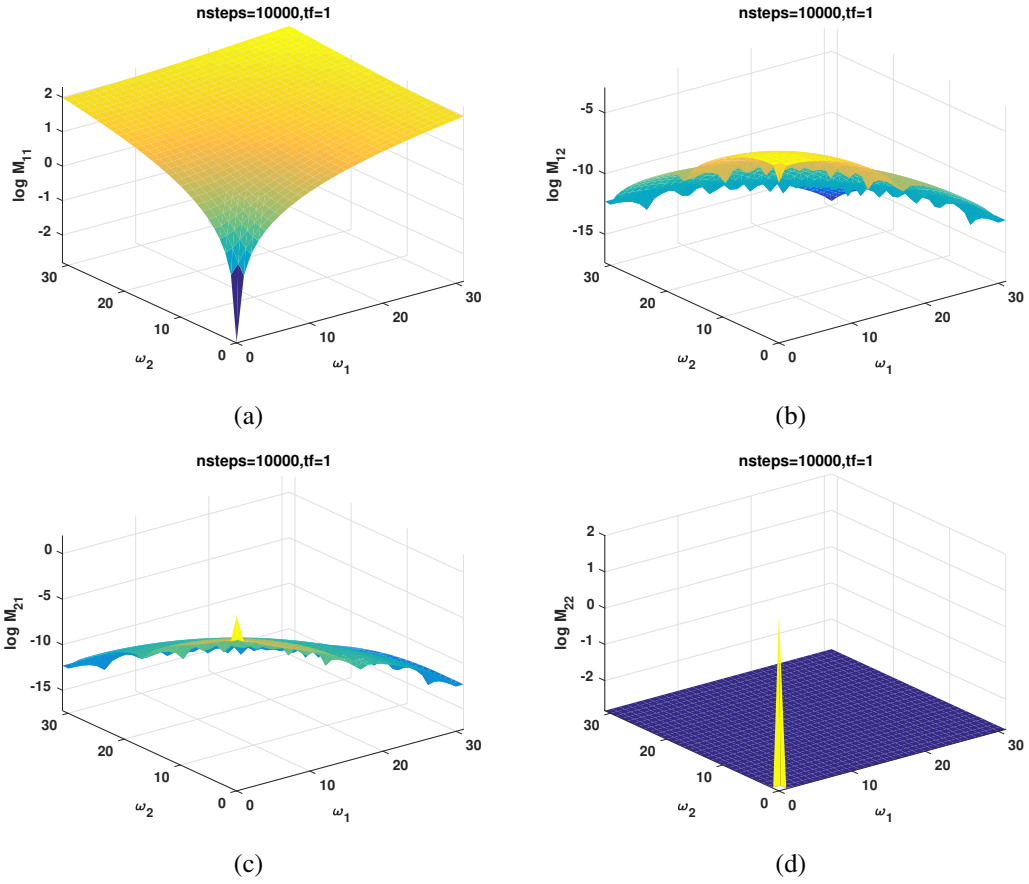

Figure 4.43: M_1 components versus frequencies (ω_1, ω_2) are shown with $nsteps = 10,000$ and $tf = 1$. Parameters are $k_{on} = 10^2\ s^{-1}$, $k_{off} = 10^{-1}\ s^{-1}$, $D_1 = 30\ \mu m^2/s$ and $D_2 = 10^{-1}\ \mu m^2/s$.

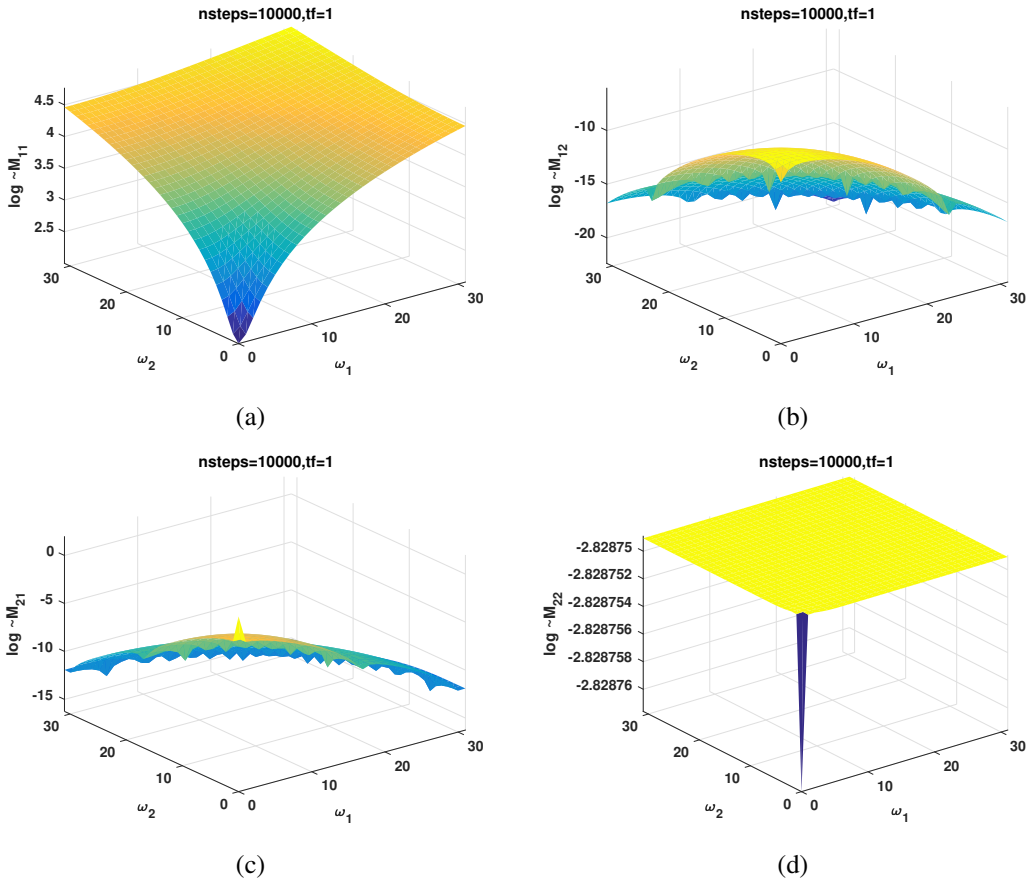

Figure 4.44: $\tilde{M}_1$ components versus frequencies (ω_1, ω_2) are shown with $nsteps = 10,000$ and $tf = 1$. Parameters are $k_{on} = 10^2\ s^{-1}$, $k_{off} = 10^{-1}\ s^{-1}$, $D_1 = 30\ \mu m^2/s$ and $D_2 = 10^{-1}\ \mu m^2/s$.

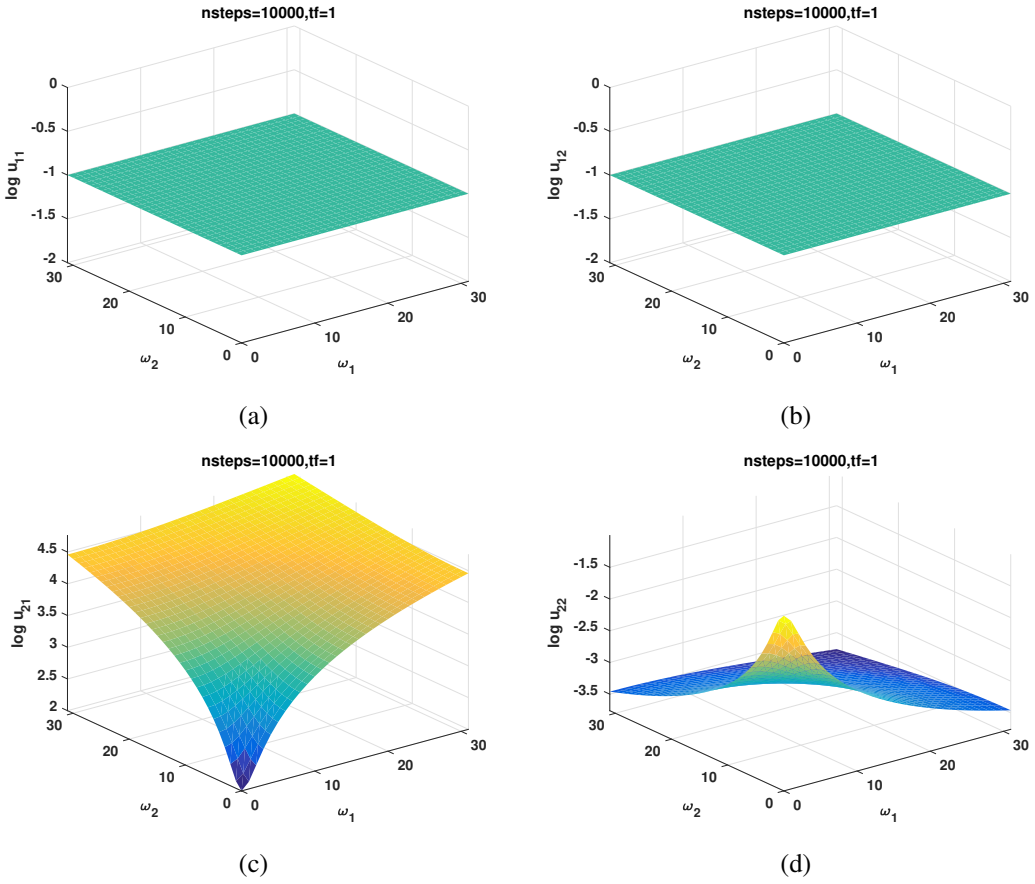

Figure 4.45: Basis function components versus frequencies (ω_1, ω_2) are shown with $nsteps = 10{,}000$ and $tf = 1$. Parameters are $k_{on} = 10^2\ s^{-1}$, $k_{off} = 10^{-1}\ s^{-1}$, $D_1 = 30\ \mu m^2/s$ and $D_2 = 10^{-1}\ \mu m^2/s$.

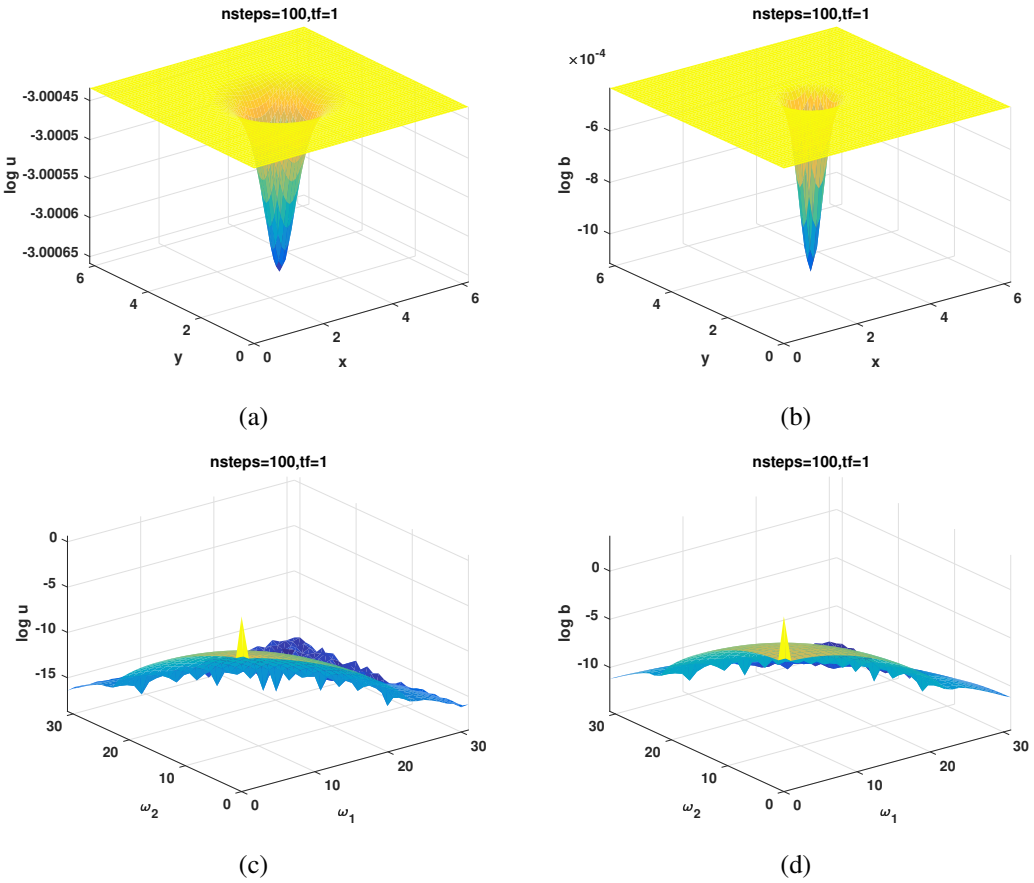

Figure 4.46: (a) and (b) solutions: u (unbound) and b (bound) versus coordinates (x,y) are shown with $nsteps = 100$ and $tf = 1$. (c) and (d) solutions: u (unbound) and b (bound) versus frequencies (ω_1, ω_2) are shown with $nsteps = 100$ and $tf = 1$. Parameters are $k_{on} = 10^2\ s^{-1}$, $k_{off} = 10^{-1}\ s^{-1}$, $D_1 = 30\ \mu m^2/s$ and $D_2 = 10^{-1}\ \mu m^2/s$.

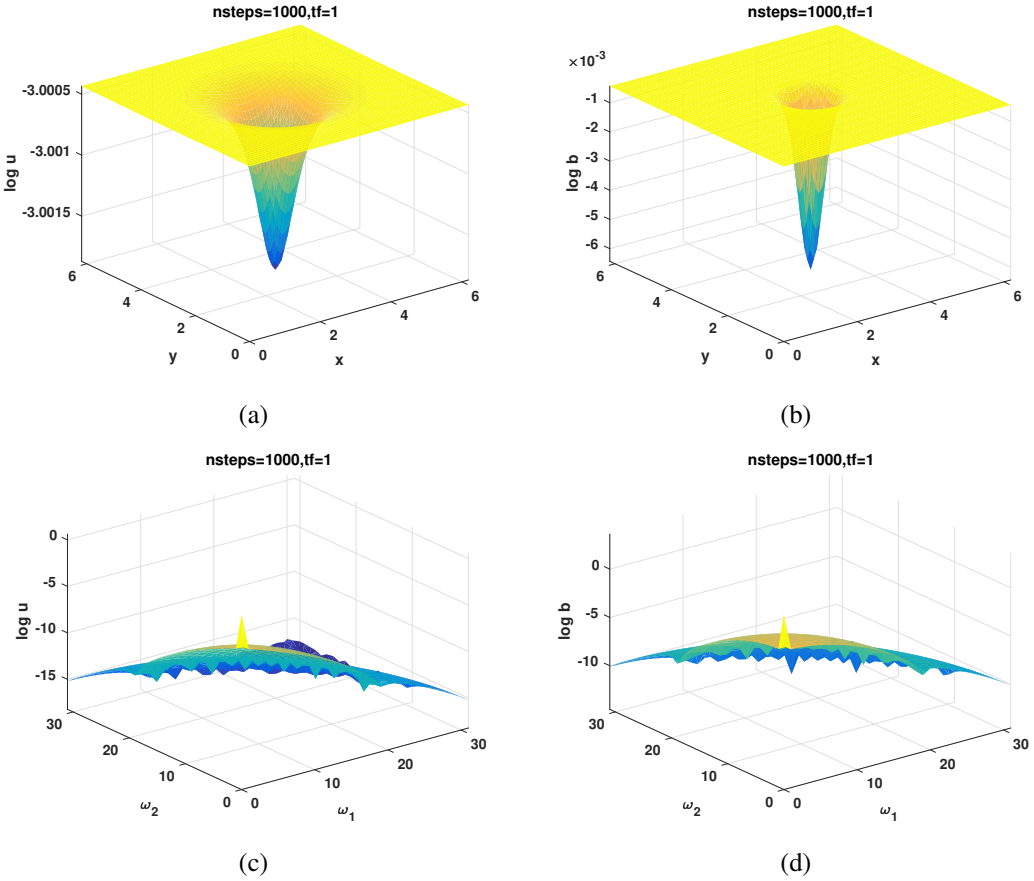

Figure 4.47: (a) and (b) solutions: u (unbound) and b (bound) versus coordinates (x,y) are shown with $nsteps = 1,000$ and $tf = 1$. (c) and (d) solutions: u (unbound) and b (bound) versus frequencies (ω_1, ω_2) are shown with $nsteps = 1,000$ and $tf = 1$. Parameters are $k_{on} = 10^2\ s^{-1}$, $k_{off} = 10^{-1}\ s^{-1}$, $D_1 = 30\ \mu m^2/s$ and $D_2 = 10^{-1}\ \mu m^2/s$.

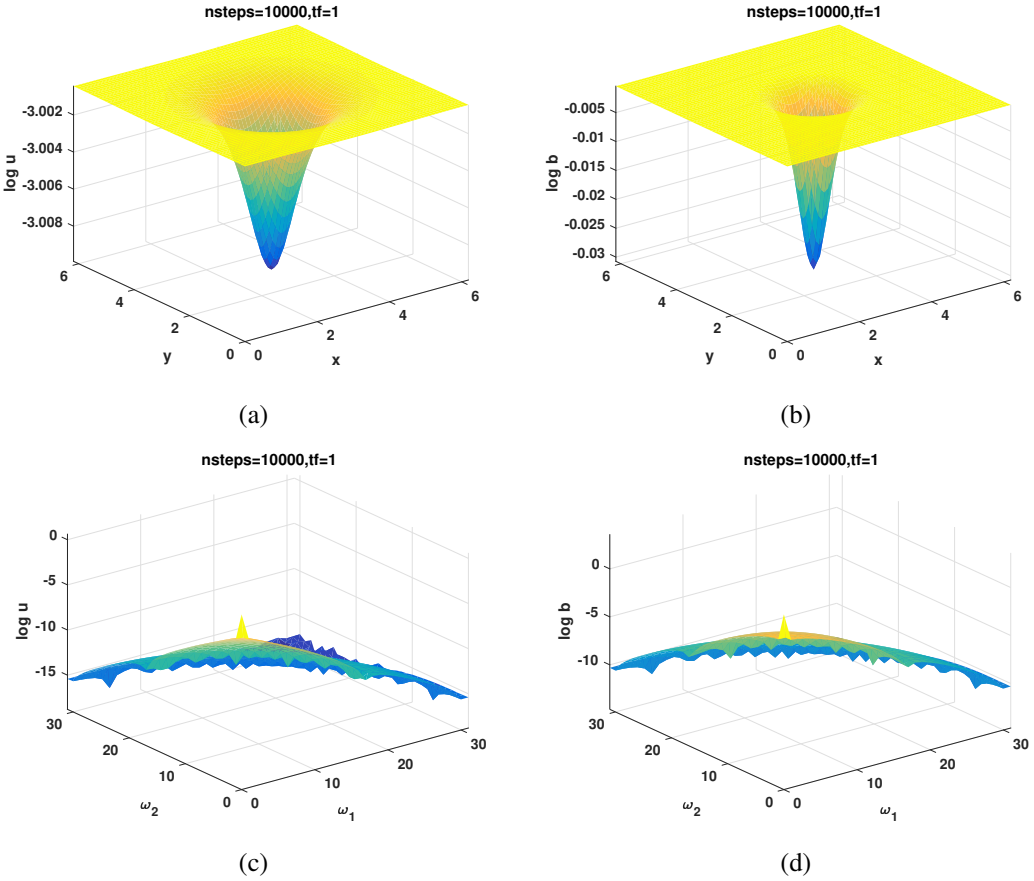

Figure 4.48: (a) and (b) solutions: u (unbound) and b (bound) versus coordinates (x,y) are shown with $nsteps = 10,000$ and $tf = 1$. (c) and (d) solutions: u (unbound) and b (bound) versus frequencies (ω_1, ω_2) are shown with $nsteps = 10,000$ and $tf = 1$. Parameters are $k_{on} = 10^2\ s^{-1}$, $k_{off} = 10^{-1}\ s^{-1}$, $D_1 = 30\ \mu m^2/s$ and $D_2 = 10^{-1}\ \mu m^2/s$.

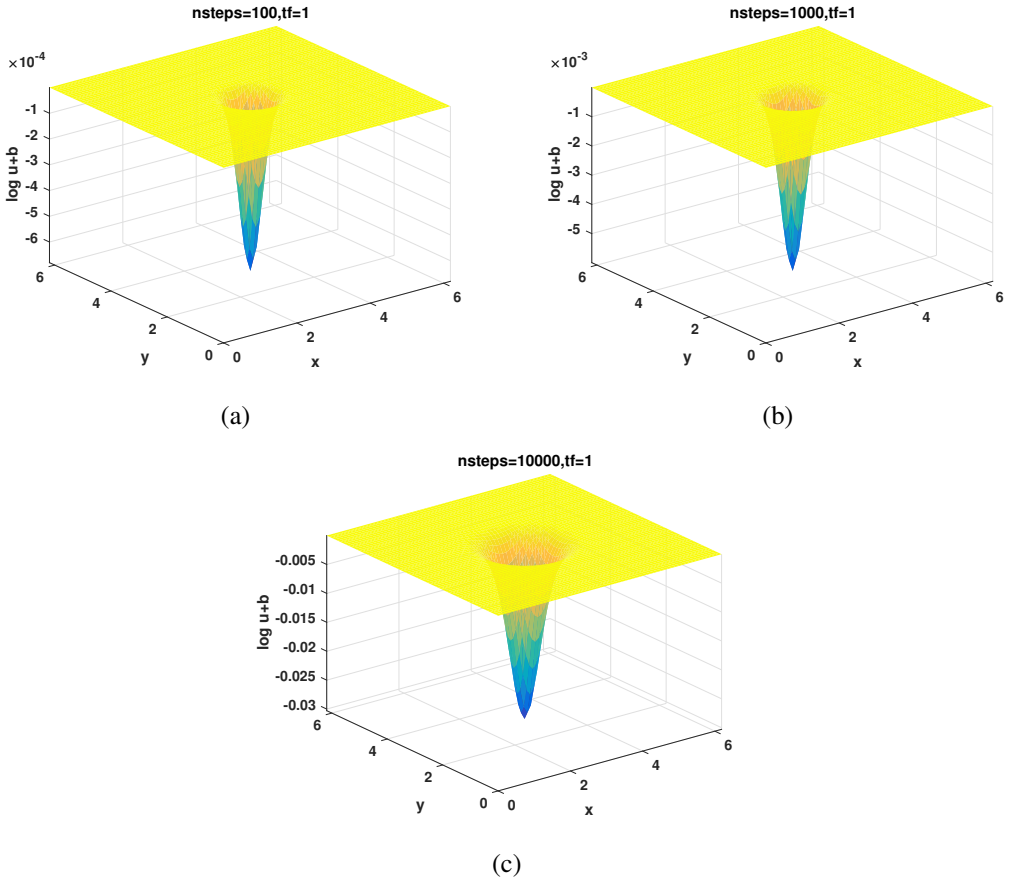

(a) (b)

(c)

Figure 4.49: Solutions $u+b$ versus coordinates (x,y) are shown with $nsteps = 100, 1,000, 10,000$ and $tf = 1$. Parameters are $k_{on} = 10^2\ s^{-1}$, $k_{off} = 10^{-1}\ s^{-1}$, $D_1 = 30\ \mu m^2/s$ and $D_2 = 10^{-1}\ \mu m^2/s$.

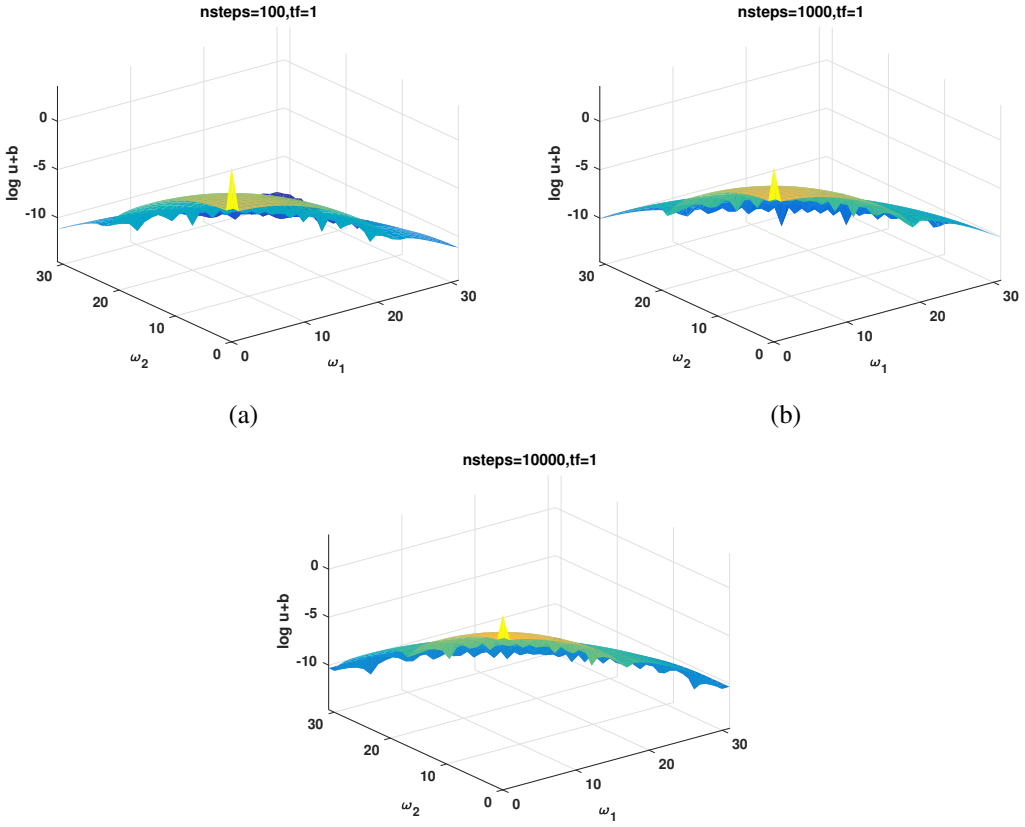

Figure 4.50: Solutions $u+b$ versus frequencies ω_1 and ω_2 are shown with $nsteps = 100, 1,000, 10,000$ and $tf = 1$. Parameters are $k_{on} = 10^2\ s^{-1}$, $k_{off} = 10^{-1}\ s^{-1}$, $D_1 = 30\ \mu m^2/s$ and $D_2 = 10^{-1}\ \mu m^2/s$.

Chapter 5

Conclusion

We applied a first-order KSS method to solve the first-order photobleaching kinetics partial differential equations with general initial conditions and the initial conditions that came from a pre-bleach steady state. It has been shown that by applying block Arnoldi iteration symbolically for each Fourier coefficient, an approximate analytical solution can be obtained that facilitates qualitative analysis of short-time behavior. The numerical results indicate satisfactory accuracy of the method for both reaction-dominated and diffusion dominated cases, which is promising for application to FRAP laboratory research. We present a simple analytical solution to this model which makes analysis feasible for scientists in the field of cell biology.

Future work will consist of proving stability and convergence, consideration of more general laser profiles, and other generalizations of interest such as generalizing time-dependent coefficients to model both the bleaching stage and recovery stage, including to three-dimensional problems as in [3]. Efficient application of higher-order KSS methods (that is, $K > 1$) will also be investigated.

Appendix A

COMPUTER RESULTS

A.1 Computer Code

```
function[x,y,w1,w2,total1,total2,total3,total4,total5,total6,absoluteErr,
relativeErr,exact,B12,B22,v11,v21,v12,v22,u11,u21,u12,u22,cons,w1m,w2m,
Rlam1,Rlam2,lam1,lam2,RM11,RM21,RM12,RM22,M11,M21,M12,M22,Tv1,Tv2]=
test2(N,nsteps,tf,coefs)
dx=2*pi/N;
dy=2*pi/N;
x=dx*(0:N-1);
y=dy*(0:N-1);
[x2,y2]=meshgrid(x,y);
x2=reshape(x2,numel(x2),1);
y2=reshape(y2,numel(y2),1);
eN2=ones(N^2,1);
kb=1.0;
I0=1.0;
w1=[0:N/2 -N/2+1:-1];
w2=[0:N/2 -N/2+1:-1];
ci=1.0;
if coefs==1
    kon=10^(-0.5);
    koff=1.e-1;
    D1 = 30;
    D2 = 1.e-4;
    rn=0.5;
elseif coefs==2
    kon=10^(3.5);
    koff=1;
```

```
    D1 = 30;
    D2 = 1.e-4;
    rn=0.5;
elseif coefs==3
    kon=255.0;
    koff=31.0;
    D1 = 45;
    D2 = 2.5;
    rn=0.6;
elseif coefs==4
    kon=1.e-2;
    koff=10;
    D1 = 30;
    D2 = 1.e-4;
    rn=0.5;
else
    kon=10^2;
    koff=10^(-1);
    D1 = 30;
    D2 = 10^(-1);
    rn=0.5;
end
Irn=(2.0*I0./pi.*rn.^2).*exp(-2.0*((x2-pi).^2+(y2-pi).^2)./rn.^2);
D=-2*eye(N)+diag(ones(N-1,1),1)+diag(ones(N-1,1),-1);
D(1,N)=1;
D(N,1)=1;
D=D/dx^2;
D=sparse(D);
Lapl=kron(D,eye(N))+kron(eye(N),D);
D3=diag(ones(N-1,1),1);
D3(N,1)=1;
D3=D3-D3';
D3=D3/(2*dx);
D3=sparse(D3);
Dx=kron(D3,eye(N));
Dy=kron(eye(N),D3);
```

```
B12=(ci.*koff)./(koff+kon)*eN2;
B22=(ci.*kon)./(koff+kon)*eN2;
L12=koff*speye(N^2);
L21=kon*speye(N^2);
L11=-kb*spdiags(Irn,0,N^2,N^2)+D1*Lapl-L21;
L22=-kb*spdiags(Irn,0,N^2,N^2)+D2*Lapl-L12;
L=[L11 L12;L21 L22];
L=sparse(L);
[w1m,w2m]=meshgrid(w1,w2);
w1m=reshape(w1m,numel(w1m),1);
w2m=reshape(w2m,numel(w2m),1);
u11=1.0.*koff*eN2;
u12=1.0.*koff*eN2;
u21=0.5.*((w1m.^2+w2m.^2).*(D1-D2)+(kon-koff))+
    0.5.*sqrt((w1m.^2+w2m.^2).^2.*(D1-D2).^2+...
    (w1m.^2+w2m.^2).*(2.0.*(D1+D2).*(kon+koff)-
    4.0.*((D1.*koff)+(D2.*kon)))+(kon+koff).^2);
u22=0.5.*((w1m.^2+w2m.^2).*(D1-D2)+(kon-koff))-
    0.5.*sqrt((w1m.^2+w2m.^2).^2.*(D1-D2).^2+...
    (w1m.^2+w2m.^2).*(2.0.*(D1+D2).*(kon+koff)-
    4.0.*((D1.*koff)+(D2.*kon)))+(kon+koff).^2);
cons=u11.*u22-u12.*u21;
v11=(u22./cons);
v21=(-u12./cons);
v12=(-u21./cons);
v22=(u11./cons);
dt=tf/nsteps;
tc = [dt:dt:tf]';
total1=zeros(N^2,nsteps);
total2=zeros(N^2,nsteps);
total3=zeros(N,N,nsteps);
total4=zeros(N,N,nsteps);
total5=zeros(N^2,nsteps);
total6=zeros(N,N,nsteps);
nstep=1;
for t=dt:dt:tf
```

```
u2=reshape(B12,N,N);
b2=reshape(B22,N,N);
Tum=fft2(u2);
Tbm=fft2(b2);
u2=reshape(u2,N^2,1);
b2=reshape(b2,N^2,1);
u2x=Dx*u2;
u2y=Dy*u2;
b2x=Dx*b2;
b2y=Dy*b2;
Tum=reshape(Tum,N^2,1);
Tbm=reshape(Tbm,N^2,1);
 vc=(v11.^2)+(v21.^2);
Tum=Tum*(2*pi/N)^2;
Tbm=Tbm*(2*pi/N)^2;
Temp1=(v11.^2.*Tum)+(v21.*v11.*Tbm);
Temp2=(v21.^2.*Tbm)+(v21.*v11.*Tum);
Temp3=(v11.^2.*conj(Tum))+(conj(v21).*conj(v11).*conj(Tbm));
Temp4=(v21.^2.*conj(Tbm))+(conj(v21).*conj(v11).*conj(Tum));
u2c=(norm(u2x,'fro')*(2*pi/N)).^2+(norm(u2y,'fro')*(2*pi/N)).^2;
b2c=(norm(b2x,'fro')*(2*pi/N)).^2+(norm(b2y,'fro')*(2*pi/N)).^2;
RM11=-(kb.*mean(Irn))+(((koff.*conj(v11).*v21)+(kon.*conj(v21).*v11)-
   (((D1.*v11.^2)+(D2.*v21.^2)).*(w1m.^2+w2m.^2))-
   (koff.*v21.^2)-(kon.*v11.^2))./(v11.^2+v21.^2));
RM12=(-4*pi^2.*kb.*(v11.^2+v21.^2).*(((myfft2(Irn.*u2)*(2*pi/N)^2).*conj(v11))
    +((myfft2(Irn.*b2)*(2*pi/N)^2).*conj(v21)))+ ...
    4*pi^2.*kb.*mean(Irn).*((Temp1).*conj(v11)+(Temp2).*conj(v21))- ...
    4*pi^2.*(w1m.^2+w2m.^2).*(v11.^2+v21.^2).*
    ((D1.*conj(v11).*Tum)+(D2.*v21.*Tbm))+ ...
    4*pi^2.*(w1m.^2+w2m.^2).*((D1.*conj(v11).*
    (Temp1))+(D2.*conj(v21).*(Temp2)))+ ...
    4*pi^2.*(v11.^2+v21.^2).*
    ((conj(v11).*(koff.*Tbm-kon.*Tum))+(conj(v21).*(kon.*Tum-koff.*Tbm)))+ ...
    4*pi^2.*(conj(v11)-conj(v21)).*((kon.*(Temp1))-(koff.*(Temp2)))./ ...
    (2*pi.*sqrt(v11.^2+v21.^2).*sqrt(16*pi^4.*(v11.^2+v21.^2).^2.*
    ((norm(u2,'fro')*(2*pi/N)).^2+(norm(b2,'fro')*(2*pi/N)).^2)- ...
```

```
    real(8*pi^2.*(v11.^2+v21.^2).*((conj(Tum).*Temp3)+(conj(Tbm).*Temp4)))+ ..
    4*pi^2.*((Temp2).^2+(Temp1).^2)));
RM21=(-4*pi^2.*kb.*(v11.^2+v21.^2).*((conj(myfft2(Irn.*u2)*(2*pi/N)^2).*v11)
    +(conj(myfft2(Irn.*b2)*(2*pi/N)^2).*v21))+ ...
    4*pi^2.*kb.*mean(Irn).*((Temp3).*v11+(Temp4).*v21)- ...
    4*pi^2.*(w1m.^2+w2m.^2).*(v11.^2+v21.^2).*
    ((D1.*v11.*conj(Tum))+(D2.*v21.*conj(Tbm)))+ ...
    4*pi^2.*(w1m.^2+w2m.^2).*((D1.*v11.*(Temp3))+(D2.*v21.*(Temp4)))+ ...
    4*pi^2.*(v11.^2+v21.^2).*((v11.*(kon.*conj(Tbm)-kon.*conj(Tum)))+
    (v21.*(koff.*conj(Tum)-koff.*conj(Tbm))))+ ...
    4*pi^2.*((v11.*kon)-(v21.*koff)).*((Temp3)-(Temp4))./ ...
    (2*pi.*sqrt(v11.^2+v21.^2).*sqrt(16*pi^4.*(v11.^2+v21.^2).^2.*
    ((norm(u2,'fro')*(2*pi/N)).^2+(norm(b2,'fro')*(2*pi/N)).^2)- ...
    real(8*pi^2.*(v11.^2+v21.^2).*((conj(Tum).*Temp3)+(conj(Tbm).*Temp4)))+ ..
    4*pi^2.*((Temp2).^2+(Temp1).^2)));
RM22=((-4*pi^2.*kon.*(Temp1).^2)-(4*pi^2.*koff.*(Temp2).^2)+ ...
    4*pi^2.*kon.*(Temp1).*(Temp4)+ ...
    4*pi^2.*koff.*(Temp3).*(Temp2)- ...
    64*pi^6.*kb.*(vc).^2.*(mean(Irn.*u2.^2)+mean(Irn.*b2.^2))+ ...
    4*pi^2.*kb.*vc.*(((myfft2(Irn.*u2)*(2*pi/N)^2).*(Temp3))+
    ((myfft2(Irn.*b2)*(2*pi/N)^2).*(Temp4)))- ...
    16*pi^4.*(vc).^2.*(D1.*(u2c)+D2.*(b2c))+ ...
    4*pi^2.*vc.*(Temp1).*((-kon.*conj(Tbm))+(D1.*(w1m.^2+w2m.^2).*
    conj(Tum))+(kon.*conj(Tum)))+ ...
    4*pi^2.*vc.*(Temp2).*((-koff.*conj(Tum))+(D2.*(w1m.^2+w2m.^2).*
    conj(Tbm))+(koff.*conj(Tbm)))- ...
    4*pi^2.*kb.*mean(Irn).*((Temp2).^2+(Temp1).^2)+ ...
    4*pi^2.*vc.*(Temp4).*((koff.*Tbm)-(kon.*Tum))- ...
    4*pi^2.*(w1m.^2+w2m.^2).*((D1.*(Temp3).^2)+(D2.*(Temp4).^2))+ ...
    4*pi^2.*vc.*((kon.*Tum)-(koff.*Tbm)).*(Temp3)+ ...
    16*pi^4.*(vc).^2.*((-kon.*(norm(u2,'fro')*(2*pi/N)).^2)+
    (4*pi^2.*koff.*mean(u2.*b2))+(4*pi^2.*kon.*mean(b2.*u2))-
    (koff.*(norm(b2,'fro')*(2*pi/N)).^2))- ...
    4*pi^2.*vc.*(w1m.^2+w2m.^2).*((D1.*Tum.*(Temp3))+(D2.*Tbm.*(Temp4)))+ ...
    4*pi^2.*kb.*vc.*((conj(myfft2(Irn.*u2)*(2*pi/N)^2).*(Temp3))+
    (conj(myfft2(Irn.*b2)*(2*pi/N)^2).*(Temp4)))./ ...
```

```
    (16*pi^4.*(vc).^2.*((norm(u2,'fro')*(2*pi/N)).^2+(norm(b2,'fro')*
    (2*pi/N)).^2)- ...
    real(8*pi^2.*vc.*((conj(Tum).*(Temp3))+(conj(Tbm).*(Temp4))))+ ...
    4*pi^2.*((Temp2).^2+(Temp1).^2));
vcc=(v12.^2)+(v22.^2);
Temp5=(v12.^2.*Tum)+(v22.*v12.*Tbm);
Temp6=(v22.^2.*Tbm)+(v22.*v12.*Tum);
Temp7=(v12.^2.*conj(Tum))+(conj(v22).*conj(v12).*conj(Tbm));
Temp8=(v22.^2.*conj(Tbm))+(conj(v22).*conj(v12).*conj(Tum));
M11=-(kb.*mean(Irn))+(((koff.*conj(v12).*v22)+(kon.*conj(v22).*v12)-
    (((D1.*v12.^2)+(D2.*v22.^2)).*(w1m.^2+w2m.^2))-
    (koff.*v22.^2)-(kon.*v12.^2))./(v12.^2+v22.^2));
M12=(-4*pi^2.*kb.*(v12.^2+v22.^2).*(((myfft2(Irn.*u2)*(2*pi/N)^2).*conj(v12))+
    ((myfft2(Irn.*b2)*(2*pi/N)^2).*conj(v22)))+ ...
    4*pi^2.*kb.*mean(Irn).*((Temp5).*conj(v12)+(Temp6).*conj(v22))- ...
    4*pi^2.*(w1m.^2+w2m.^2).*(v12.^2+v22.^2).*
    ((D1.*conj(v12).*Tum)+(D2.*v22.*Tbm))+ ...
    4*pi^2.*(w1m.^2+w2m.^2).*((D1.*conj(v12).*(Temp5))+(D2.*conj(v22).*
    (Temp6)))+ ...
    4*pi^2.*(v12.^2+v22.^2).*((conj(v12).*(koff.*Tbm-kon.*Tum))+
    (conj(v22).*(kon.*Tum-koff.*Tbm)))+ ...
    4*pi^2.*(conj(v12)-conj(v22)).*((kon.*(Temp5))-(koff.*(Temp6)))./ ...
    (2*pi.*sqrt(v12.^2+v22.^2).*sqrt(16*pi^4.*(v12.^2+v22.^2).^2.*
    ((norm(u2,'fro')*(2*pi/N)).^2+(norm(b2,'fro')*(2*pi/N)).^2)- ...
    real(8*pi^2.*(v12.^2+v22.^2).*((conj(Tum).*Temp7)+(conj(Tbm).*
    Temp8)))+ ...
    4*pi^2.*((Temp6).^2+(Temp5).^2)));
M21=(-4*pi^2.*kb.*(v12.^2+v22.^2).*((conj(myfft2(Irn.*u2)*(2*pi/N)^2).*v12)+
   (conj(myfft2(Irn.*b2)*(2*pi/N)^2).*v22))+ ...
    4*pi^2.*kb.*mean(Irn).*((Temp7).*v12+(Temp8).*v22)- ...
    4*pi^2.*(w1m.^2+w2m.^2).*(v12.^2+v22.^2).*
    ((D1.*v12.*conj(Tum))+(D2.*v22.*conj(Tbm)))+ ...
    4*pi^2.*(w1m.^2+w2m.^2).*((D1.*v12.*(Temp7))+(D2.*v22.*(Temp8)))+ ...
    4*pi^2.*(v12.^2+v22.^2).*((v12.*(kon.*conj(Tbm)-kon.*conj(Tum)))+
    (v22.*(koff.*conj(Tum)-koff.*conj(Tbm))))+ ...
    4*pi^2.*((v12.*kon)-(v22.*koff)).*((Temp7)-(Temp8)))./ ...
```

```
    (2*pi.*sqrt(v12.^2+v22.^2).*sqrt(16*pi^4.*(v12.^2+v22.^2).^2.*
    ((norm(u2,'fro')*(2*pi/N)).^2+(norm(b2,'fro')*(2*pi/N)).^2)- ...
    real(8*pi^2.*(v12.^2+v22.^2).*((conj(Tum).*Temp7)+(conj(Tbm).*Temp8)))+ ..
    4*pi^2.*((Temp6).^2+(Temp5).^2)));
M22=((-4*pi^2.*kon.*(Temp5).^2)-(4*pi^2.*koff.*(Temp6).^2)+ ...
    4*pi^2.*kon.*(Temp5).*(Temp8)+ ...
    4*pi^2.*koff.*(Temp7).*(Temp6)- ...
    64*pi^6.*kb.*(vcc).^2.*(mean(Irn.*u2.^2)+mean(Irn.*b2.^2))+ ...
    4*pi^2.*kb.*vcc.*(((myfft2(Irn.*u2)*(2*pi/N)^2).*(Temp7))+
    ((myfft2(Irn.*b2)*(2*pi/N)^2).*(Temp8)))- ...
    16*pi^4.*(vcc).^2.*(D1.*(u2c)+D2.*(b2c))+ ...
    4*pi^2.*vcc.*(Temp5).*
    ((-kon.*conj(Tbm))+(D1.*(w1m.^2+w2m.^2).*conj(Tum))+(kon.*conj(Tum)))+ ...
    4*pi^2.*vcc.*(Temp6).*
    ((-koff.*conj(Tum))+(D2.*(w1m.^2+w2m.^2).*conj(Tbm))+(koff.*conj(Tbm)))- .
    4*pi^2.*kb.*mean(Irn).*((Temp6).^2+(Temp5).^2)+ ...
    4*pi^2.*vcc.*(Temp8).*((koff.*Tbm)-(kon.*Tum))- ...
    4*pi^2.*(w1m.^2+w2m.^2).*((D1.*(Temp7).^2)+(D2.*(Temp8).^2))+ ...
    4*pi^2.*vcc.*((kon.*Tum)-(koff.*Tbm)).*(Temp7)+ ...
    16*pi^4.*(vcc).^2.*((-kon.*(norm(u2,'fro')*(2*pi/N)).^2)+
    (4*pi^2.*koff.*mean(u2.*b2))+
    (4*pi^2.*kon.*mean(b2.*u2))-(koff.*(norm(b2,'fro')*(2*pi/N)).^2))- ...
    4*pi^2.*vcc.*(w1m.^2+w2m.^2).*((D1.*Tum.*(Temp7))+(D2.*Tbm.*(Temp8)))+ ...
    4*pi^2.*kb.*vcc.*((conj(myfft2(Irn.*u2)*(2*pi/N)^2).*(Temp7))+
    (conj(myfft2(Irn.*b2)*(2*pi/N)^2).*(Temp8)))./ ...
    (16*pi^4.*(vcc).^2.*((norm(u2,'fro')*(2*pi/N)).^2+(norm(b2,'fro')*
    (2*pi/N)).^2)- ...
    real(8*pi^2.*vcc.*((conj(Tum).*(Temp7))+(conj(Tbm).*(Temp8))))+ ...
    4*pi^2.*((Temp6).^2+(Temp5).^2));
TrRM=RM11+RM22;
TrM=M11+M22;
DetRM=RM11.*RM22-RM12.*RM21;
DetM=M11.*M22-M12.*M21;
DiscRM=sqrt(TrRM.^2-4*DetRM);
DiscM=sqrt(TrM.^2-4*DetM);
Rlam1=(TrRM+DiscRM)/2;
```

```
Rlam2=(TrRM-DiscRM)/2;
lam1=(TrM+DiscM)/2;
lam2=(TrM-DiscM)/2;
Tum=Tum/(2*pi/N)^2;
Tbm=Tbm/(2*pi/N)^2;
p=L11*u2+L12*b2;
q=L21*u2+L22*b2;
p2=reshape(p,N,N);
q2=reshape(q,N,N);
Tpm=fft2(p2);
Tqm=fft2(q2);
Tpm=reshape(Tpm,N^2,1);
Tqm=reshape(Tqm,N^2,1);
Rc1=((exp(Rlam2*dt)-exp(Rlam1*dt))./(Rlam2-Rlam1));
Rc0=exp(Rlam2*dt)-Rc1.*Rlam2;
c1=((exp(lam2*dt)-exp(lam1*dt))./(lam2-lam1));
c0=exp(lam2*dt)-c1.*lam2;
Tv1=u11.*(Rc0.*((u22./cons).*Tum+(-u12./cons).*Tbm))+...
    u11.*(Rc1.*((u22./cons).*Tpm+(-u12./cons).*Tqm))+...
    u12.*(c0.*((-u21./cons).*Tum+(u11./cons).*Tbm))+...
    u12.*(c1.*((-u21./cons).*Tpm+(u11./cons).*Tqm));
Tv2=u21.*(Rc0.*((u22./cons).*Tum+(-u12./cons).*Tbm))+...
    u21.*(Rc1.*((u22./cons).*Tpm+(-u12./cons).*Tqm))+...
    u22.*(c0.*((-u21./cons).*Tum+(u11./cons).*Tbm))+...
    u22.*(c1.*((-u21./cons).*Tpm+(u11./cons).*Tqm));
Tv1=reshape(Tv1,N,N);
Tv2=reshape(Tv2,N,N);
v1=ifft2(Tv1);
v2=ifft2(Tv2);
v1=reshape(v1,N^2,1);
v2=reshape(v2,N^2,1);
vv=[v1;v2];
B12=v1;
B22=v2;
Sf=vv;
total1(:,nstep)=B12;
```

```
    total2(:,nstep)=B22;
    total3(:,:,nstep)=Tv1;
    total4(:,:,nstep)=Tv2;
    T=B12+B22;
    total5(:,nstep)=T;
    Tv=Tv1+Tv2;
    total6(:,:,nstep)=Tv;
    nstep=nstep+1;
end
[exact1,exact2]=refsoln(coefs,64,tf);
exact=exact1+exact2;
exact1=reshape(exact1,64,64);
exact2=reshape(exact2,64,64);
r=64/N;
Sf=reshape(Sf,numel(Sf),1);
Sf1=Sf(1:end/2);
Sf2=Sf(end/2+1:end);
Sf1=reshape(Sf1,N,N);
Sf2=reshape(Sf2,N,N);
absoluteErr1=norm(Sf1-exact1(1:r:64,1:r:64),'inf');
relativeErr1=norm(Sf1-exact1(1:r:64,1:r:64),'inf')./
norm(exact1(1:r:64,1:r:64),'inf');
absoluteErr2=norm(Sf2-exact2(1:r:64,1:r:64),'inf');
relativeErr2=norm(Sf2-exact2(1:r:64,1:r:64),'inf')./
norm(exact2(1:r:64,1:r:64),'inf');
absoluteErr=absoluteErr1+absoluteErr2
relativeErr=relativeErr1+relativeErr2
```

BIBLIOGRAPHY

[1] M. J. Abbett. Boundary condition calculation procedures for inviscid supersonic flow fields. In *Proceedings, AIAA Computational Fluid Dynamics Conference, Palm Springs, CA., July 19-20, 1973*, pages 153–172, New York, 1973. American Institute of Aeronautics and Astronautics, AIAA.

[2] M. J. Berger. Stability of interfaces with mesh refinement. Paper 83-42, ICASE, NASA Langley Research Center, Hampton, August 1983.

[3] K. Braeckmans, L. Peeters, N. N. Sanders, S. C. De Smedt, and J. Demeester. Three-dimensional fluorescence recovery after photobleaching with the confocal scanning laser microscope. *Biophysical Journal*, 85:2240–2252, 2003.

[4] J. Braga, J. M. P. Desterro, and M Carmo-Fonseca. Intracellular macromolecular mobility measured by fluorescence recovery after photobleaching with confocal laser scanning microscopes. *Molecular Biology Of The Cell*, 15:4749, 2004.

[5] Alexandru Cibotarica, James V. Lambers, and Elisabeth M. Palchak. Solution of nonlinear time-dependent pdes through componentwise approximation of matrix functions. *Journal of Computational Physics*, 321:1120–1143, 2016.

[6] L. Reichel D. Calvetti, S.-M. Kim. Quadrature rules based on the arnoldi process. *SIAM J. Matrix Anal.*, 26:765–781, 2005.

[7] G. H. Golub and Charles F. Van Loan. *Matrix Computations*. The John Hopkins University Press, 3rd ed edition, 1996.

[8] G. H. Golub and G. Meurant. *Matrices, moments and quadrature*. Proceedings of the 15th Dundee Conference, June-July 1993,. Longman Scientific and Technical, 1994.

[9] B. Gustafsson. Numerical boundary conditions. In B. E. Engquist, S. Osher, and R. C. J. Somerville, editors, *Large-Scale Computations in Fluid Mechanics*, pages 279–308. AMS, Providence, 1985. Lectures in Applied Mathematics, Vol. 22, Part 1.

[10] P. Jeanteur. *RNA trafficking and nuclear structure dynamics*. spinger, 2008.

[11] Minchul Kang, Charles A. Day, Emmanuele DiBenedetto, and Anne K. Kenworthy. A quantitative approach to analyze binding diffusion kinetics by confocal frap. *Biophysicsl Journal*, 99:2737–2747, 2010.

[12] Minchul Kang, Charles A. Day, Kimberly Drake, Anne K. Kenworthy, and Emmanuele DiBenedetto. A generalization of theory for two-dimensional fluorescence recovery after photobleaching applicable to confocal laser scanning microscopes. *Biophysicsl Journal*, 97:1501–1511, 2009.

[13] Minchul Kang and Anne K. Kenworthy. A closed-form analytic expression for frap formula for the binding diffusion model. *Biophysical Journal: Biophysical Letters*, (doi:10.1529/biophysj.108.135913), 2008.

[14] Adel. Kouroush, Hubert J. Identification of biomolecule mass transport and binding rate parameters in living cells by inverse modeling. *BioMed Central Ltd.*, 3(1):36, 2006.

[15] U. Kubitscheck. *Fluorescence microscopy : From principles to biological applications*. Weinheim: Wiley-Blackwell, http://dx.doi.org/10.1002/9783527671595., 2013.

[16] James V. Lambers. Enhancement of krylov subspace spectral methods by block lanczos iteration. *Electron. T. Numer. Ana.*, 31:86–109, 2008.

[17] James V. Lambers. An explicit, stable, high-order spectral method for the wave equation based on block gaussian quadrature. *IAENG Journal of Applied Mathematics*, 38:333–348, 2008.

[18] James V. Lambers. A spectral time-domain method for computational electrodynamics. *Adv. Appl. Math. Mech.*, 6:781–798, 2009.

[19] T. May. *Boundary Conditions in the Numerical Integration of Hyperbolic Equations*. PhD thesis, University of Reading, Reading, May 1978.

[20] Y. Saad. *Numerical Methods for Large Eigenvalue Problems*. Halsted Press, New York, 1992.

[21] Anthony E. Siegman. *Lasers*. University Science Books, Sausalito, California, 1986.

[22] B. L. Sprague, R. L. Pego, D. A. Stavreva, and J. G. McNally. Analysis of binding reactions by fluorescence recovery after photobleaching. *Biophys. J.*, 86:3473–3495., 2004.